# UTILIZING PRESYNAPTIC STRUCTURE-FUNCTION PROPERTIES TO INFORM THE DESIGN OF NOVEL THERAPIES FOR NEUROMUSCULAR DISEASE

by

**Tyler B. Tarr**

BS Neuroscience, University of Pittsburgh, 2010

Submitted to the Graduate Faculty of the

Kenneth P. Dietrich School of Arts and Sciences in partial fulfillment

of the requirements for the degree of

Doctor of Philosophy

University of Pittsburgh

2015

UNIVERSITY OF PITTSBURGH

KENNETH P. DEITRICH SCHOOL OF ARTS AND SCIENCES

This dissertation was presented

by

Tyler B. Tarr

It was defended on

August 10, 2015

and approved by

Chair: Stephen D. Meriney, PhD, Professor, Neuroscience

Edda Thiels, PhD, Associate Professor, Neurobiology

Jon W. Johnson, PhD, Professor, Neuroscience

German Barrionuevo, MD, Professor, Neuroscience

Anne-Marie Oswald, PhD, Assistant Professor, Neuroscience

Alan D. Grinnell, PhD, Professor, University of California, Los Angeles

Markus Dittrich, PhD, Director of Biomedical Applications Group, Pittsburgh Supercomputing Center & Carnegie Mellon University

**UTILIZING PRESYNAPTIC STRUCTURE-FUNCTION PROPERTIES TO INFORM THE DESIGN OF NOVEL THERAPIES FOR NEUROMUSCULAR DISEASE**

Tyler B. Tarr, PhD

University of Pittsburgh, 2015

The mammalian neuromuscular junction (NMJ) is consistently reliable, but disorders with a synaptic locus can adversely affect this reliability and lead to muscle weakness. One such disorder is Lambert-Eaton myasthenic syndrome (LEMS), an autoimmune disorder that causes a reduction in neurotransmitter release at the NMJ by reducing the number of release-relevant presynaptic calcium channels. In addition to removing calcium channels, it is hypothesized that LEMS causes a disruption in the organization of release sites, or active zones. Therefore, understanding how active zone structure and organization regulate functional properties in both normal and diseased NMJs would be beneficial for the targeting of treatment for synaptic pathologies. Here we show evidence suggesting that the mammalian NMJ is built with hundreds to thousands of unreliable single-vesicle release sites, and this organization leads to both overall reliability during single action potentials and a conservation of resources such that reliability is maintained during periods of high-frequency activity. We then show that this unreliability at a single-vesicle level likely has two low probability components, the low probability of a calcium channel opening near a vesicle and the low probability that a vesicle will be released even when a nearby channel does open. Furthermore, the low probability of these two components becomes pathologically low in LEMS, and targeting both components simultaneously with a potassium channel blocker and a novel calcium channel agonist leads to a supra-linear increase in transmitter release at LEMS model synapses. Although this dual treatment completely restores

the magnitude of transmitter release, the short-term plasticity characteristics are not restored to normal levels. Using an MCell model of the mouse NMJ active zone, we show that simply reducing the number of channels does not recapitulate the short-term facilitation observed experimentally in LEMS model mouse NMJs. Instead, it seems that a combination of a reduction in the number of channels tightly coupled to the vesicle and an increase in the number of channels that are loosely coupled to vesicles is more representative of LEMS short-term plasticity characteristics. This information could help determine novel treatment approaches for LEMS and other synaptic disorders.

## TABLE OF CONTENTS

## LIST OF TABLES

## LIST OF FIGURES

# PREFACE

Some sections of the General Introduction and the General Discussion have been published in two separate review articles. The following sections or portions of them have been published in *Trends in Neurosciences* in 2013 (citation below): Section 1.1.2.2, Section 1.2.1, and Section 6.5. The following sections or portions of them have been published in *Molecular Neurobiology* in 2015 (citation below): Section 1.2, Section 1.2.1, Section 1.3, Section 1.4, Section 1.4.1, Section 1.4.2, and Section 1.4.3. Minor formatting changes and changes to the numbering of figures and tables have been made to preserve consistency with the rest of this dissertation document.

# 1.0 GENERAL INTRODUCTION

## 1.1 NEUROTRANSMITTER RELEASE FROM PRESYNAPTIC TERMINALS

Many decades ago, it was determined that the primary means of communication between cells in the nervous system was chemical neurotransmitter release at sites of contact called synapses. Although there are some synapses with direct electrical connections between the two cells, the vast majority of synapses are chemical. Thus, neurotransmitter release from the presynaptic terminal of the synapse is a vital process in the overall function of the nervous system. Understanding the properties and regulation of neurotransmitter release is therefore important from a basic biological standpoint and a disease standpoint, since many diseases of the nervous system have a synaptic locus.

Release of neurotransmitter into the synaptic cleft occurs as a result of the fusion of neurotransmitter-containing vesicles into the presynaptic terminal membrane. This vesicle fusion occurs following an action-potential-evoked depolarization of the presynaptic terminal, which allows an influx of calcium and subsequent triggering of vesicle fusion. Although calcium-triggered secretion of neurotransmitter seems straightforward, this process, as well as its regulation, is highly complex and remains incompletely understood.

### 1.1.1 Calcium-triggered neurotransmitter release

Much of our understanding of the process of neurotransmitter release comes from the work of Bernard Katz and colleagues. Their work led to the discovery that neurotransmitter is released in defined "packets", or quanta, and that this quantal release is dependent on external calcium (Katz, 1969). It was eventually determined that voltage-gated calcium channels (VGCCs) are the gate by which external calcium can influence neurotransmitter release (Llinas et al., 1972; Llinas and Nicholson, 1975; Tsien, 1983). When an action potential invades the presynaptic terminal, VGCCs open in response to this depolarization and allow calcium to come into the terminal from the extracellular space. The relationship between calcium concentration and neurotransmitter release is close to the third or fourth order (Dodge and Rahamimoff, 1967), such that a small change in calcium influx leads to a large change in neurotransmitter release. The potential mechanisms underlying the nonlinear relationship between calcium and neurotransmitter release is discussed in more detail below (Section 1.1.2.1).

#### 1.1.1.1 Voltage-gated calcium channels

VGCCs are transmembrane proteins that respond to a change in voltage across the membrane to open and allow a flux of calcium ions across the membrane. VGCCs consist of a pore-forming $\alpha 1$ subunit and its auxiliary subunits, which are the $\alpha 2$, $\beta$, $\delta$, and/or $\gamma$ subunits (Catterall, 2011). For the sake of simplicity, I will be focusing on the $\alpha 1$ subunit, but it should be noted that the various auxiliary subunits come in multiple variants and play important roles in the regulation of channel function. The $\alpha 1$ subunit consists of approximately 2000 amino acid residues, the sequence of which has four domains that have six transmembrane segments each (Takahashi et al., 1987; Tanabe et al., 1987). Of particular importance is the S4 segment in each domain, which

has been shown to be the voltage sensor in multiple voltage-dependent cation channels (Bezanilla, 2000). It is thought that this segment moves from a more internal position to a more external position in response to a depolarization of voltage across the membrane (Stock et al., 2013).

There are three different subfamilies of the α1 subunit: $Ca_v1$ (L-type), $Ca_v2$ (P/Q-, N- and R-type) and $Ca_v3$ (T-type) (Hille, 2001). With respect to synaptic transmission, the majority of synapses utilize P/Q-type ($Ca_v2.1$) or N-type ($Ca_v2.2$) channels to trigger neurotransmitter release, although R-type ($Ca_v2.3$) can contribute at some mixed-channel synapses and L-type can control release in specialized ribbon synapses (Catterall, 2011). Each of the $Ca_v2$ channels has the fortuitous property of being selectively sensitive to a specific blocker, thus allowing the identification of channel subtypes at a synapse. P/Q-type channels can be blocked selectively with spider toxin ω-agatoxin IVA (Mintz et al., 1992), N-type channels are selectively sensitive to the cone snail toxin ω-conotoxin GVIA (Olivera et al., 1984), and R-type channels are selectively blocked by the tarantula toxin SNX-482 (Newcomb et al., 1998). Therefore, the effect of each channel on synaptic transmission at a particular synapse can be determined by utilizing that channel's selective blocker. In addition to their selective blockers, the $Ca_v2$ channels (as well as the $Ca_v1$ and $Ca_v3$ channels) are blocked by certain divalent and trivalent ions, such as cadmium and lanthanum (Lansman et al., 1986). However, it should be noted that these divalent and trivalent ions block the channel by permeating slowly through the channel pore, which prevents other permeable ions, such as calcium and barium, from passing through the pore (Lansman et al., 1986).

#### 1.1.1.2 Calcium homeostasis mechanisms in the presynaptic terminal

As previously mentioned, there is a highly nonlinear relationship between calcium influx and neurotransmitter release (Jenkinson, 1957; Dodge and Rahamimoff, 1967), so it is vital that the presynaptic terminal tightly regulates the concentration of free calcium. There are many mechanisms for keeping the intracellular calcium concentration at very low levels, in the range of ~10-100 nM (Naraghi and Neher, 1997). Some of the players in the regulation of intracellular calcium concentration include fixed and mobile buffers, such as parvalbumin and calbindin, the sodium/calcium exchanger, the calcium/magnesium pump, and internal storage compartments, such as mitochondria and the endoplasmic reticulum (Rusakov, 2006). These work in concert to spatially and temporally restrict changes in the free calcium concentration in the presynaptic terminal. The fixed and mobile buffers are the most relevant for the work discussed below since they are likely to be the biggest contributors to calcium homeostasis on shorter timescales, such as the timescales of a single or a few action potentials. The relevance of buffers is especially true in our MCell model of the NMJ, which includes fixed buffers, but no exchangers/pumps or internal sequestering compartments (discussed in more detail below; also see (Dittrich et al., 2013; Ma et al., 2015). The exchangers/pumps and the sequestering of calcium into organelles works on a slower timescale and therefore are not likely to play a major role in my work presented below, although the possibility that these contribute to neurotransmitter release, especially during trains of stimuli, cannot be discounted and will be considered further in the Discussion.

### 1.1.2 Active zones are the sites of vesicle fusion

The sites of neurotransmitter release are often called active zones, which is an ultrastructural term for the sites where vesicle docking and fusion occur. Active zones are electron-dense areas on the inner part of the presynaptic membrane, directly opposing the postsynaptic density, where vesicles locate (or dock) very close to the terminal membrane (Zhai and Bellen, 2004). Additionally, freeze-fracture electron microscopy has shown that vesicles do actually fuse with the terminal membrane at these active zone sites shortly after an action potential invades the presynaptic terminal (Heuser et al., 1979). Active zones come in many different configurations (Zhai and Bellen, 2004), and these configurations can lead to vastly different functional properties (see 1.1.2.2 for more detail). For example, recent studies have highlighted the importance of calcium channel number and organization within the active zone for the functional output of the synapse. Studies on various rodent hippocampal synapses have shown that release probability scales with the size of the active zone (Holderith et al., 2012) and also that release characteristics are greatly affected by the number and organization of calcium channels within an active zone (Scimemi and Diamond, 2012). Similarly, at the rodent calyx of Held synapse, the number and position of calcium channels relative to the individual synaptic vesicle release sites influences the observed neurotransmitter release characteristics (Sheng et al., 2012). Importantly, certain neurological disorders have been associated with changes in presynaptic active zone structure/organization (Nagel et al., 1988; Mato et al., 2005; Upreti et al., 2012; Wondolowski and Dickman, 2013), highlighting the clinical importance of a detailed understanding of synapse function at the level of individual active zone proteins. However, it should be noted that for many years the idea that active zone structure played an important role in the function of neurotransmitter release was disputed based on evidence from phasic and tonic synapses in the

crayfish and lizard. Interestingly, phasic synapses release much more neurotransmitter compared to tonic synapses (Parnas and Atwood, 1966; Msghina et al., 1999), but the active zone ultrastructure of these two synapses is not markedly different (Govind and Pearce, 2003). Based on the evidence from many different synapses, it seems that active zone organization could be one way in which many synapses can regulate their activity and achieve different functional outputs, although other mechanisms can surely play a role as well.

#### 1.1.2.1 Release-relevant proteins within the active zone

In addition to the VGCCs that trigger vesicle fusion, there are many proteins that are relevant to the process of neurotransmitter release. Probably the most critical of these release machinery proteins is the calcium sensor for release, usually synaptotagmin 1 or 2, and a group of proteins involved with the vesicle fusion process called the SNAP (Soluble NSF (N-ethylmaleimide-sensitive factor) Attachment Protein) Receptor (SNARE) complex (Sudhof, 2012). The SNARE protein complex includes the vesicle membrane-associated protein synaptobrevin (or VAMP) and the terminal membrane proteins syntaxin and SNAP-25 (Sudhof, 2012). When enough calcium ions bind to the sensor synaptotagmin, a yet-to-be-determined process is initiated that allows the SNARE proteins to fuse the vesicle membrane to the terminal membrane, thus unloading the contents of the vesicle into the synaptic cleft.

Due to the approximate fourth order relationship between external calcium (and therefore calcium influx) and neurotransmitter release, a small change in calcium influx leads to large changes in release (Jenkinson, 1957; Dodge and Rahamimoff, 1967). Something about the interaction between calcium ions and the release sensor synaptotagmin leads to this molecular cooperativity. It is not unreasonable then to hypothesize ~4-5 cooperative binding sites, and multiple models have been constructed under this hypothesized scenario (Bennett et al., 2000;

Schneggenburger and Neher, 2000; Bollmann and Sakmann, 2005). These models basically assume a spatially uniform concentration of calcium in the region near the sensor, and that the binding of calcium to a sensor (according to an association rate constant) will affect the binding of calcium to the next sensor (by altering the association rate constant for the next sensor). However, recent work in our laboratory suggests another possible scenario that can give a fourth-order molecular cooperativity, one in which there is an excess number of independent binding sites (Dittrich et al., 2013). In this study, a 3-dimensional MCell model (Kerr et al., 2008) of the frog neuromuscular junction (NMJ) active zone was developed using decades of experimental data at this synapse as constraints (Dittrich et al., 2013). By having an excess number of binding sites (40) with no binding site cooperativity, the model could accurately reproduce the experimentally observed fourth-order relationship between calcium concentration and release, as well as other experimentally observed parameters such as average release probability and release latency (Dittrich et al., 2013). This excess binding site hypothesis is also attractive because it agrees with biochemical data on the number of synaptotagmin molecules and SNARE complexes per vesicle, which have shown that there are ~15 copies of synaptotagmin per vesicle (Takamori et al., 2006; Mutch et al., 2011) and that three to eight SNARE complexes initiate vesicle fusion to the terminal membrane (Chapman, 2002; Han et al., 2004). Since the model had 40 calcium binding sites located at the bottom of the vesicle and the proposed sensor at the frog NMJ (synaptotagmin) has 5 calcium binding sites per molecule, then our model would have 8 synaptotagmin molecules on the bottom of the vesicle (Dittrich et al., 2013), which agrees nicely with both sets of biochemical data.

#### 1.1.2.2 Functional organization of the active zone

To aid in the discussion of sub-active zone mechanisms for transmitter release, we compare and contrast two concepts that are often used when discussing calcium-triggered vesicle fusion: nanodomain and microdomain coupling of calcium to transmitter release (Figure 1) (Eggermann et al., 2012). These concepts are used to classify calcium signals that synaptic vesicles are exposed to during an action potential into two main categories. Nanodomain coupling refers to vesicle release triggered by the localized calcium signal in close vicinity to the mouth of a single calcium channel after activation (Figure 1). Cellular imaging and computational modeling of single calcium channels predict that the calcium concentration in such a nanodomain can be as high as hundreds of μM (Simon and Llinas, 1985; Llinas et al., 1992). However, because the spatial extent of the nanodomain is so small, the actual number of calcium ions present is also small, typically only a few hundred ions (Stanley, 1993). During nanodomain-coupled vesicle release, a synaptic vesicle is located within this calcium nanodomain and the calcium concentration is sufficiently high to trigger vesicle fusion and transmitter release (Llinas et al., 1982; Stanley, 1993). Under this scenario, only a fast-binding calcium buffer, such as BAPTA, can effectively compete with the calcium sensor for transmitter release.

By contrast, microdomain calcium signals are produced by the summed, overlapping calcium clouds generated by calcium entry through multiple open calcium channels that are not tightly associated with one another or the vesicle release sites in an active zone (essentially increasing background calcium near the vesicle; Figure 1), with a spatial extent ranging from 100 nm to 1 μm (Neher and Sakaba, 2008). When transmitter release is triggered by a microdomain of calcium, many channels need to open to generate a calcium concentration near vesicles that is high enough to cause vesicle fusion. In this scenario, even relatively slow binding buffers, such

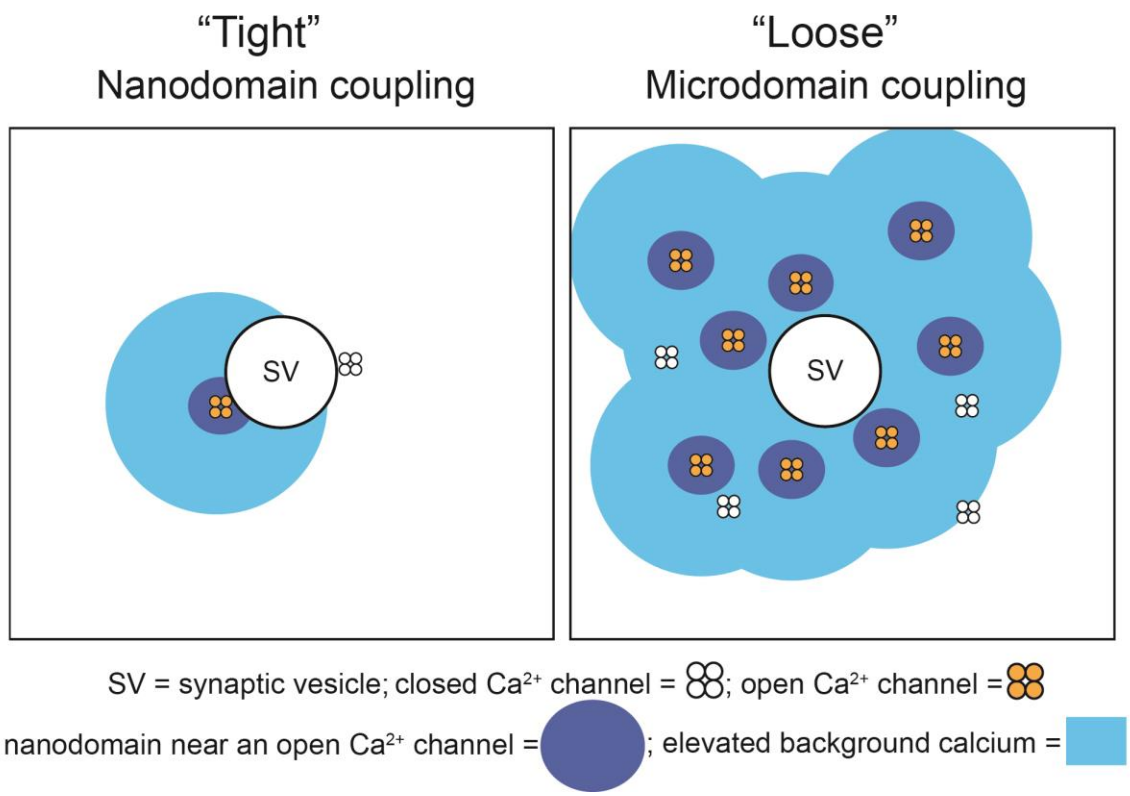


**Figure 1. Schematic diagram that compares nanodomain and microdomain coupling of a single vesicle release site to calcium channels.**

Nanodomain coupling occurs when vesicle fusion at single vesicle release sites is triggered by the local calcium flux through a single or very small number of open calcium channel(s) (dark-blue regions). Microdomain coupling occurs when vesicle fusion at single vesicle release sites is triggered by the summed calcium flux through many loosely-coupled calcium channels that essentially increases background calcium in the active zone region (light-blue regions). Figure reproduced from Tarr et al. (2013a).

as EGTA (in addition to BAPTA), can effectively compete with the calcium sensor for transmitter release.

Nanodomain and microdomain calcium signals may be mixed at some synapses due to a range of calcium channel-to-vesicle release site distances. This type of non-uniform topographic relation would produce a large variability in the calcium transient sensed by different vesicles, resulting in heterogeneity of their release probability during an action potential. Indeed, a numerical model that reproduced most experimental data of the immature calyx of Held synapse predicted that vesicles located at various distances would be released with probabilities that are inversely related to coupling distances, and ranged from 100% to less than 1% (Meinrenken et al., 2002).

## 1.2 THE NEUOROMUSCULAR JUNCTION AS A MODEL SYNAPSE

The neuromuscular junction (NMJ) is a strong, reliable synapse that consistently brings the postsynaptic muscle fiber to threshold. The large presynaptic terminal of the NMJ contains hundreds of individual neurotransmitter release sites, or active zones, where synaptic vesicle docking and fusion occur to mediate the release of neurotransmitter (Zhai and Bellen, 2004). Much of the reliability of the NMJ stems from the large safety margin for neuromuscular transmission, meaning that more neurotransmitter is released in response to each presynaptic action potential than is necessary to cause the postsynaptic cell to reach threshold (Wood and Slater, 2001). Even as muscle fibers grow and require a larger amount of input, there are compensatory increases in other parameters, such as nerve terminal size, in order keep the large safety margin for transmission (Grinnell, 1995). This excess neurotransmitter release ensures that

the postsynaptic muscle cell is depolarized beyond what is required to reach threshold and initiate muscle contraction, even during periods of high-frequency activity.

### 1.2.1 The properties of the frog and mammalian NMJs

The NMJ is a large model synapse that has been studied extensively for decades, especially with respect to presynaptic properties of neurotransmitter release (Katz, 1969). This synapse has been especially valuable for studying the properties of neurotransmitter release for several reasons: It is a very large, peripheral synapse that is amenable to experimental study, and since there is only one presynaptic terminal per postsynaptic muscle fiber, it has been relatively easy to interpret experimental results. This synapse releases more chemical neurotransmitter than is required to bring the postsynaptic muscle cell to threshold (it is strong), and it can do this repeatedly (it is reliable) during short periods of high-frequency activity (bursts of 5–10 action potentials at 50–100 Hz in "fast" muscles (Hennig and Lomo, 1985)). Although the NMJ has been the focus of numerous studies of neurotransmitter release, the exact mechanisms by which the NMJ achieves strength and reliability are not completely understood.

The adult frog NMJ is the classic model NMJ preparation that has played a critical role in our understanding of the basic mechanisms of synaptic transmission (Katz, 1969). A presynaptic action potential leads to the release of ~350 quanta from the entire large nerve terminal (Katz and Miledi, 1979). This magnitude of transmitter release is more than sufficient to bring the postsynaptic muscle cell to threshold, resulting in reliable muscle contraction (Wood and Slater, 2001). Ultrastructurally, the frog NMJ contains an average of 700 linear (1µm long) active zones separated from one another by about 1µm (Heuser et al., 1974; Katz and Miledi, 1979).

Freeze fracture and electron microscope tomography have provided detailed structural information demonstrating that these active zones each contain ~25-40 docked synaptic vesicles arranged in a double row along the length of this structure, each tightly associated with vesicle release machinery and "ready" for calcium-triggered fusion (Heuser et al., 1979; Pawson et al., 1998; Harlow et al., 2001; Rizzoli and Betz, 2005). Based on the number of released quanta and the number of active zones per synapse, each active zone releases on average a single vesicle every other action potential stimulus (probability of release / active zone = 0.5). Thus, the probability of release for any single synaptic vesicle is very small. This unreliable release within each active zone ensures that the NMJ retains a large fraction of its available docked vesicles (a conservation of resources), even during repeated stimulation, resulting in strong and reliable release from the whole NMJ under sustained activity.

Frog NMJ active zones also contain ~200-250 intramembranous particles (some of which are thought to be calcium channels) arranged in two parallel rows between the double row of vesicles (Heuser et al., 1974; Heuser et al., 1979; Pawson et al., 1998). Combining high-resolution calcium imaging techniques with variance analysis of imaged calcium signals has enabled the study of voltage-gated calcium channel properties in small neuronal compartments inaccessible to standard electrophysiological techniques (Sabatini and Svoboda, 2000). This method has previously revealed the stochastic opening of a small number of calcium channels in both presynaptic boutons and postsynaptic spines (Frenguelli and Malinow, 1996; Sabatini and Svoboda, 2000). Initial work demonstrated the feasibility of imaging presynaptic calcium entry at frog NMJ active zones (Wachman et al., 2004). A subsequent study used single pixel optical fluctuation analysis (SPOFA) of the imaged action potential-evoked increase in calcium fluorescence at the frog NMJ to estimate the number and opening probability of calcium

channels during an action potential at single active zones (Luo et al., 2011). This work identified the mechanisms that govern the low probability of transmitter release at active zones in the frog NMJ, including a paucity of voltage-gated calcium channels (30-40 per active zone, which represents only about 15-20% of total intramembranous particles identified in freeze fracture studies), a low probability of calcium channel opening during an action potential stimulus (0.2 – 0.3), and the rare triggering of synaptic vesicle fusion when a calcium channel does open and allow local calcium flux (Luo et al., 2011). Interestingly, these data predict that the total number of presynaptic calcium channels within an individual active zone coincides roughly with the number of docked synaptic vesicles and that during an action potential only ~6-10 calcium channels open in each active zone. This quantitative relationship suggests that each single vesicle release site in the frog NMJ associates on average with only a single voltage-gated calcium channel, and that vesicle fusion is triggered by the nanodomain of relatively high calcium concentration near the mouth of a single open calcium channel.

These findings are also consistent with previous studies at this synapse that have proposed that calcium flux through only one or two calcium channels can trigger transmitter release (Yoshikami et al., 1989; Shahrezaei et al., 2006). Experiments combining high resolution calcium imaging and MCell (Kerr et al., 2008) computer modeling have provided evidence that each vesicle fusion event at this synapse is controlled predominately by a single calcium channel positioned nearby. Further, it appears that calcium flux through this nearby channel triggers vesicle fusion with a low probability (5~10%) (Luo et al., 2011).

The mammalian NMJ is composed of hundreds of small, spatially isolated neurotransmitter release sites, or active zones (Figure 2A, B). Within each active zone, there is a single row of ~2–3 docked synaptic vesicles between two double rows of intramembranous

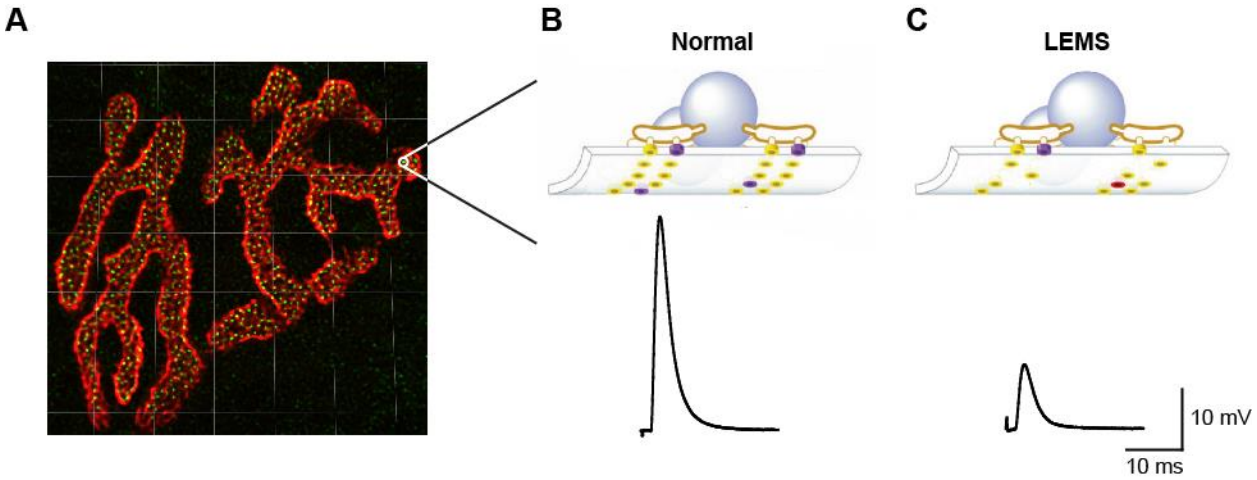


**Figure 2. Active zone organization in healthy and LEMS model NMJs.**

**A.** A single mouse NMJ showing postsynaptic acetylcholine receptors (pretzel-shaped structure stained red) and presynaptic active zone neurotransmitter release sites (green spots within red stain). Each grid line segment = 5 μm. **B.** Schematic of an individual active zone (top) along with a sample average end plate potential (EPP; a measure of the strength of neurotransmitter release) trace (bottom) from a healthy mouse NMJ. **C.** Schematic of an individual active zone (top) along with a sample average EPP trace from a LEMS model mouse NMJ (bottom). Schematics of active zones (**B**, **C**) include synaptic vesicles (blue spheres), P/Q-type calcium channels (purple cylinders), other calcium channel subtypes (red cylinders), and active zone proteins other than calcium channels (yellow cylinders). **A** Modified from Meriney and Dittrich (2013). **B, C** Modified from Urbano et al. (2003) (Copyright 2003 National Academy of Sciences, USA). Figure reproduced from Tarr et al. (2015).

particles (Nagwaney et al., 2009), a portion of which are thought to be the P/Q-type calcium channels required for neurotransmitter release. The estimated length of each punctate active zone is between ~80 nm (determined by measurements of the double row of intramembranous particles observed in electron microscopy (Fukunaga et al., 1983; Nagwaney et al., 2009)) and ~250 nm (determined by confocal imaging of the active zone protein bassoon (Ruiz et al., 2011)). The larger measurement made with confocal imaging of bassoon immunoreactivity may simply be at the limit of light microscopy resolution, or this larger measurement may reflect the possibility that the bassoon proteins in the active zone encompass a larger area as compared to the space occupied by the intramembranous particles of the active zone. Each small active zone is separated from each of its neighboring active zones by approximately 500 nm (Ruiz et al., 2011). At the mouse NMJ, there are ~850 active zones per NMJ (Figure 2A) (Ruiz et al., 2011; Chen et al., 2012), but despite the large number of active zones, only ~100 vesicles are released with each action potential stimulus (Tarr et al., 2013b). This means that the average probability of release per active zone is only ~0.12 and the average probability of release per vesicle (assuming two vesicles per active zone) is only ~0.06. Therefore, each individual vesicle has a very low probability of release during any one action potential, but since there are thousands of vesicles ready to be released in each NMJ, the total number of vesicles released per action potential is easily sufficient to bring the postsynaptic muscle cell to threshold. Furthermore, the low probability of release for any one vesicle means that significant depression will not occur during brief periods of high-frequency activity. Therefore, we view the NMJ as a strong and reliable synapse constructed of thousands of unreliable single-vesicle release sites (Meriney and Dittrich, 2013; Tarr et al., 2013a), with each of these unreliable single-vesicle release sites being

composed of a single vesicle docked at the active zone and a small number of closely associated calcium channels.

## 1.3 LAMBERT-EATON MYASTHENIC SYNDROME

Lambert-Eaton myasthenic syndrome (LEMS) is an autoimmune disease that attacks the neuromuscular active zone. The incidence of LEMS is estimated to be only about 0.48 per million (Wirtz et al., 2003), making LEMS a relatively rare disease. Despite its rarity, LEMS is well known as a classic paraneoplastic disorder. About 50–60 % of LEMS cases are paraneoplastic, most commonly observed in older individuals who have been long-term cigarette smokers and have developed a small-cell lung cancer tumor (Titulaer et al., 2011b). The remaining LEMS patients tend to be younger, do not have a history of smoking, and do not have an underlying tumor. In these patients, the cause of LEMS is unknown (Titulaer et al., 2008). LEMS patients most commonly experience debilitating muscle weakness but can also suffer from autonomic symptoms and reduced tendon reflexes (Titulaer et al., 2011a). In both tumor-associated LEMS and the idiopathic form of LEMS, the clinical symptoms are generally attributed to an autoantibody-mediated reduction in the number of P/Q-type voltage-gated calcium channels at the presynaptic terminal of the NMJ (Vincent et al., 1989; Lennon et al., 1995). In the case of tumor-associated LEMS, P/Q-type calcium channels are expressed by the small cell lung cancer cells, and antibodies to P/Q-type calcium channels are produced as part of the patient's immune response to the tumor (Roberts et al., 1985). The reduction in the number of presynaptic P/Q-type calcium channels leads to a reduction in the calcium influx that occurs in

response to a presynaptic action potential. With decreased presynaptic calcium influx, the probability of synaptic vesicle fusion is also lowered, resulting in less neurotransmitter (acetylcholine) release per presynaptic action potential (Figure 2C). Because less neurotransmitter is released per action potential, each presynaptic action potential is less likely to trigger a postsynaptic muscle contraction. The NMJ may attempt to compensate for the loss of P/Q-type calcium channels in LEMS in part by upregulating the expression of other calcium channel subtypes (Flink and Atchison, 2002; Oh et al., 2007), but this compensation is not sufficient to restore normal levels of neurotransmitter release (Smith et al., 1995). The upregulation of other calcium channel subunits may be insufficient because there are simply fewer calcium channels per active zone relative to healthy conditions. Another possibility is that the other calcium channel subtypes may not be located in the same positions relative to docked synaptic vesicles as the P/Q-type calcium channels in healthy active zones (Urbano et al., 2003). If the calcium channels are located farther away from docked synaptic vesicles, then they will not be able to contribute the same levels of calcium ions that are normally required to trigger the release of a synaptic vesicle. In addition to having less neurotransmitter release due to a reduced calcium influx, LEMS synapses also have disruptions in the overall structure of the presynaptic release site caused by calcium channel removal, which may also contribute to the reduction in neurotransmitter release (Fukunaga et al., 1983). Furthermore, previous studies have demonstrated that the interaction between presynaptic calcium channels and laminin β2 is critical for the maintenance of active zone organization (Nishimune et al., 2004; Chen et al., 2011), suggesting that removal of calcium channels in LEMS could lead to a disruption in the overall organization of active zones. Since the structural organization of active zones is important to synapse function (Holderith et al., 2012; Sheng et al., 2012; tom Dieck et al., 2012; Shahidullah

et al., 2013), it seems plausible that disruption of active zone organization due to autoimmune attack of active zone proteins could be partly responsible for the deficits in neurotransmitter release in LEMS.

Although antibodies to P/Q-type calcium channels are present in most LEMS patients and are generally considered responsible for the symptoms of LEMS, antibodies to other critical proteins involved in neurotransmitter release have also been detected in LEMS patients. These include antibodies to other calcium channel subtypes, such as N-type and L-type channels (Johnston et al., 1994; Lennon et al., 1995; Meriney et al., 1996; Motomura et al., 1997). Antibodies to these other calcium channel subtypes could contribute to the autonomic symptoms observed in some LEMS patients (Waterman et al., 1997). In addition, other presynaptic proteins can also be targeted by LEMS antibodies, including synaptotagmin and M1 muscarinic acetylcholine receptors (Takamori, 2008). Synaptotagmin is considered to be the calcium sensor for fast, synchronous neurotransmitter release at most synapses (Südhof, 2013). M1 muscarinic acetylcholine receptors are located on the presynaptic terminal of the NMJ and have been shown to be involved in the modulation of neurotransmitter release (Santafe et al., 2006). Interestingly, some LEMS patients are seronegative for P/Q-type calcium channel antibodies. Despite not having a detectable level of P/Q-type calcium channel antibodies, these seronegative patients have a similar clinical presentation as seropositive LEMS patients (Nakao et al., 2002; Oh et al., 2007). The symptoms in seronegative LEMS patients may be caused by antibodies to other presynaptic proteins such as synaptotagmin or M1 muscarinic receptors. Another possibility is that these patients may have P/Q-type calcium channel antibodies at levels below what is detectable with diagnostic assays.

LEMS is diagnosed using a combination of clinical symptoms, electrophysiological measurements, and tests to determine antibody levels (Titulaer et al., 2011a). The most prominent symptom in LEMS patients is muscle weakness of the proximal limbs, although the weakness does eventually progress distally (Titulaer et al., 2011a). LEMS patients also commonly report symptoms associated with autonomic dysfunction, which can include dry mouth, erectile dysfunction in men, and constipation (O'Suilleabhain et al., 1998; Titulaer et al., 2011a). It is also common for LEMS patients to present with reduced tendon reflexes (O'Neill et al., 1988; Titulaer et al., 2011a). In terms of electrophysiological measurements to diagnose LEMS, repetitive nerve stimulation (RNS) is often used (2001). The results of the RNS test in LEMS patients show a decrease in the compound muscle action potential (CMAP) amplitude during low-frequency stimulation (2-5 Hz) and an increase in CMAP amplitude during post-exercise stimulation or during high-frequency stimulation (Oh et al., 2005). Lastly, antibody panels to test for the presence of antibodies to calcium channels can be used in the diagnosis of LEMS (Titulaer et al., 2011a).

## 1.4 TREATMENT OPTIONS FOR LEMS

There is no cure for LEMS and few treatment options are available to alleviate the symptoms. If LEMS is present along with small cell lung cancer, then cancer therapy is the priority. In LEMS patients with an associated tumor, successful treatment of the tumor also alleviates the symptoms of LEMS (Mason et al., 1997; Wang et al., 2006). The simultaneous alleviation of LEMS is presumably due to the fact that the removal/reduction of the tumor has removed the underlying

cause of LEMS in these patients. If LEMS presents without an associated tumor or if LEMS symptoms are not alleviated during or following cancer treatment, then treatment can include drugs that alleviate the symptoms associated with LEMS and/or immunomodulatory therapies. As discussed below, immunosuppression may only be recommended for those patients in whom symptomatic treatment is not effective (Lindquist and Stangel, 2011).

### 1.4.1 3,4-Diaminopyridine as a symptomatic treatment option

Symptomatic treatment strategies that increase neurotransmitter release have emerged as the primary therapeutic approach (Verschuuren et al., 2006; Keogh et al., 2011; Lindquist and Stangel, 2011; Maddison, 2012; van Sonderen et al., 2013). The most common symptomatic treatment option is 3,4-diaminopyridine (3,4-DAP), a voltage-gated $K^+$ channel inhibitor that broadens the presynaptic action potential (Kirsch and Narahashi, 1978). The broadening of the presynaptic action potential allows more voltage-gated calcium channels to open, thus increasing calcium entry into the nerve terminal during each action potential. 3,4-DAP can be used alone or, less commonly, in combination with an acetylcholinesterase inhibitor. Although 3,4-DAP increases neurotransmitter release, there are dose-limiting side effects, such as paresthesia, difficulty sleeping, and, paradoxically, fatigue and deterioration in muscle strength that prevent adequate symptomatic relief for many LEMS patients (Sanders et al., 2000; Oh et al., 2009; Wirtz et al., 2009; Lindquist and Stangel, 2011; Sedehizadeh et al., 2012). The latter two may be due to reported effects on axonal $K^+$ channels that limit firing frequencies (Miralles and Solsona, 1998) and/or reduction in activity-dependent facilitation caused by 3,4-DAP (Thomsen and Wilson, 1983). Thus, 3,4-DAP indirectly increases calcium entry into the nerve terminal, but due

to dose-dependent limitations (3,4-DAP doses <80 mg/day) (Lindquist and Stangel, 2011), 3,4-DAP often does not provide enough symptomatic relief for patients to return to normal activity (Sedehizadeh et al., 2012).

### 1.4.2 Immunomodulatory therapies

If patients do not receive enough relief from 3,4-DAP, the next line of treatment usually involves some form of immunomodulatory therapy. Immunosuppressive drugs are usually given, with the combination of prednisolone and azathioprine being the most common. Studies have reported that LEMS patients show significant improvement following the combination treatment of prednisolone and azathioprine (Newsom-Davis and Murray, 1984; Maddison et al., 2001). The combined prednisolone and azathioprine treatment strategy received support from a study that compared the effectiveness of the combined prednisolone plus azathioprine treatment versus prednisolone alone in treating myasthenia gravis (Palace et al., 1998). In this study, adding azathioprine to the treatment protocol resulted in fewer side effects and a lower number of treatment failures (Palace et al., 1998). Additionally, there is evidence that LEMS patients taking high doses of prednisolone alone only experienced a mild to moderate improvement (Tim et al., 1998; Tim et al., 2000), lending further support to the use of the combined prednisolone and azathioprine treatment. However, immunosuppressants have generally not been favored, as side effects may be severe and include leukopenia, liver dysfunction, nausea, vomiting, and hair loss (Lindquist and Stangel, 2011).

Two other immunomodulatory treatment options for LEMS patients include intravenous immunoglobulin (IVIg) and plasma exchange. A randomized, crossover trial has reported

significant improvements that last for several weeks in LEMS patients treated with IVIg (Bain et al., 1996). Multiple case reports have also supported the potential benefits of using IVIg to treat LEMS (Bird, 1992; Takano et al., 1994; Muchnik et al., 1997). The beneficial effects of IVIg treatment in LEMS patients seem to result from the decline in circulating calcium channel antibodies (Bain et al., 1996), although the exact mechanism by which IVIg reduces antibody titer remains unknown. Plasma exchange is another treatment approach that temporarily reduces calcium channel antibody titer. Plasma exchange induces a rapid improvement in LEMS symptoms that diminishes after approximately 6 weeks (Newsom-Davis and Murray, 1984). Other treatment options are available, and more comprehensive discussions of the available therapeutic approaches for LEMS can be found elsewhere (Titulaer et al., 2011a; Maddison, 2012; Antoine and Camdessanche, 2013; van Sonderen et al., 2013).

### 1.4.3 Calcium channel agonists as a potential therapeutic approach

Considering that 3,4-DAP is not completely effective for all LEMS patients due to dose-limiting side effects, the development of alternative symptomatic treatment options that are as effective or even superior to 3,4-DAP would be greatly beneficial to the LEMS patient population. As 3,4-DAP indirectly increases the calcium influx by prolonging the action potential duration and therefore increasing the number of calcium channels that open during an action potential, a more direct approach to increase calcium influx might be beneficial. These ideas are explored more thoroughly in Chapters 3 and 4.

# 2.0 CHAPTER ONE: TWO LOW-PROBABILITY COMPONENTS OF TRANSMITTER RELEASE AT THE ACTIVE ZONES OF MAMMALIAN NMJS

## 2.1 INTRODUCTION

Although the mammalian NMJ is a reliable synapse, the way this reliability is achieved is not well understood. Even during bursts of high-frequency stimuli, the presynaptic terminal of the NMJ easily releases enough neurotransmitter to bring the postsynaptic cell to threshold (Wood and Slater, 2001). In order to further understand how this synapse can function in such a manner, it is necessary to understand how the individual components that make up the terminal function. Unfortunately, the mammalian NMJ is a difficult preparation to manipulate experimentally, so studies at the level of the individual release sites, or active zones, have been lacking. The exception to this has been studies on the ultrastructure of the mouse NMJ active zones using freeze-fracture electron microscopy (EM) (Ellisman et al., 1976; Fukunaga et al., 1983) and 3-D reconstructions of the active zone using EM tomography (Nagwaney et al., 2009). These studies have found that the mouse NMJ active zones are punctate and have two double rows of intramembranous particles on either side of a single row of two to three vesicles. Further, studies have used an antibody to the presynaptic active zone protein bassoon to identify and count active zones at the light microscope level (Nishimune et al., 2004; Ruiz et al., 2011; Chen et al., 2012). The authors of these studies concluded that there are 500-1000 active zones per mouse

neuromuscular synapse (depending on age and muscle type) and that active zones are spaced regularly at about 500 nm from one another (Nishimune et al., 2004; Ruiz et al., 2011; Chen et al., 2012). Other than ultrastructural studies, the studies on the mouse NMJ that specifically focus on active zone properties have by necessity been indirect. For example, evidence found using a binomial analysis to estimate the number of release sites and the probability of release ($P_r$) per release site suggests there are a small number of release sites that have a high average $P_r$ (Wang et al., 2010).

A similar preparation that has a longer history of study and is more amenable to experimental manipulations is the frog NMJ. Like the mammalian NMJ, the frog NMJ has hundreds of active zones and very reliably brings the postsynaptic cell to threshold, even during periods of high-frequency activity. Importantly, multiple studies have been performed at the frog NMJ to determine some key sub-active zone parameters. Previous reports have estimated that the number of calcium channels per active zone is relatively low, such that there is a near 1:1 channel to vesicle ratio (Shahrezaei et al., 2006; Luo et al., 2011). Additionally, the probability that any one channel opens in response to a presynaptic action potential has been estimated to be quite low (~0.2). Even when a channel does open, the probability that a nearby vesicle will be released is likely very low (~0.05; (Luo et al., 2011; Luo et al., 2015)). Based on this information on sub-active zone structure-function relationships, as well as decades of research on the physiology and ultrastructure of the frog NMJ, our lab recently built an MCell computer model of the frog NMJ active zone that closely recapitulates multiple physiological parameters observed at this synapse, such as the average $P_r$ per active zone, synaptic latency, and the non-linear relationship between calcium and transmitter release (Dittrich et al., 2013). From this model as well as experimental results, it was estimated that for most release events, a majority of

the calcium ions contributing to release come from a single nearby channel, with a small percentage of the ions coming from neighboring channels (Luo et al., 2015). The model was then improved so that it also matches the short-term plasticity characteristics at the frog NMJ (Ma et al., 2015).

Because many of the experiments looking at individual active zone properties at the frog NMJ are not as feasible in the less tractable mouse NMJ, we sought to use the frog NMJ active zone model to help inform us about the structure-function relationships at the mouse NMJ active zones. Specifically, we initially wondered whether a simple rearrangement of the frog NMJ active zone model into a mouse NMJ active zone configuration would lead to a recapitulation of the physiological characteristics we can observe at the mouse NMJ. If the model could closely match the experimental constraints, it could help us predict those parameters that are not easily measured experimentally. We first made multiple physiological measurements, such as quantal content, $P_r$ per active zone, and short-term plasticity characteristics, and combined these data with published data on the calcium release relationship (molecular cooperativity) and synaptic latency at the mouse NMJ in order to have parameters that our model must match to be considered viable. Here, we found the mouse NMJ has a low average $P_r$ per active zone, and it very consistently has little short-term facilitation or depression. We also estimated the calcium channel-release site cooperativity (or the average number of channels that contribute to the release of single vesicle) in order to have an additional parameter for our model to match to confirm its viability. We found that there is a linear or nearly linear relationship between the number of channels and release, which means that one or very few channels normally contribute to the release of a vesicle (similar to results determined at the frog NMJ). Having these constraints in place, we rearranged our frog NMJ active zone model into the mouse NMJ active

zone organization and found that our mouse NMJ active zone model closely matched all of our experimental parameters. Our results suggest that the structure of active zones, especially the number and organization of calcium channels relative to docked vesicles, has a major influence on the overall function of the synapse.

## 2.2 METHODS

### 2.2.1 Intracellular recordings at mouse NMJs

Mice were killed by $CO_2$ inhalation followed by thoracotomy in accordance with procedures approved by the University of Pittsburgh IACUC, and intracellular recordings of transmitter release were made in the mouse epitrochleoanconeus (ETA) *ex vivo* nerve–muscle preparation as previously described (Tarr et al., 2013b). The extracellular saline contained 150 mM NaCl, 5 mM KCl, 11 mM dextrose, 10 mM Hepes, 1 mM $MgCl_2$ and 2 mM $CaCl_2$ (pH 7.3–7.4). In some experiments, the 10 mM HEPES was substituted with 10 mM BES buffer. The nerve was stimulated with a suction electrode, and muscle contractions were blocked by exposure to 1 μM μ-conotoxin GIIIB (Alomone Labs Ltd, Jerusalem, Israel), a peptide toxin that specifically blocks sodium channels muscle fibers (Hong and Chang, 1989). Microelectrode recordings were performed using ~40–60 MΩ borosilicate electrodes filled with 3M potassium acetate. For the experiments with ω-agatoxin, recordings were made in the continued presences of the toxin. Spontaneous miniature synaptic events [miniature endplate potentials (mEPPs)] were collected for 1–2 min in each muscle fiber, and then 10–20 nerve-evoked synaptic events [endplate

potentials (EPPs)] were collected with an inter-stimulus interval of 5 s. The traces were corrected for non-linear summation using the following equation:

$$\bar{v}' = \bar{v}/(1 - \frac{f\bar{v}}{|E|}) \qquad \text{Eqn.1}$$

where $\bar{v}'$ is the EPP amplitude if the individual quanta summed linearly, $\bar{v}$ is the measured mean EPP amplitude, $f$ is a constant that is dependent on the duration of transmitter action relative to the membrane time constant (0.8 gives a good fit for the mouse muscle), and $E$ is the difference between the measured resting potential of the muscle fiber and the reversal potential of the receptors being activated by neurotransmitter (acetylcholine receptors, which can be considered to have a reversal potential of 0 mV) (McLachlan and Martin, 1981). To calculate quantal content, the peak of the average corrected EPP waveform was divided by the peak of the average mEPP waveform recorded from each NMJ. This ratio calculates the average number of quanta that are released following each presynaptic action potential. To evaluate effects on short-term synaptic plasticity, either a pair of EPPs or a train of 10 EPPs with varying interstimulus intervals (10-100 Hz) was collected. Data were collected using an Axoclamp 900A and digitized at 10 kHz for subsequent analysis using pClamp 10 software.

### 2.2.2 Bassoon immunohistochemistry

The ETA *ex vivo* nerve-muscle preparation was dissected and placed in an extracellular saline (detailed in the previous section) containing ~3 μg/mL Alexa 594-conjugated α-bungarotoxin (BTX) for 30 min to label the postsynaptic acetylcholine receptors. The tissue was then washed and fixed in 2% (w/v) paraformaldehyde in phosphate-buffered saline (PBS) for 20 minutes at room temperature. The tissue was then permeabilized and blocked in a PBS solution containing

2% (w/v) bovine serum albumin (BSA), 2% (v/v) rabbit serum and 0.5% Triton-X 100. After block, the tissue was incubated in the primary antibody (1:600 dilution of SAP7F407 clone of mouse anti-bassoon IgG subtype 2a; Assay Designs #VAM-PS003) for 12-16 hours on a rocker platform at room temperature. Following washout of the primary antibody (three 15-minute washes), the tissue was incubated in the secondary antibody (1:1000 dilution of Alexa-488 goat anti-mouse IgG 2a; Molecular Probes #A21131) for 4-6 hours on a rocker platform at room temperature. Finally, after 3 15-minute washes, the tissue was mounted on glass slides under #1.5 cover glass using Prolong Gold mounting media (Life Technologies).

### 2.2.3 Confocal imaging

Mounted tissue was imaged on a Leica TCS SP5 spectral confocal microscope. Alexa-488 bassoon antibody staining was imaged using 488 nm laser excitation and photon collection between 492-560 nm. Alexa 594 labeled α-bungarotoxin staining was imaged using 564nm laser excitation and photon collection between 568-750 nm. Confocal scanning occurred using the resonance scanner at 8000 Hz and images were collected using line-scan averaging after 96 sweeps. Regions of interest were scanned using image stacks at 0.25 µm intervals sufficient to include the entire NMJ (typically 5-10 optical slices). Brightest projection images were made from these stacks and photon collections from both wavelengths were superimposed in pseudocolor to generate composite images representing α-bungarotoxin staining for acetylcholine receptors and bassoon immunoreactivity. The number of bassoon puncta within each NMJ was counted by hand within α-bungarotoxin-stained regions of the image.

### 2.2.4 Presynaptic calcium imaging

Imaging of calcium influx into the presynaptic terminal of the mouse NMJ was performed as previously described in the frog NMJ (Wachman et al., 2004; Luo et al., 2011). Briefly, the ETA nerve-muscle preparation was dissected out and placed in a HEPES-buffered extracellular saline (described above). The nerve was drawn into a Vaseline well containing 30 mM fluo-2 leakage-resistant (TEFLabs) calcium-sensitive dye dissolved in distilled water, and the nerve was subsequently cut close to the muscle while in the dye. The dye was loaded for 4-5 hours at room temperature, and then another 1-2 hours at 4 °C. The preparation was then washed and bathed in BES-buffered saline (as described above) and mounted in a 35 mm dish with Sylgard. The nerve was stimulated with a suction electrode and muscle twitch was blocked by 1 μM μ-conotoxin GIIIB. Postsynaptic acetylcholine receptors were labeled with 2 μg/mL Alexa 594-conjugated α-bungarotoxin (BTX), which was also used to focus on terminal and evaluate the possibility of z-axis drift. Following addition of ω-agatoxin, images were collected in the continued presence of the toxin. Images were collected with a 1 ms illumination time that occurred 1.5 ms following the initiation of acquisition (with and without stimulation of the nerve). Images were collected on a liquid nitrogen-cooled, deep electron well CCD camera (LN 1300B, Princeton Instruments) with a pixel size of 200 nm. Twenty Hz trains of 10 stimuli were collected without nerve stimulation and then with nerve stimulation. To determine the action potential-induced increase in presynaptic calcium influx, the sum of each of these 10 photon collections in each train was subtracted from background (un-stimulated) images to yield a subtracted ΔF/F image. Images were aligned and analyzed in ImageJ. Alignment was performed using the TurboReg plugin for ImageJ (Thevenaz et al., 1998). Following alignment, a mask of each terminal was manually drawn using the BTX stain as a guide. The total intensity within this mask was then determined

in both the background and stimulated images to determine the stimulation-induced change in fluorescence signal before and after ω-agatoxin.

### 2.2.5 Statistical analysis

Statistical analysis was performed using either GraphPad Prism Version 5.0 (GraphPad Software, Inc., La Jolla, CA, USA) or Origin 7 (OriginLab Corp., Northampton, MA, USA). Data are presented as the mean ± s.e.m. unless otherwise noted. The significance level was set at $P < 0.05$ for all statistical tests.

## 2.3 RESULTS

### 2.3.1 Average $P_r$ per active zone

We first wanted to determine whether the average probability of release (Pr) per active zone was low in our ETA nerve-muscle preparation. In order to do this, we measured both the quantal content and the number of active zones. Since the size of the active zone, and therefore the number of active zones, increases with age (Chen et al., 2012), we restricted the age window of the mice to 4-6 weeks of age for both the quantal content and the bassoon immunohistochemistry experiments. Using classical intracellular microelectrode recordings, we found a quantal content of 75.15 ± 3.79 (n = 23). For the determination of the number of active zones, we used the immunohistochemically-tagged active zone protein bassoon as a marker for active zones (Nishimune et al., 2004). For each terminal (see Figure 2A for a sample terminal image), the

number of bassoon spots was manually counted, giving an average number of active zones per terminal of 686.0 ± 72.51 (n = 8). If we assume functional homogeneity across active zones, we can make a rough estimate of the average Pr per active zone. Using the quantal content and active zone data obtained, we estimated the average Pr per active zone to be ~0.10-0.12.

### 2.3.2 Short-term plasticity characteristics

After determining the average release characteristics for a single stimulus in our ETA nerve-muscle preparation, we sought to determine the average short-term plasticity characteristics using both paired-pulse and 10-stimuli high-frequency train protocols with varying interstimulus intervals. Figure 3A,B shows a comparison of the paired-pulse ratio (PPR) for each of the 10 interstimulus intervals tested. There was very little variability in PPR short-term plasticity characteristics at the mouse NMJ, regardless of the frequency of the paired-pulse stimulus. Similarly, there was very little variability in short-term plasticity characteristics during trains of 10 stimuli at varying frequencies (Figure 3C). Trains of 10 stimuli at 10, 20, 50 and 100Hz were remarkably similar to one another, with each frequency showing very little or no facilitation during the first few pulses and similar depression to ~65-70% of the first EPP by the 10th stimulus in the train (Figure 3C). Therefore, unlike the frog NMJ, which shows wide variability in short-term plasticity characteristics among individual NMJs and between different stimulus frequencies (Ma et al., 2015), the mouse NMJ shows remarkably consistent short-term plasticity characteristics among individual NMJs, regardless of stimulus frequency.

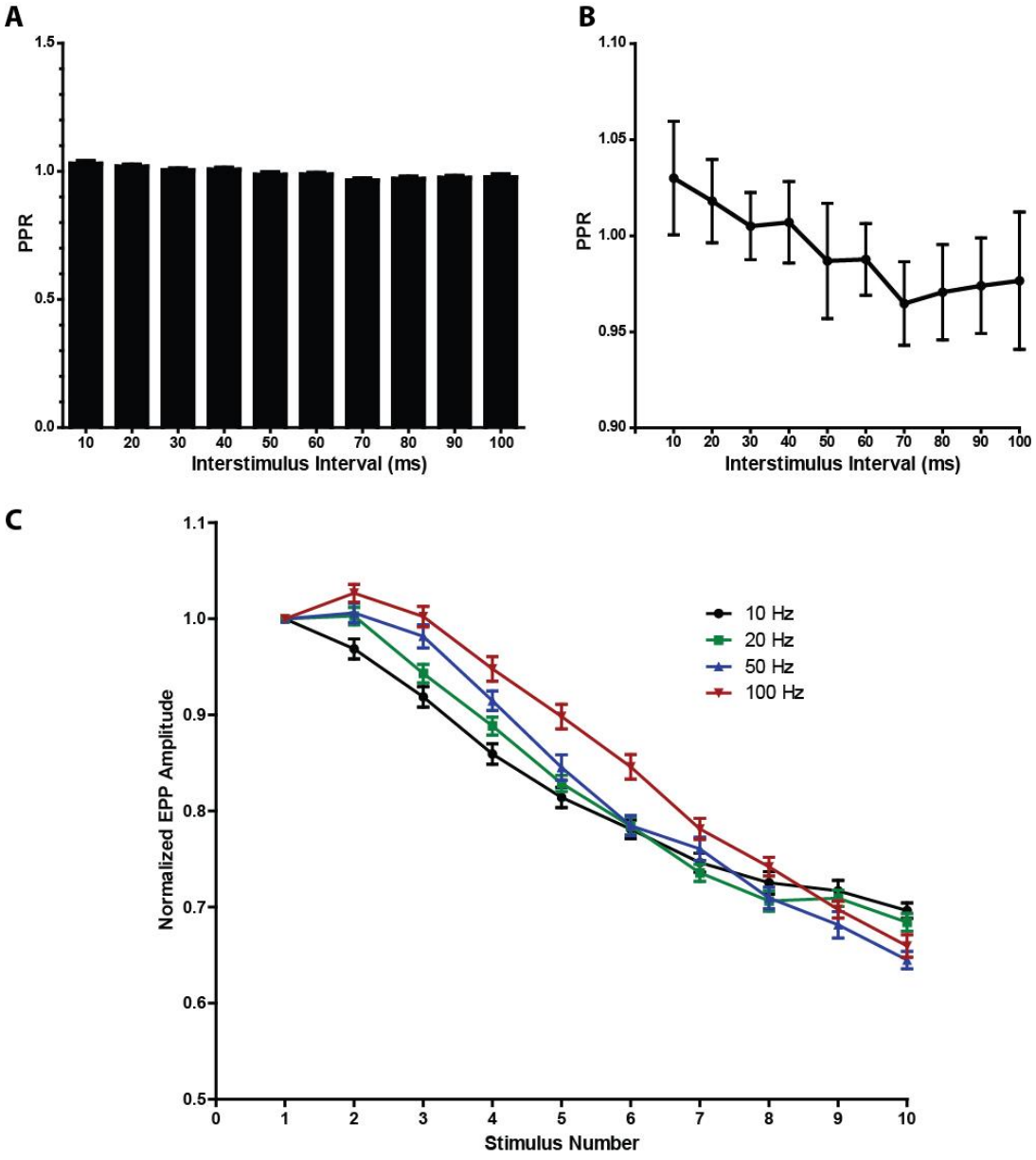


**Figure 3. Short-term plasticity at the mouse NMJ.**

**A, B.** PPR at control mouse NMJ at different interstimulus intervals from 10-100 ms. **C.** Short-term plasticity during trains of 10 stimuli at 4 different frequencies at mouse NMJ all show small little or no facilitation and a small amount of depression.

### 2.3.3 The number of calcium channels contributing to release

To estimate the number of channels that normally contribute to release, we first set out to determine the calcium channel-release site cooperativity by measuring the effect of blocking a particular portion of calcium channels on both neurotransmitter release and calcium influx. Since P/Q-type calcium channels control release at the mouse NMJ, we used ω-agatoxin to specifically block a significant fraction of these channels. If a certain concentration of ω-agatoxin reduces both neurotransmitter release and calcium influx to the same extent (linear relationship), then, on average, one channel on average contributes to the release of a single vesicle. On the other hand, if a certain concentration of agatoxin reduces neurotransmitter release to a much greater extent compared to the reduction in calcium influx (non-linear relationship), then the molecular cooperativity of the sensor for release is reached and many channels on average are contributing to the release of a single vesicle (Eggermann et al., 2012; Tarr et al., 2013a). The difference between these two extremes ($1^{st}$-order and $4^{th}$-order channel-release site relationship) is particularly apparent at concentrations of blocker that reduce neurotransmitter release by 75% or more. We chose 25 nM ω-agatoxin, which reduced quantal content to 0.23 ± 0.02 (n = 15) of control levels (Figure 4A). We then tested this concentration of ω-agatoxin in calcium imaging experiments to determine the percent change in calcium influx at this level of block. Interestingly, the fraction of calcium influx remaining after block in 25 nM ω-agatoxin was 0.19 ± 0.04 (n = 8) of control levels (Figure 4B). If this point is plotted on a log-log plot that contains the lines for 1st, $2^{nd}$-, $3^{rd}$-, and $4^{th}$-order relationships (Figure 4C), our data fall very close to a $1^{st}$-order, or linear, relationship between calcium channels and neurotransmitter release. This linear relationship between the reduction of channels and the reduction of transmitter release suggests that, on average, one or very few channels contribute to the release of a single vesicle.

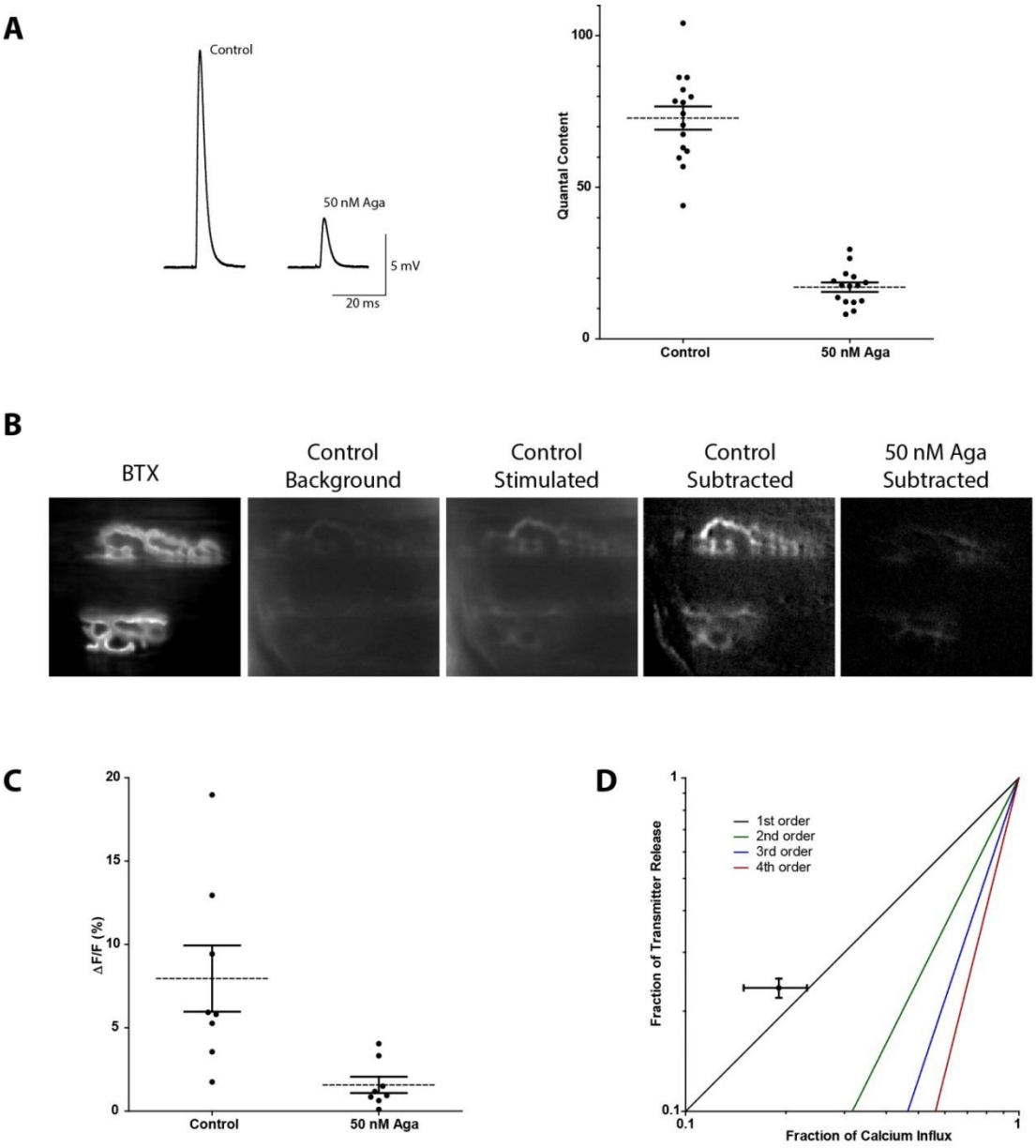


**Figure 4. A small number of calcium channels contribute to vesicle release.**

**A.** Sample EPP traces and plot of quantal content show the decrease following 50 nM ω-agatoxin (Aga) at mouse NMJ. **B.** Sample images show postsynaptic BTX stain (left) along with sample images of the same NMJs taken at 20 Hz without (Control Background) and with (Control Stimulated) nerve stimulation in a control NMJ. Subtracted images on far right show the terminal calcium signal after subtracting the Background from the Stimulated images before (Control Subtracted) and after (50 nM Aga Subtracted). **C.** Imaging data plotted to show the average decrease following 50 nM Aga. **D.** Log-log plot showing the approximate 1$^{st}$-order relationship between calcium influx and transmitter release at the mouse NMJ.

To support our data using ω-agatoxin, we also performed paired-pulse experiments before and after the addition of the ionic blockers cadmium or manganese, which has been used previously to estimate the numbers of channels contributing to the release of a vesicle (Scimemi and Diamond, 2012). Cadmium slowly permeates calcium channels (compared to calcium), such that on the time scale of a single action potential, cadmium is essentially a channel blocker (Lansman et al., 1986; Scimemi and Diamond, 2012). Manganese also slowly permeates the calcium channel relative to calcium, but not as slowly as cadmium; therefore, manganese produces a fast "flicker" block of the calcium channel (Lansman et al., 1986; Scimemi and Diamond, 2012) and results in less calcium coming in through open channels. Hence, application of manganese is similar to lowering extracellular calcium, whereas cadmium approaches an "all-or-none" channel block. If only a single channel contributes to the release of a vesicle, then only manganese should lead to an increase in PPR. If many channels contribute to the release of a vesicle, then both cadmium and manganese should increase PPR because both ions will simply reduce the amount of calcium influx and therefore the concentration of calcium around a vesicle (assuming cadmium is used at less than saturating concentrations so that not all open channels are blocked). We chose a concentration of both cadmium (25 μM) and manganese (500 μM) that reduced quantal content by >50% in order to have the best chance to increase the PPR. 25 μM cadmium reduced the quantal content from 82.73 ± 3.02 to 18.81 ± 1.21 (n = 17), which is a decrease of ~77%. However, there was no significant change in the PPR, which was 1.09 ± 0.008 before and 1.10 ± 0.02 (n = 17; p = 0.34, Student's paired *t* test) after 25 μM cadmium (Figure 5A). These findings agree with the results obtained with ω-agatoxin above and suggest that one or very few channels contribute to release. When the stimulation frequency of 50 Hz was

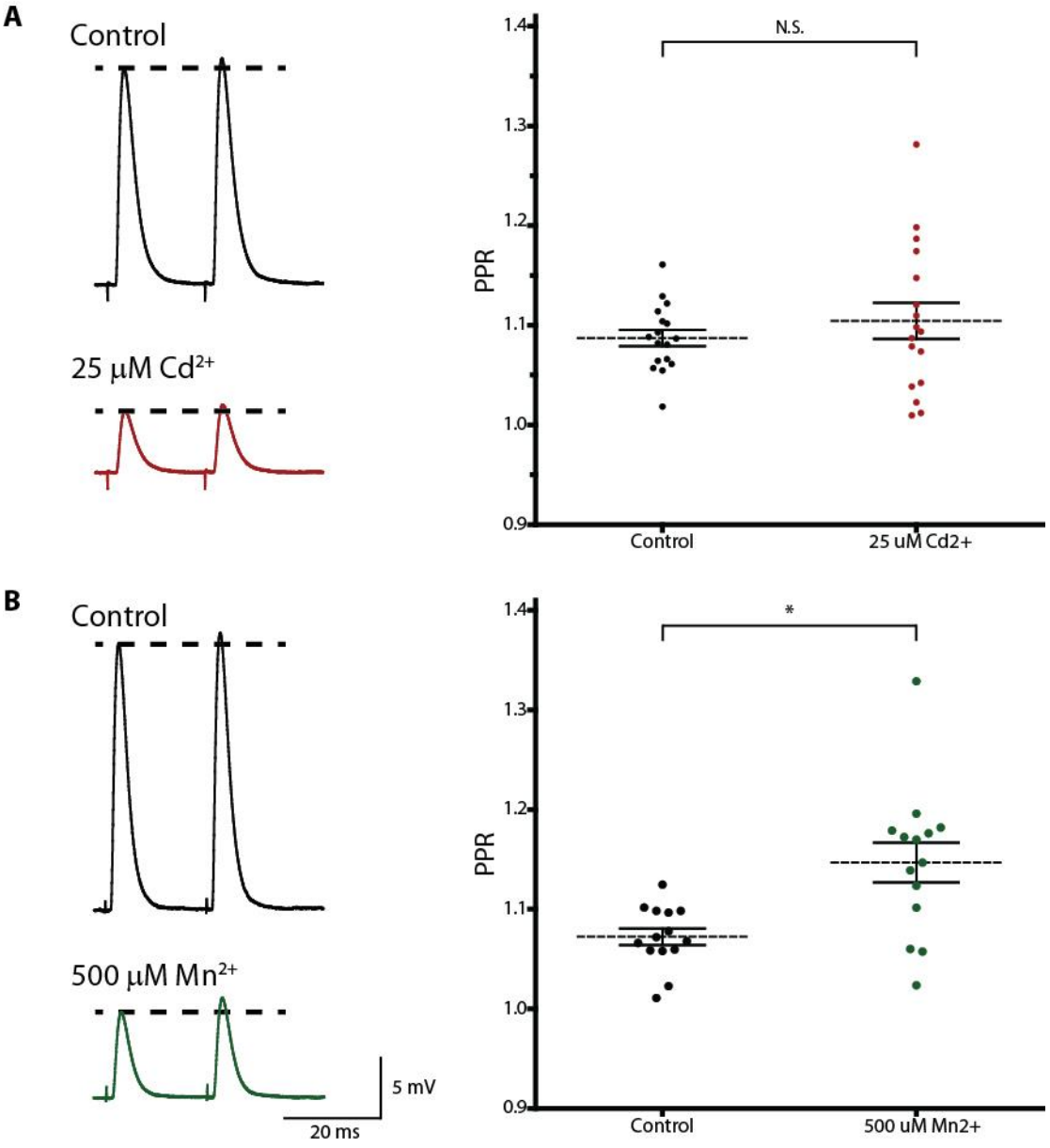


**Figure 5. Cadmium does not increase paired-pulse facilitation at the mouse NMJ.**

**A.** Sample traces (left) and plot of average data (right) before (black) and after (red) 25 μM cadmium showing that cadmium does not significantly change PPR at the mouse NMJ. **B.** Sample traces and plot of average data before (black) and after (green) 500 μM manganese shows that manganese does significantly increase PPR at the mouse NMJ, although the overall change is small.

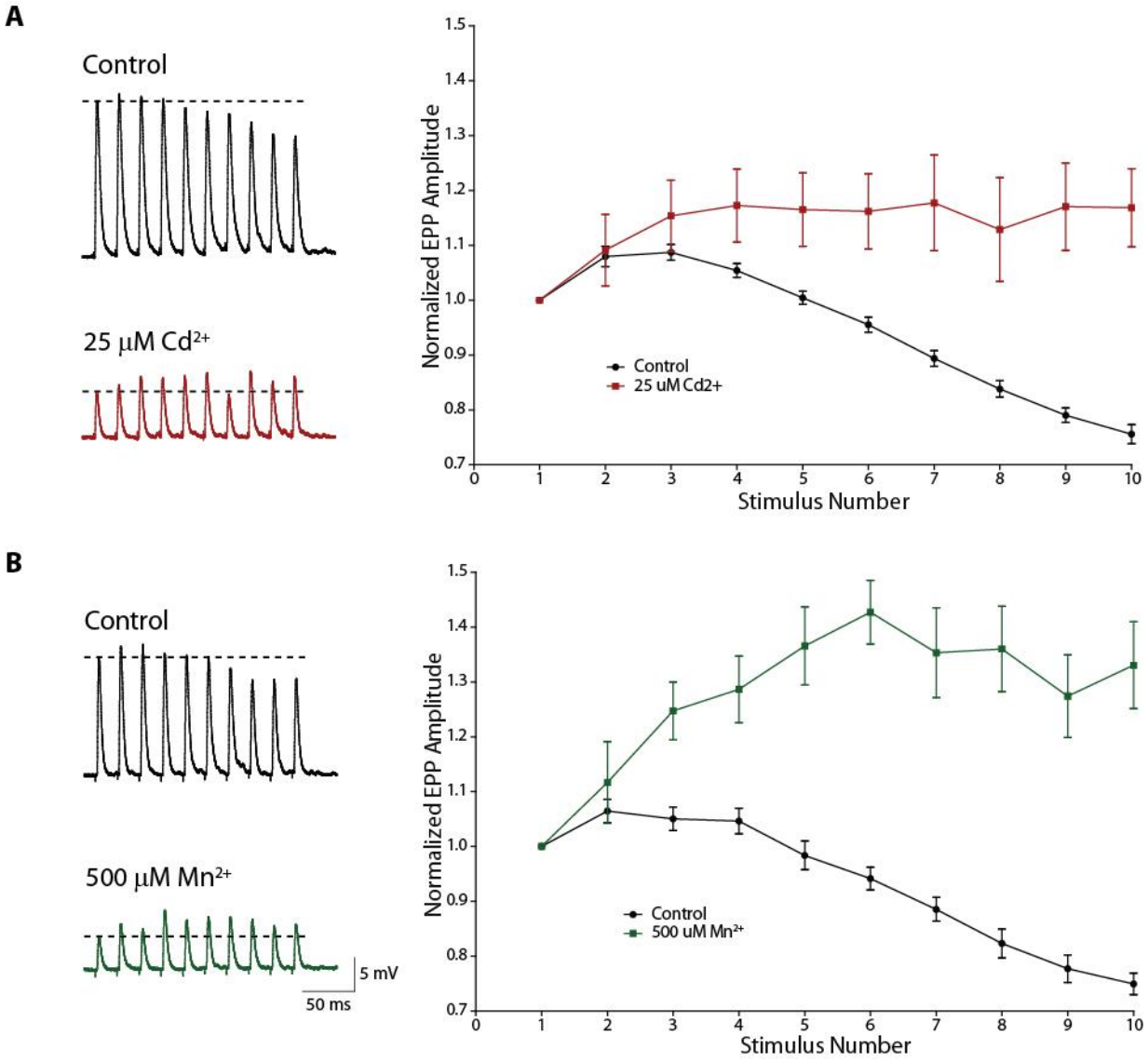


**Figure 6. Cadmium and manganese increase facilitation during high-frequency trains.**

**A.** Sample traces (left) and plot of average data (right) for trains of 10 stimuli at 50 Hz show that cadmium can increase facilitation during longer trains of activity. **B.** Similarly, manganese also causes a greater facilitation during longer trains of activity.

extended to a train of 10 stimuli, 25 μM cadmium did significantly increase facilitation at the 10th stimulus (normalized to the 1st stimulus in the train) from 0.76 ± 0.02 to 1.17 ± 0.07 (n = 17; $p < 0.05$, Student's paired *t* test; Figure 6A). 500 μM manganese reduced quantal content by ~68%, from 71.19 ± 5.48 to 21.80 ± 1.00 (n = 14). In contrast to cadmium, 500 μM manganese did significantly increase the PPR, which increased from 1.07 ± 0.008 to 1.15 ± 0.02 (n = 14; $p < 0.05$, Student's paired *t* test; Figure 5B). The increase in facilitation due to 500 μM manganese was even more apparent during a train of 10 stimuli at 50 Hz, with manganese significantly increasing facilitation at the 10th stimulus (normalized to the first stimulus in the train) from 0.75 ± 0.02 to 1.33 ± 0.08 (n = 14; $p < 0.05$, Student's paired *t* test; Figure 6B).

## 2.4 DISCUSSION

Here we present data that suggest the mouse NMJ is a reliable synapse that is built with many unreliable single-vesicle release sites, a structural unit similar to what has previously been called the "synaptosecretosome" or "secretosome" (O'Connor et al., 1993; Bennett, 1996; Bennett et al., 1997). We believe that the mouse NMJ active zone configuration is advantageous not only because of its reliability, but also because it allows for a conservation of resources (neurotransmitter-containing vesicles), such that reliability is maintained even in cases of high-frequency activity.

### 2.4.1 The active zones of the mouse NMJ have a low $P_r$ on average

We made measurements of the quantal content and the number of active zones to estimate the average Pr per active zone at the mouse NMJ. Although not a novel experiment, we wanted to determine this property at our nerve-muscle preparation, the ETA of the mouse. We found an average Pr per active zone of ~0.10-0.12, and if we assume 2 vesicles per active zone (Nagwaney et al., 2009), then the average probability of release per vesicle is only ~0.05. Therefore, like the frog NMJ, the mouse NMJ has a low probability of release per vesicle on average. Although the NMJ as a whole is a reliable, strong synapse, having a low probability of release per single vesicle makes sense for the function of the NMJ. With hundreds to thousands of docked vesicles, there is overall reliability in spite of the unreliability of the individual components. Additionally, there is continued reliability during physiological bursts of activity because of the conservation of resources. Having fewer release sites, and therefore fewer vesicles, with a higher probability of release would in theory lead to more depression and the possibility of failures during physiological high-frequency bursts of action potentials. It is important to note that functional homogeneity across all active zones is an assumption made mostly because of experimental limitations at the NMJ. At this synapse, experimental tools have not yet been developed that allow sub-active zone mapping of the spatial distribution of single vesicle transmitter release events along the length of the NMJ. In the absence of such direct study, other indirect or lower resolution methods have been used to examine details of transmitter release from these synapses (see General Discussion for more detail).

One report using a binomial analysis of transmitter release estimated that there are few release sites (<100) that have a high probability of release (~0.8-1.0; (Wang et al., 2010)). These results are hard to reconcile with the relatively small amount of depression during trains of high-

frequency activity at the mouse NMJ (Figure 3), unless the mouse NMJ has unusually fast vesicle refilling times. Additionally, a binomial analysis cannot specifically say what the "release sites" actually mean. Nonetheless, it remains unknown why a disconnect exists between findings such as ours and those found using binomial analysis.

### 2.4.2 The mouse NMJ lacks significant short-term plasticity

As mentioned above, the mouse NMJ shows neither significant short-term facilitation nor significant short-term depression during trains of high-frequency stimuli (Figure 3). Furthermore, this lack of short-term plasticity is evident regardless of the stimulation frequency, so much so that there is no appreciable difference across the range of frequencies from 10 to 100 Hz. The lack of short-term depression is not all that surprising given the average low probability of release per vesicle, although the low probability of release per vesicle contradicts the predictions based on the results using binomial analysis (Wang et al., 2010). Short-term plasticity is generally a balance between the probability of release and a depletion of readily releasable, or docked, vesicles (Zucker and Regehr, 2002). Therefore, since we hypothesize there are many docked vesicles with a low probability of release, we would not expect to observe significant depression during high-frequency trains of action potentials. Instead, a low probability of release and negligible depletion of docked vesicles should lead to see significant facilitation. Some other mechanism appears to restrict the amount of facilitation that can occur at the mouse NMJ.

In collaboration with Markus Dittrich and colleagues at the Pittsburgh Supercomputing Center, we have explored the properties of the mouse NMJ using an MCell model of the mouse NMJ active zone (Ma, 2014). This MCell model of the mouse NMJ active zone was recently built by rearranging our previously validated MCell model of the frog NMJ into the active zone

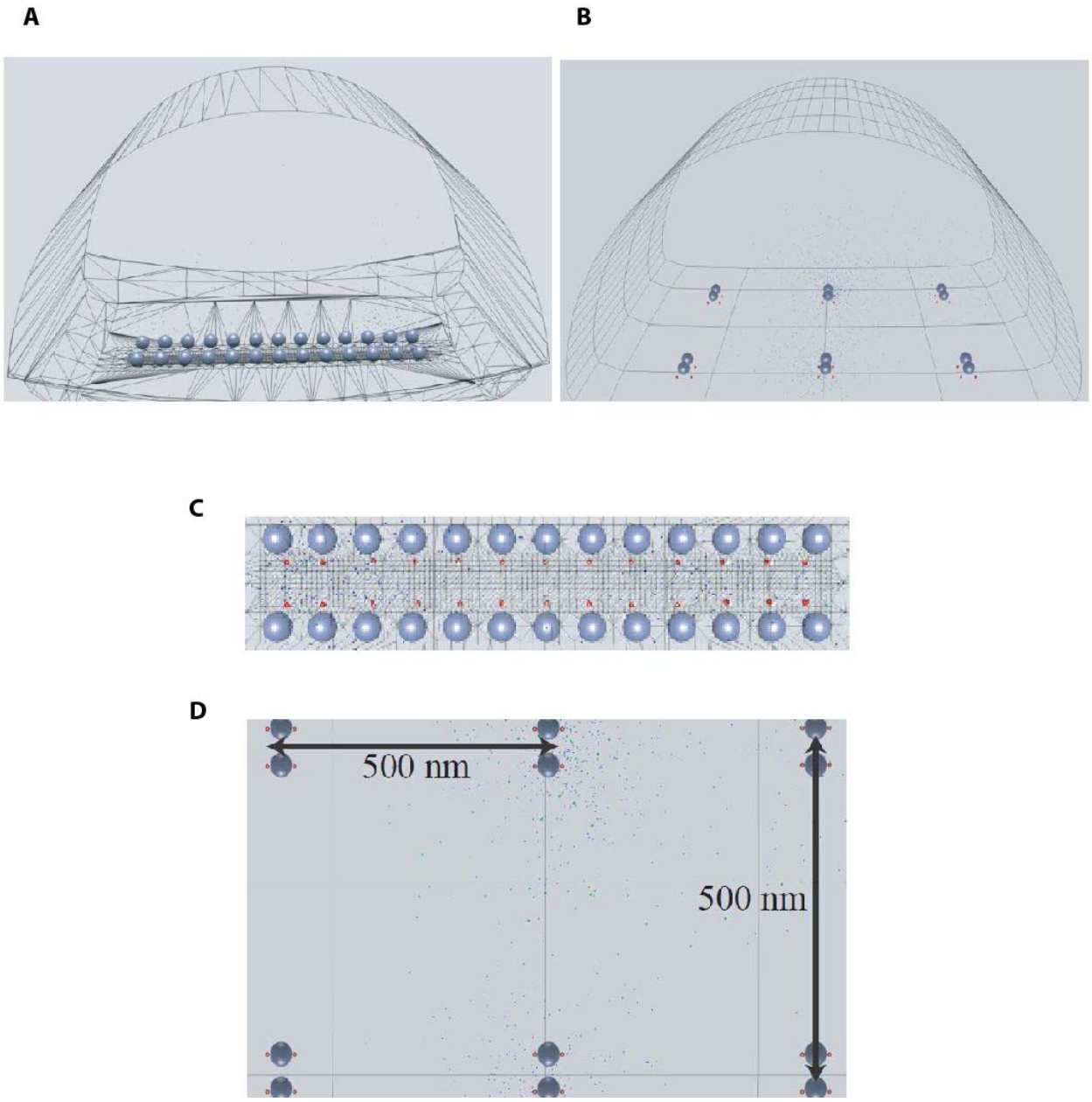


**Figure 7. Geometry of mouse and frog MCell models.**

Whole terminal view of (**A**) frog containing one active zone and (**B**) mouse NMJ model containing 6 active zones. Top view (**C**) of the active zone at frog NMJ model. (**D**) Top view of the active zone arrangement in mouse NMJ model (adapted from Ma, 2014).

organization of the mouse NMJ. We have shown that by simply rearranging the ultrastructure of the frog NMJ into the ultrastructure of the mouse NMJ (Figure 7), without any changes to other parameters, we can switch the functional properties of the frog NMJ into the functional properties of the mouse NMJ, especially with respect to short-term plasticity characteristics (Ma, 2014). The frog NMJ shows significant facilitation during high-frequency trains of stimuli, but the rearrangement into the active zone structure of the mouse NMJ changes the output of the model such that it closely matches the experimentally measured probability of release and lack of short-term plasticity at the mouse NMJ (Figure 8). Important model constraints, such as the $4^{th}$-order molecular cooperativity and release latency, are not altered following this active zone reconfiguration. Since this mouse model so closely matches the physiological characteristics of the mouse NMJ, we used this model to help inform our understanding of short-term plasticity at the mouse NMJ. Specifically, we used the model to help explain the lack of short-term facilitation at the mouse NMJ given the low probability of release per vesicle. What we determined from this analysis is that the structure of the mouse active zone (small, punctate active zones with only ~2 vesicles) is the most influential factor behind the lack of facilitation. Although there are 4 rows of intramembranous particles for each row of vesicles in the mouse NMJ (the frog has 2 rows of intramembranous particles for each row of vesicles), which suggests that the calcium channel-to-vesicle ratio is likely higher in the mouse than in the frog, the calcium channels are spatially more sparse in the mouse than in the frog. With fewer calcium channels in the active zone, and a predicted low probability of calcium channel opening during an action potential, it is less likely that vesicles in the mouse NMJ (compared to vesicles in the frog NMJ) would experience the opening of nearby calcium channels on consecutive stimuli. In other words, it is less likely that there will be a residual calcium effect from a previous stimulus

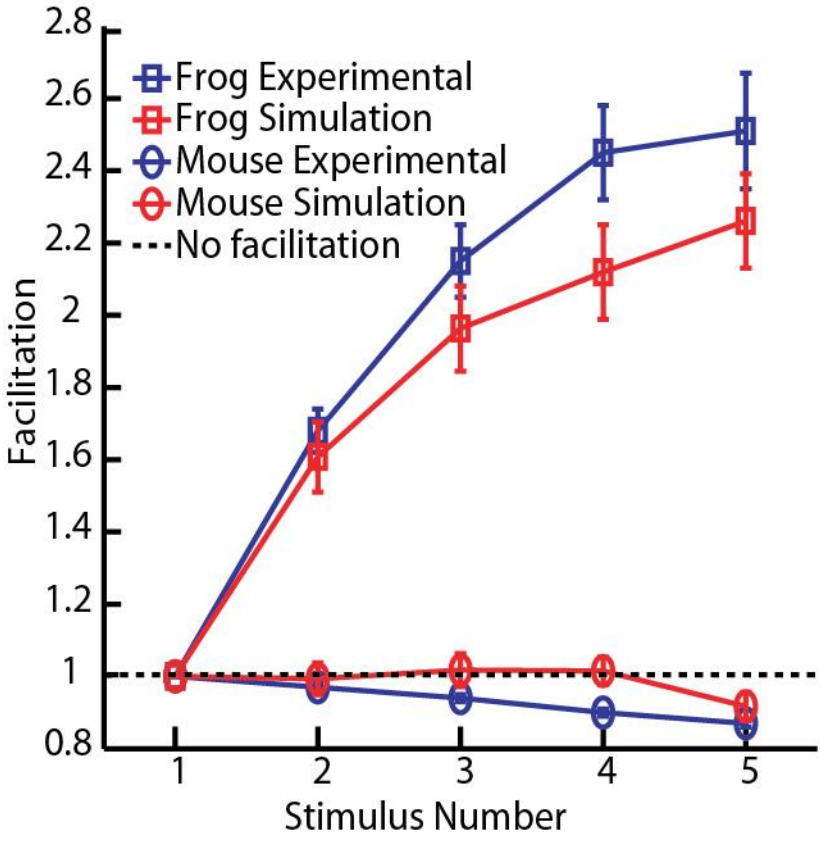


**Figure 8. Short-term plasticity at frog and mouse NMJs.**

Facilitation during a five-pulse train at 100 Hz at the frog NMJ (squares) and mouse NMJ (circles) as seen in both simulation (red) and experimental data (blue) (adapted from Ma, 2014).

in the mouse NMJ. This hypothesis was supported in our MCell model, which showed that the effect of residual calcium in a train of stimuli was much lower in the mouse compared to the frog, and therefore, there was much less facilitation in the mouse (Figure 9). Interestingly, both the mouse and frog NMJs show nearly identical short-term plasticity characteristics in the absence of residual calcium effects (Figure 9). In other words, if you did not allow calcium ions from one stimulus in the train to contribute to release in subsequent stimuli, both the frog and the mouse NMJ models showed nearly identical short-term plasticity characteristics. Furthermore, if you take the frog active zone model and continually remove channels, while not changing the vesicle number, you can keep lowering facilitation until you eventually reach the short-term plasticity level of the mouse (Figure 10). Therefore, it seems that even with a low probability of release per vesicle, short-term facilitation can be significantly restricted if the organization of the active zone prevents significant overlap of calcium channel domains.

One issue with our mouse NMJ active zone model is that many assumptions are made when we rearrange the frog active zone into the mouse active zone. First, we assume there is no significant difference in the relative number of calcium channels and their properties between the frog and mouse. We have experimental data suggesting a 1:1 relationship between the number of calcium channels and the number of vesicles in the frog (Luo et al., 2011), but we have no such data for the mouse. Since the number of rows of intramembranous particles relative to rows of vesicles in the mouse is twice the number compared to frog (Harlow et al., 2001; Nagwaney et al., 2009), and if calcium channels are arranged similarly in mouse and frog, then there would be two calcium channels adjacent to each vesicle in the mouse (compared to one channel per vesicle in the frog model). Additionally, we assume the calcium channels in the mouse have same low probability of opening during an action potential as the calcium channels in the frog do (~0.2).

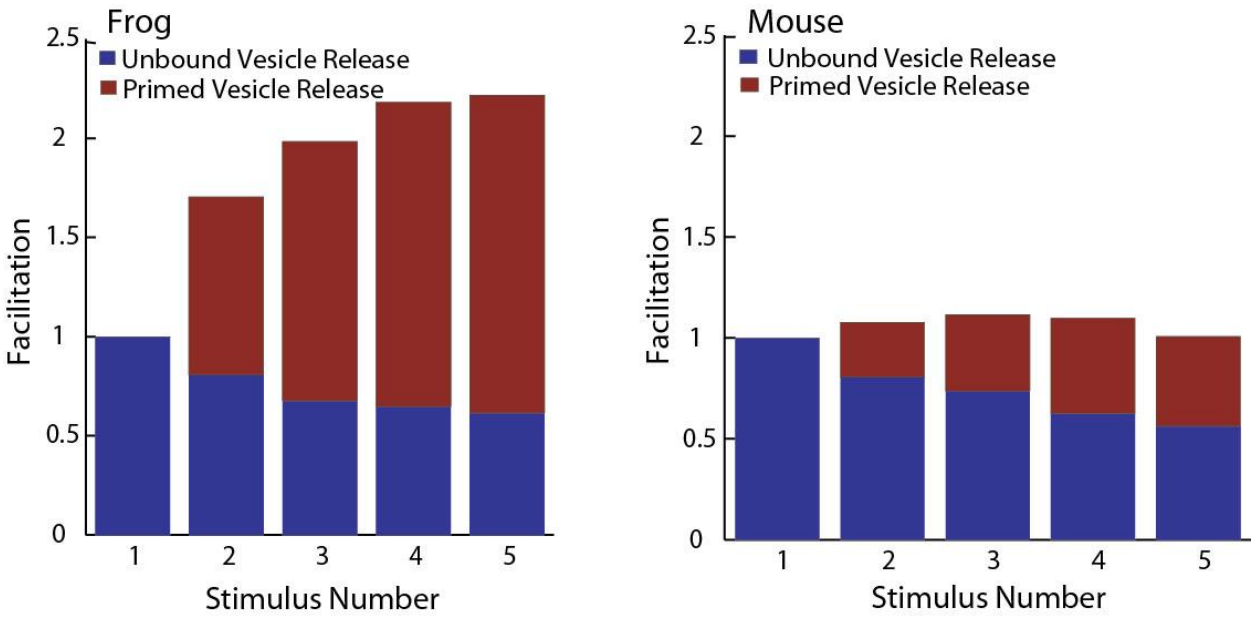


**Figure 9. Facilitation decomposition in frog and mouse models.**

Fraction of contribution from primed (red) and unbound (blue) vesicles at frog and mouse NMJ. Primed vesicles are vesicles that have a bound calcium ion from a previous stimulus. Mouse and frog show similar short-term plasticity if primed vesicle release is removed from the equation (adapted from Ma, 2014).

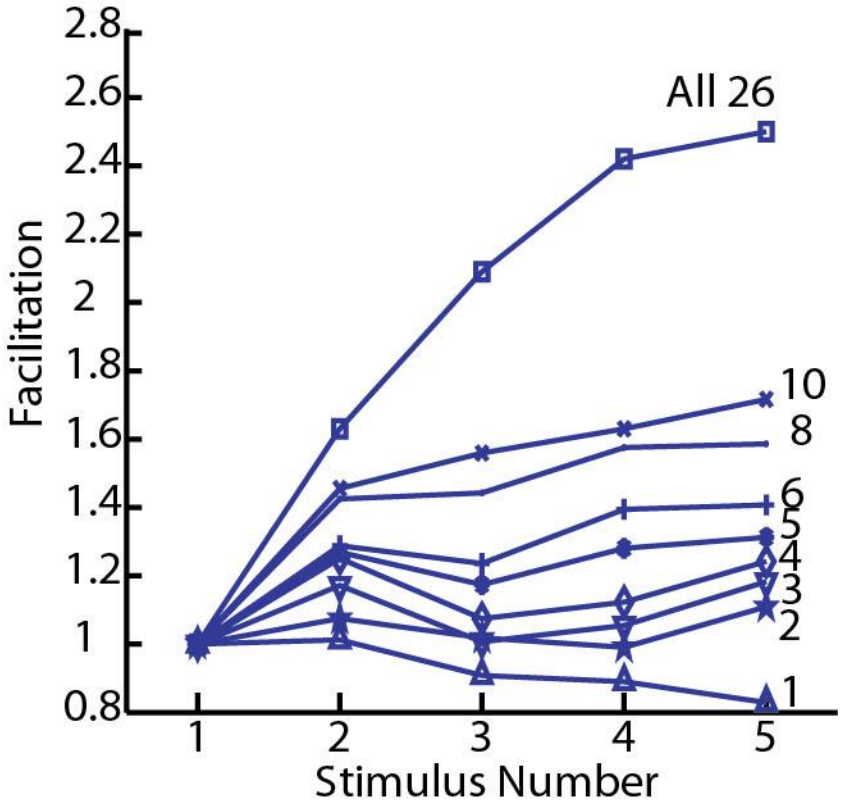


**Figure 10. Analysis of short-term plasticity in frog model.**

**A.** Facilitation of frog NMJ active zone with different number of available VGCCs. Calcium channels were randomly removed from the frog active zone model and the effect on short-term plasticity was observed. Number besides each curve indicates number of VGCCs remaining (out of the initial 26) (adapted from Ma, 2014).

Finally, we also assume there is no difference in the single channel function (e.g. conductance, mean open time, etc.) between the P/Q-type calcium channels in the mouse NMJ active zone and the N-type calcium channels in the frog NMJ active zone. Despite these assumptions, we feel confident that our mouse NMJ active zone model is a good estimation of the actual situation. For instance, if the number of calcium channels and/or their probability of opening during an action potential were significantly higher than what we have in our mouse model, then certain parameters such as the probability of release and the amount of short-term depression would likely be much higher. Despite the uncertainties discussed above, we believe it is particularly striking that the simple rearrangement of active zone structure can lead to very different functional properties, suggesting that active zone organization plays a vital role in the individual active zone and the synapse as a whole.

### 2.4.3 A small number of channels contributes to the release of a vesicle at the mouse NMJ

In support of our modeling data, we determined that the number of calcium channels that contribute to the release of an individual vesicle was low, possibly as low as a single channel. Using ω-agatoxin to block a significant portion of presynaptic calcium channels, we found that both neurotransmitter release and calcium influx were blocked to a similar extent (Figure 4). Although we cannot be certain that the relationship between neurotransmitter release and calcium influx is exactly linear, we are confident that this relationship is at least close to linear, which is similar to what is seen in the frog NMJ (Luo et al., 2015). The linear relationship between calcium channels and vesicles is further supported in our paired-pulse experiments in which cadmium did not cause a significant increase in paired-pulse facilitation (Figure 5). Since cadmium has a slow unbinding rate (Chow, 1991), it basically blocks the channel for the

duration of the action potential. Therefore, if only one channel usually contributes to the release of a vesicle, the cadmium block will simply remove that single-vesicle release site and there should be no change in facilitation. This finding matched a previous report that argued for a nearly linear relationship between calcium channels and neurotransmitter release at the CA3-CA1 Schaeffer collateral synapse in the hippocampus (Scimemi and Diamond, 2012). Manganese, on the other hand, has a very fast unbinding rate, so it produces a "flicker block" of the channel and reduces the amount of calcium influx when the channel opens (Lansman et al., 1986), which is similar to reducing extracellular calcium. Manganese is expected to increase facilitation in all cases and acts as a positive control. Interestingly, although manganese did significantly increase paired-pulse facilitation (as expected based on its theoretical mimicking of reducing extracellular calcium (Scimemi and Diamond, 2012)), the increase in facilitation was not great. This is likely due to the organization of the mouse NMJ active zone. Since we hypothesize that there is little overlap in calcium channel domains at the mouse NMJ active zones and that there is a low probability that an active zone will have an open channel on consecutive stimuli (based on the hypothesized small number of channels per active zone and their hypothesized low probability of opening during action potential), manganese cannot greatly increase facilitation in a paired-pulse protocol when residual calcium has little effect. However, the mouse NMJ can be pushed to facilitate in the presence of blockers during longer periods of high-frequency activity when residual calcium can be given more opportunity to elicit an effect (Figure 6). These data, therefore, give credence to some of the assumptions that were made in our mouse NMJ active zone model and give us confidence that model findings are reasonable.

# 3.0 CHAPTER TWO: EVALUATION OF A NOVEL CALCIUM CHANNEL AGONIST FOR THERAPEUTIC POTENTIAL IN LAMBERT–EATON MYASTHENIC SYNDROME

***Preface***

We developed a novel calcium channel agonist that is selective for N- and P/Q-type calcium channels, which are the calcium channels that regulate transmitter release at most synapses. We have shown that this new molecule (GV-58) slows the deactivation of channels, resulting in a large increase in presynaptic calcium entry during activity. GV-58 was developed as a modification of (R)-roscovitine, which was previously shown to be a calcium channel agonist, in addition to its known cyclin-dependent kinase activity. In comparison with the parent molecule, (R)-roscovitine, GV-58 has a ∼20-fold less potent cyclin-dependent kinase antagonist effect, a ∼3- to 4-fold more potent calcium channel agonist effect, and ∼4-fold higher efficacy as a calcium channel agonist. We have further evaluated GV-58 in a passive transfer mouse model of Lambert–Eaton myasthenic syndrome and have shown that weakened Lambert–Eaton myasthenic syndrome-model neuromuscular synapses are significantly strengthened following exposure to GV-58. This new calcium channel agonist has potential as a lead compound in the development of new therapeutic approaches to a variety of disorders that result in neuromuscular weakness.

**The results of this chapter have been published in the *Journal of Neuroscience* in 2013, and the citation for this article is given below. Minor formatting changes and changes to the numbering of figures and tables have been made to preserve consistency with the rest of this dissertation document.**

**Tarr TB, Malick W, Liang M, Valdomir G, Frasso M, Lacomis D, Reddel SW, Garcia-Ocano A, Wipf P, Meriney SD (2013) Evaluation of a novel calcium channel agonist for therapeutic potential in Lambert-Eaton Myasthenic Syndrome. *J. Neurosci.* 33:10559-67**

## 3.1 INTRODUCTION

Lambert–Eaton myasthenic syndrome (LEMS) is an autoimmune disorder of the neuromuscular junction (NMJ) that is characterized by debilitating muscle weakness (Lambert et al., 1956). Although LEMS is often a paraneoplastic syndrome associated with small cell lung cancer, it can also be idiopathic (Titulaer et al., 2011b). This muscle weakness has been shown to be due to an auto-antibody-mediated removal of a fraction of presynaptic P/Q-type ($Ca_v2.1$) calcium channels, which provide the calcium flux that normally triggers transmitter release at the mammalian NMJ (Katz et al., 1996). Despite a LEMS-induced compensatory expression of other calcium channel types, the overall effect is a decrease in the quantal content of transmitter release from the NMJ (Vincent et al., 1989; Smith et al., 1995; Flink and Atchison, 2002). There is no cure for LEMS, and currently there are few symptomatic treatment options available. One of the most common therapeutic approaches is the use of the potassium channel blocker 3,4-diaminopyridine (DAP), which indirectly increases presynaptic calcium entry by broadening the action potential waveform, leading to an increase in transmitter release (Verschuuren et al., 2006; Oh et al., 2009; Wirtz et al., 2009). However, DAP is only partially effective in LEMS, and there are dose-limiting side-effects including paresthesia, gastric symptoms, insomnia, and less commonly, seizures (Verschuuren et al., 2006; Oh et al., 2009; Titulaer et al., 2011a). It would therefore be beneficial to have access to more treatment options. An alternative strategy would be to directly target the presynaptic calcium channels involved in transmitter release.

(*R*)-roscovitine, a compound that was originally developed as a cyclin-dependent kinase (Cdk) inhibitor (Meijer et al., 1997), also displays direct calcium channel agonist effects that are

independent of Cdk effects (Yan et al., 2002; Buraei et al., 2005; Cho and Meriney, 2006). (*R*)-roscovitine slows the deactivation kinetics of N- and P/Q-type calcium channels by increasing their mean open time (DeStefino et al., 2010), which leads to an increase in transmitter release at synapses (Yan et al., 2002; Cho and Meriney, 2006). Although (*R*)-roscovitine does target the calcium channels involved in transmitter release at the NMJ, the potent (*R*)-roscovitine-mediated inhibition of Cdks presents a potential source of undesirable side-effects if used for the treatment of LEMS. Therefore, we set out to develop a novel analog of (*R*)-roscovitine with both reduced Cdk antagonist effects and stronger calcium channel agonist effects.

Using strategic medicinal chemistry modifications to the purine scaffold, we modified selected side chains present in (*R*)-roscovitine and characterized the resulting compounds by patch-clamp electrophysiological measurements of calcium current, as well as in secondary kinase assays (Liang et al., 2012). Analogs that displayed reduced Cdk activity and strong agonist effects on calcium current were further evaluated using electrophysiological recordings of transmitter release from LEMS model mouse neuromuscular junctions. The most promising analog that emerged from these studies, GV-58, has ~20-fold lower potency as a Cdk antagonist, ~3- to 4-fold higher potency as a calcium channel agonist, and ~4-fold higher efficacy as a calcium channel agonist compared with the parent molecule, (*R*)-roscovitine.

## 3.2 MATERIALS AND METHODS

### 3.2.1 Chemistry

(*R*)-roscovitine analogs were synthesized as reported previously (Liang et al., 2012) and used after they passed quality control analysis (liquid chromatography-mass spectrometry purity >92%).

### 3.2.2 Cell lines expressing calcium channels

Initial screenings of (*R*)-roscovitine derivatives on N-type calcium channels were performed using a tsA-201 cell line that stably expressed the subunits of the N-type calcium channel splice variant present in mammalian brain and spinal cord: $Ca_v2.2$ rnα1B-c (Cav2.2 e[24a,Δ31a]), $Ca_vβ3$, and $Ca_vα2δ1$. For subsequent evaluation of effects on N-, P/Q-, or L-type channels, tsA-201 cells were transiently transfected with $Ca_v2.2$, $Ca_v2.1$, or $Ca_v1.3$, in combination with $Ca_vβ3$ and $Ca_vα2δ1$ (Addgene) using FuGENE 6 (Promega). All cells were maintained in DMEM supplemented with 10% fetal bovine serum. For the stable cell line expressing N-type channels, 25 μg/ml zeocin, 5 μg/ml blasticidin, and 25 μg/ml hygromycin were added as selection agents.

### 3.2.3 Whole-cell perforated patch clamp recordings

To assess the effects of (*R*)-roscovitine analogs, whole-cell currents through calcium channels were recorded using perforated patch methods as previously described (White et al., 1997; Yazejian et al., 1997; Cho and Meriney, 2006). Briefly, the pipette solution consisted of 70 mM

$Cs_2SO_4$, 60 mM CsCl, 1 mM $MgCl_2$, 10 mM 4-(2-hydroxyethyl)-1-piperazineethanesulfonic acid (HEPES) at pH 7.4. Cultured cells were bathed in a saline composed of 130 mM choline chloride (ChCl), 10 mM tetraethylammonium chloride (TEA-Cl), 2 mM $CaCl_2$, 1 mM $MgCl_2$, 10 mM HEPES, at pH 7.4. Patch pipettes were fabricated from borosilicate glass and pulled to a resistance of ~1 MΩ. Before each experiment, a stock solution consisting of 3 mg of amphotericin-B dissolved into 50 µl of anhydrous DMSO was made. The tips of the pipettes were dipped into pipette solution that did not contain amphotericin-B for 5–10 s, and then backfilled with pipette solution that contained amphotericin-B (7 µl amphotericin-B stock solution mixed into 500 µl pipette solution, freshly made every hour). Using this approach, perforated patch access resistances were 7.41 ± 1.75 MΩ (mean ± SD, n = 68). Capacitive currents and passive membrane responses to voltage commands were subtracted from the data. Currents were amplified by an Axopatch 200B amplifier, filtered at 5 kHz, and digitized at 10 kHz for subsequent analysis using pClamp 10 software (Molecular Devices). The liquid junction potential was subtracted during recordings. The tail current integral was measured before and after application of a compound, with the integral of each trace normalized to its peak. All experiments were performed at room temperature (22°C). Stock solutions of (*R*)-roscovitine and the analog compounds were dissolved in DMSO at either 50 or 100 mM and stored at −20°C. (*R*)-roscovitine and the analog compounds were bath applied via a glass pipette in a ~1.5 ml static bath chamber during whole-cell recordings of calcium current. Control recordings performed with 0.1–1% DMSO alone added to the drug delivery pipette solution revealed no significant effects on whole-cell calcium currents. All other salts and chemicals were obtained from Sigma-Aldrich.

### 3.2.4 Kinase screen of novel analogs

Each of the three novel analogs, along with the parent compound (*R*)-roscovitine, was tested for kinase activity using the EMD Millipore KinaseProfiler service. Each compound's kinase inhibitory activity was tested at three different concentrations (0.2, 2, and 20 μM) on five different kinases: Cdk1 cyclinB(h), cdk2 cyclinA(h), cdk5 p35(h), mitogen-activated protein kinase [MAPK1(h)], and myosin light-chain kinase [MLCK(h)]. All kinases were tested in the presence of 10 μM ATP.

### 3.2.5 LEMS passive transfer

To test GV-58 in a LEMS model NMJ, we used an established LEMS passive-transfer mouse model (Fukunaga et al., 1983; Lang et al., 1984; Fukuoka et al., 1987; Smith et al., 1995; Xu et al., 1998; Flink and Atchison, 2002). To perform this passive transfer of LEMS, mice were injected with the serum of patients diagnosed with LEMS. Collection of serum from LEMS patients was performed following the guidelines set forth by the University of Pittsburgh Institutional Review Board (IRB). Serum from patients aBC2 and aCB was collected using plasmapheresis. All other patient serum samples were obtained by collecting patient blood samples in serum separator tubes (BD Vacutainer Plus, BD Bioscience), which were spun down in a clinical centrifuge according to the manufacturer's specifications to isolate the serum. Each serum sample was tested for the presence of voltage-gated calcium channel antibodies using a calcium channel antibody radioimmune assay (Kronus RIA kit). Control serum was obtained from the University of Pittsburgh Medical Center blood bank. All serum, including control serum, was filtered with a 0.22 μm filter before the injection protocol. Adult female CFW mice

(2–3-months-old at beginning of passive transfer; weighing 25–32 g; Charles River Laboratories) were divided into two groups: one group that received LEMS serum, and a control group that received control serum. Mice received an intraperitoneal injection on day 1 of the treatment phase with 300 mg/kg cyclophosphamide to suppress immune responses, and were injected intraperitoneally once per day for 24–30 consecutive days with either 1.5 ml serum from LEMS patients or 1.5 ml control serum. In all cases, experimenters were blinded to the injection conditions.

### 3.2.6 Intracellular recordings at mouse NMJs

Following the passive transfer protocol, intracellular recordings to assess the LEMS-mediated deficit in transmitter release were made in an *ex vivo* nerve-muscle preparation. A thin upper arm muscle, the epitrochleoanconeus (ETA), was chosen for these recordings (Bradley et al., 1989; Rogozhin et al., 2008). This ex vivo nerve-muscle preparation was placed in a bath containing the following in mM: 118 NaCl, 3.45 KCl, 11 dextrose, 26.2 $NaHCO_3$, 1.7 $NaH_2PO_4$, 0.7 $MgCl_2$, 2 $CaCl_2$, pH 7.4. The nerve was stimulated with a suction electrode and muscle contractions were blocked by exposure to 1 μM μ-conotoxin GIIIB (Alomone Labs). Microelectrode recordings were performed using ~40–60 MΩ borosilicate electrodes filled with 3 M potassium acetate. Spontaneous miniature synaptic events (mEPPs) were collected for 1–2 min in each muscle fiber, followed by single nerve-evoked synaptic activity (10–30 EPPs) that was collected with an interstimulus interval of 5 s. A train of 10 EPPs was also collected in each muscle fiber using an interstimulus interval of 20 ms. To analyze the data, both the amplitudes and the areas under the waveforms (integral) were determined after correcting each digitized point in each trace for nonlinear summation (McLachlan and Martin, 1981). Data were collected using an Axoclamp

900A and digitized at 10 kHz for subsequent analysis using pClamp 10 software (Molecular Devices).

### 3.2.7 Statistical analysis

Statistical analysis was performed using either GraphPad Prism 5 or Origin 7 (OriginLab). For the dose–response analyses on calcium current, each concentration of the four different compounds was tested in 3–6 cells. For the dose–response analyses on kinase activity, each of the three concentrations was tested in duplicates (n = 2) for every compound except (R)-roscovitine, which was sent for kinase screening three times (n = 6 for each concentration). Dose–response curves for agonists were fit using the following equation: y = ymax/(1 + (EC50/[S])nH), where [S] is the agonist concentration and nH is the Hill coefficient. Antagonist inhibition curves were fit with the equation: y = ymax/(1 + ([A]/IC50)nH), where [A] is the antagonist concentration and nH is the Hill coefficient. The fits were not weighted. Data are presented as mean ± SEM unless otherwise noted.

## 3.3 RESULTS

### 3.3.1 Effect of novel analogs of (*R*)-roscovitine on calcium channel function

We previously reported the synthesis and structure of 24 novel analogs of (*R*)-roscovitine (Liang et al., 2012). Briefly, after an analysis of the available literature data for (*R*)-roscovitine analogs, we decided to primarily investigate replacements of the benzylamine and isopropyl side chains

of the parent lead structure. The new compounds were generated using this strategy and probed for relative structure-activity relationships of Cdk versus calcium channel interactions (Liang et al., 2012). We initially screened the effect of these novel analogs of (*R*)-roscovitine on calcium channel function using the whole-cell patch-clamp technique on tsA-201 cells expressing N-type ($Ca_v2.2$) calcium channels. Among the 24 compounds synthesized and tested, three compounds in particular exhibited a strong agonist effect on the calcium channel tail currents: GV-05, ML-50, and GV-58 (Figure 11A). For comparison, the effect of (*R*)-roscovitine on N-type tail currents was also determined. By measuring the tail current integrals (first normalizing each trace to its peak tail current amplitude and then normalizing to control integrals), the EC50 values of (*R*)-roscovitine, GV-05, ML-50, and GV-58 on N-type calcium channels, which were reported previously (Liang et al., 2012), were determined and are listed in Table 1. The maximal fold-increase in the tail current integral relative to control was ~8-fold, ~13-fold, ~25-fold, and ~32-fold, when modified by (*R*)-roscovitine, GV-05, ML-50, and GV-58, respectively (Figure 11B,C).

**Table 1. Comparison of (R)-roscovitine and novel analogs EC50/IC50 values (in µM) for activity at calcium channels and kinases.**

| | N-type ($Ca_v2.2$) | P/Q-type ($Ca_v2.1$) | L-type ($Ca_v1.3$) | Cdk1 | Cdk2 | Cdk5 | MAPK | MLCK |
|---|---|---|---|---|---|---|---|---|
| (*R*)-roscovitine | 27.58 ± 1.65 | 120* | >100† | 0.89 ± 0.01 | 0.15 ± 0.004 | 0.14 ± 0.01 | >20‡ | >20‡ |
| GV-05 | 30.02 ± 1.87 | N.D. | N.D. | 10.46 ± 2.77 | 3.04 ± 0.17 | 2.81 ± 0.91 | >20‡ | >20‡ |
| ML-50 | 11.29 ± 1.48 | N.D. | N.D. | 1.77 ± 0.04 | 0.26 ± 0.0002 | 0.27 ± 0.01 | >20‡ | 19.45 ± 8.65 |
| GV-58 | 7.21 ± 0.86 | 8.81 ± 1.07 | >100† | >20‡ | 3.29 ± 0.43 | 3.03 ± 0.32 | >20‡ | >20‡ |

*Literature $EC_{50}$ value for (*R*)-roscovitine on P/Q-type calcium channels taken from Buraei et al. (2007).

†No measureable agonist effect on L-type calcium channels up to 100 µM.

‡20 µM was the highest concentration used in kinase screens; therefore, an $IC_{50}$ above 20 µM could not be reliably determined.

N.D. = Not determined

### 3.3.2 Effect of novel analogs of (*R*)-roscovitine on kinase activity

In addition to seeking a compound with greater calcium channel agonist activity than (*R*)-roscovitine, we also sought to synthesize a compound with reduced Cdk antagonist activity. We used a commercial kinase screen that tested the effect of these novel compounds and (*R*)-roscovitine on several kinases, including cdk1, cdk2, cdk5, MAPK1, and MLCK (Table 1). We were focused on reducing the antagonist activity of our novel analogs on these three Cdks because (*R*)-roscovitine is a potent inhibitor of all three (Meijer et al., 1997). The IC50 values for

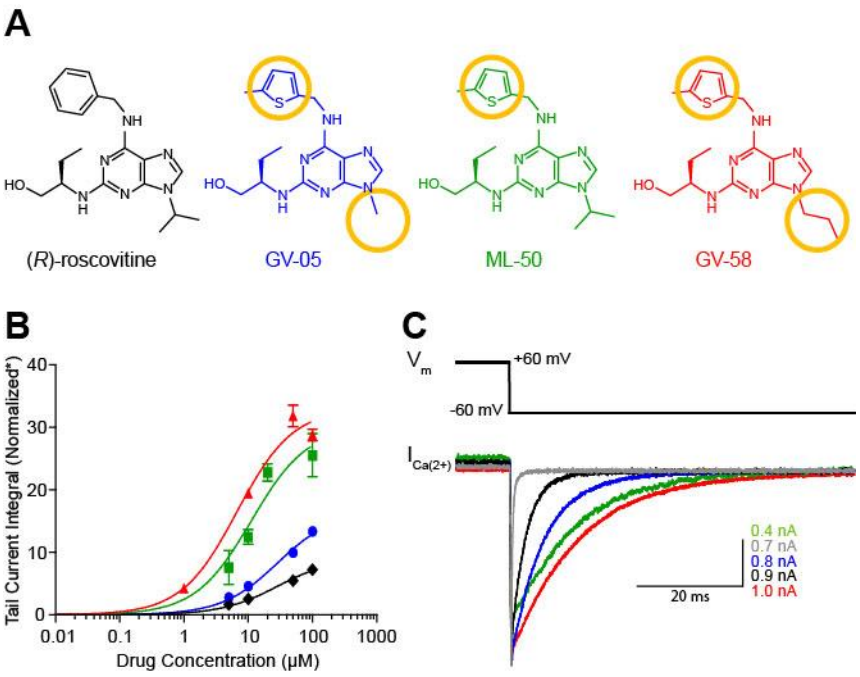


**Figure 11. GV-58 shows increased calcium channel activity compared with (R)-roscovitine.**

**A**, Structure of (*R*)-roscovitine and the three novel analogs with the strongest calcium current agonist effects of the 24 analogs screened. Yellow circles indicate structural differences compared with (*R*)-roscovitine. **B.** Calcium channel agonist activity dose–response curves for each of the compounds shown in **A**. *Each analog-modified tail current integral was normalized to its peak tail current and then divided by its respective control (untreated) tail current integral (also normalized to its respective peak current) to calculate the final value. **C.** Representative tail current traces are displayed for each of the compounds, along with a control tail current trace (gray trace). Each trace was obtained from a different cell and normalized at the peak for comparison. For **B** and **C**, data are color-coded to match the colored structures in **A**. Error bars indicate SEM.

cdk1, cdk2, and cdk5 inhibition following exposure to (*R*)-roscovitine, GV-05, ML-50, and GV-58 are shown in Table 1 (IC50 values for cdk2 determined in our kinase screen were reported previously (Liang et al., 2012)). Together, the data on calcium channel and Cdk activity show that GV-58 displays the most desirable properties of the compounds we have synthesized and tested thus far, as it displays both a greatly increased calcium channel agonist activity and a decreased Cdk antagonist activity compared with the parent molecule (*R*)-roscovitine (Table 1). For this reason, we chose GV-58 as our lead compound of interest and used it as the focus of the remainder of this study.

### 3.3.3 Selectivity of GV-58 for N- and P/Q-type calcium channels

Using our lead compound with the best profile (GV-58), we then tested the agonist activity on P/Q-type channels ($Ca_v2.1$) and L-type ($Ca_v1.3$) channels using the same voltage-clamp protocol. We found that the $EC_{50}$ value for GV-58 was very similar for both P/Q-type and N-type channels (8.81 ± 1.07 μM vs 7.21 ± 0.86 μM for P/Q- and N-type channels, respectively). Additionally, GV-58 increased the P/Q-type channel tail current integral by ~33-fold compared with control, similar to its effect on N-type channels (~32-fold). Finally, GV-58 had no agonist activity (up to 100 μM) on the L-type α-subunit we tested ($Ca_v1.3$; Table 1). In summary, GV-58 greatly improved upon (*R*)-roscovitine in terms of our properties of interest, with a ~4-fold increase in efficacy as an agonist for N- and P/Q-type calcium channels, a ~3- to 4-fold increase in potency as an agonist for N- and P/Q-type calcium channels, and a ~20-fold decrease in potency as a Cdk antagonist.

### 3.3.4 Evaluating LEMS passive transfer model mice

Having developed a novel calcium channel analog with reduced Cdk activity and potent calcium channel agonist activity, we then tested this analog in LEMS model mice. We used an established LEMS passive-transfer mouse model (Fukunaga et al., 1983; Lang et al., 1984; Fukuoka et al., 1987; Smith et al., 1995; Xu et al., 1998; Flink and Atchison, 2002), which involves daily injections of IgG or whole serum taken from patients who were diagnosed with LEMS. Using this approach, we tested the effects of whole serum injections from eight LEMS patients by measuring the quantal content in mouse ETA neuromuscular junctions following the passive transfer protocol (Figure 12A), and comparing them to the quantal content of mice that underwent a passive transfer protocol with injections of control human serum. The clinical profile for each LEMS patient whose serum was studied is shown in Table 2. Several patients' serum caused no significant change in quantal content compared with control (Figure 12A, black bars; $p > 0.05$, one-way ANOVA with Tukey's *post hoc* test), whereas other patient's serum showed moderate to strong changes in quantal content compared with control (Figure 12A, white bars; $p < 0.05$, one-way ANOVA with Tukey's *post hoc* test). In addition to testing quantal content following our passive transfer protocol, we also performed an antibody radioimmune assay to determine the level of calcium channel antibodies in each patient's serum (Figure 12B). In general, those serum samples that significantly decreased quantal content had detectable levels of calcium channel antibodies, although the level of these antibodies did not seem to correspond precisely to the level of quantal content decrease (Figure 12A,B). Our aim was to choose a single patient's serum for repeated testing of our novel calcium channel agonist to have a consistent passive transfer effect in every mouse. For these studies, we chose the serum from patient aBC2 because the quantal content following the passive transfer with this serum (40.5 ± 9.9; mean ±

**Table 2. Clinical data of each LEMS patient from whom serum was obtained and tested for this study.**

| Patient | Age | Age at Diagnosis | CMAP increment | ANNA1 (+/-) | P/Q-type $Ca^{2+}$ channel antibodies (+/-) |
|---|---|---|---|---|---|
| PB | 62 | 52 | 500% | - | + |
| EB | 66 | 57 | 331% | - | + |
| PG | 71 | 68 | 1300% | - | + |
| JS | 56 | 42 | 109% | N.D. | - |
| aBC2 | 30 | 20 | 800-1600% | + | + |
| SH | 61 | 55 | 78% | + | + |
| LE | 54 | 45 | 400% | - | + |
| aCB | 71 | 65 | 315% | - | + |

CMAP increment is a common diagnostic marker for LEMS and refers to the increase in compound muscle action potential (CMAP) size following a short exercise period (~10 seconds; Oh et al., 2007).

ANNA1 = anti-neuronal nuclear antibody type I, which is also known as "anti-Hu".

N.D. = Not determined

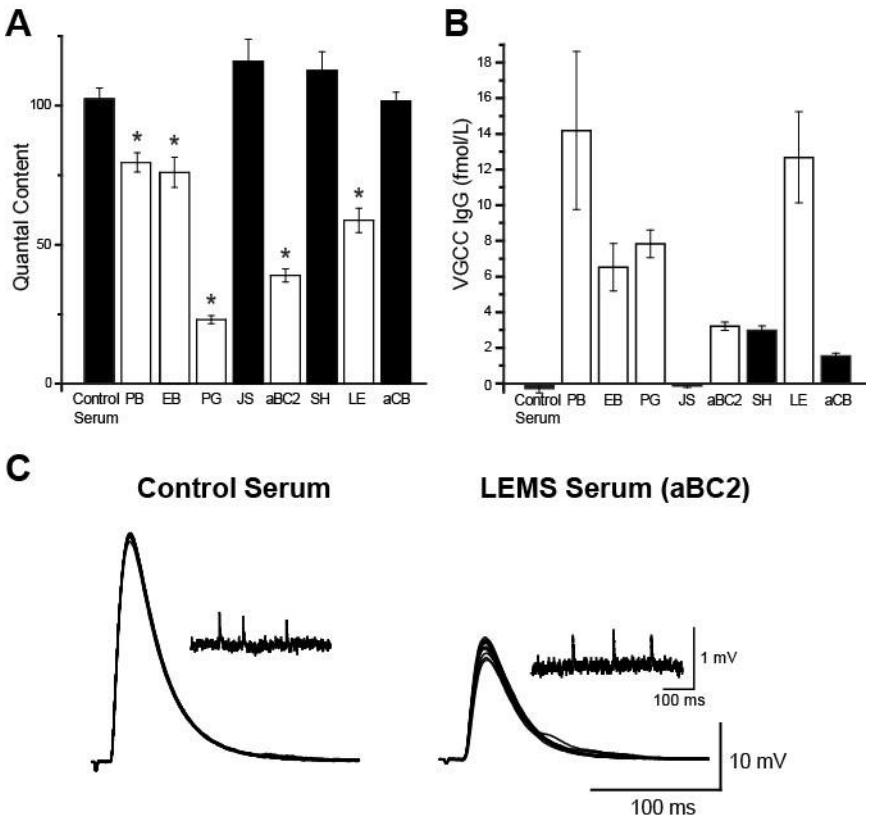


**Figure 12. Screening LEMS patient sera for passive transfer to mice.**

**A.** Each patient's serum was evaluated in our LEMS passive transfer model by measuring quantal content following the passive transfer protocol. White bars with an asterisk (*) indicate a significant decrease in quantal content compared with control serum-treated NMJs, whereas black bars indicate no significant difference from control serum-treated NMJs. **B.** Each serum shown in **A** was also evaluated for levels of voltage-gated calcium channel (VGCC) antibodies. The level of these antibodies in serum did not always correlate with the degree of the decrease in quantal content. **C.** Sample mEPP (insets) and EPP traces from a representative control (left) and aBC2 serum-treated (right) NMJ. Error bars indicate SEM; * indicates significance ( $p < 0.05$).

SD, n = 49 terminals) was significantly reduced compared with control serum (102.4 ± 25.1; mean ± SD, n = 41 terminals, $p < 0.05$, one-way ANOVA with Tukey's *post hoc* test; Figure 12A,C). EPP amplitude following passive transfer with aBC2 serum was also significantly smaller than EPP amplitude of NMJs injected with control serum (14.15 ± 0.64 mV, n = 49 vs 34.61 ± 1.37 mV, n = 41 for aBC2 serum-treated NMJs and control serum-treated NMJs, respectively; $p < 0.05$, Student's *t* test), but mEPP amplitude was not significantly different between the two conditions (data not shown). Additionally, we had sufficient serum from patient aBC2 to perform all of the desired experiments. Therefore, all of the following experiments were performed using mice that underwent our passive transfer protocol using serum aBC2.

### 3.3.5 GV-58 restores function in LEMS passive transfer NMJs

Having developed a consistent LEMS passive transfer protocol, we tested the effect of our novel compound (GV-58) on action potential-evoked transmitter release from LEMS passive transfer mouse NMJs. EPP amplitude and quantal content were determined in the vehicle (0.05–0.1% DMSO) before a 30 min incubation in 50 μM GV-58, which was then followed by repeated EPP amplitude and quantal content measurements from the same NMJs with the GV-58 still present in the bath. EPP amplitude was significantly increased from 13.00 ± 0.56 mV (n = 73 terminals) in vehicle-treated aBC2 serum NMJs to 19.44 ± 0.98 mV (n = 73 terminals; $p < 0.05$, Student's paired *t* test) following application of 50 μM GV-58 (Figure 13A,B). The quantal content (determined by dividing the EPP peak amplitude by the mEPP peak amplitude) in the LEMS passive transfer vehicle control NMJs was 38.0 ± 12.8 (mean ± SD, n = 73 terminals), and was significantly increased after GV-58 exposure to 56.0 ± 15.2 (mean ± SD, n = 73 terminals; $p < 0.05$, Student's paired *t* test; Figure 13D). Furthermore, when the quantal content was determined

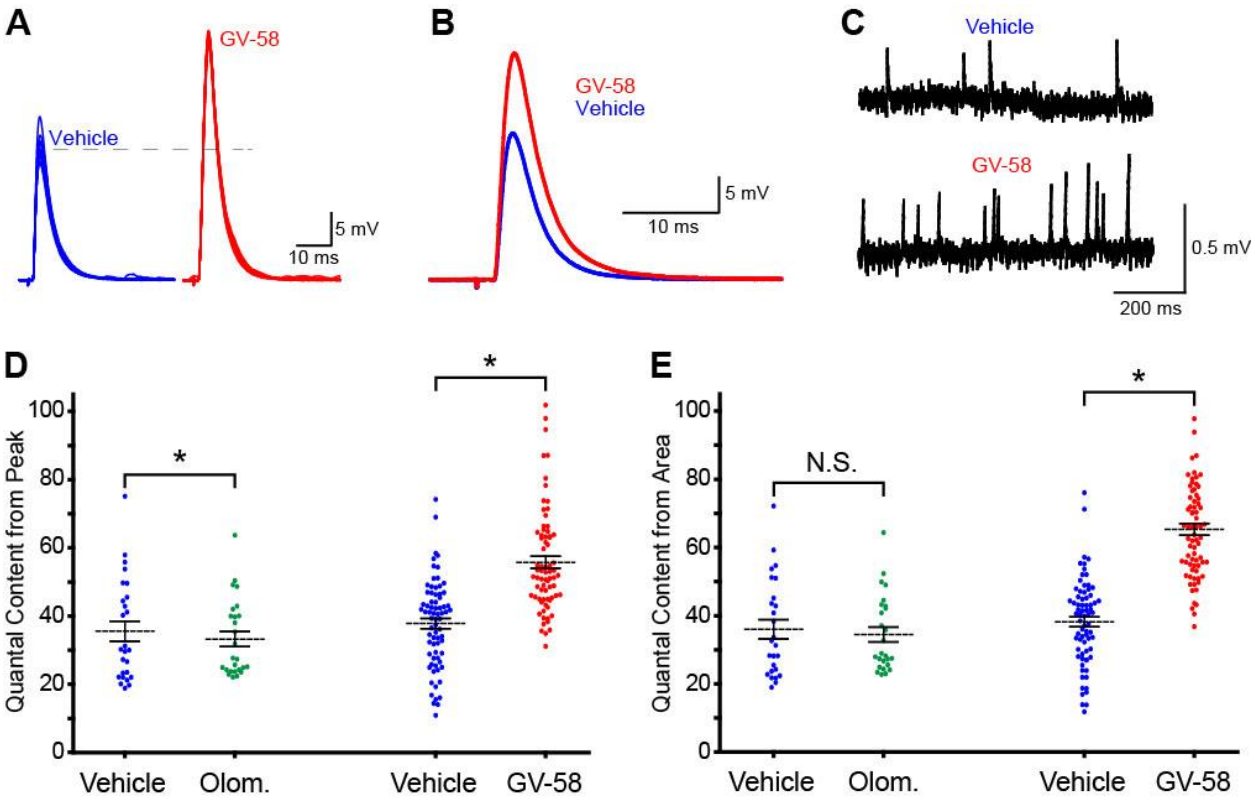


**Figure 13. GV-58 increases transmitter release at LEMS model NMJs.**

**A.** Sample traces (overlay of 10 traces in each example) show the increase in EPP amplitude following a 30 min incubation in 50 μM GV-58 (red) relative to vehicle control (0.05 – 0.1% DMSO; blue). Dashed line indicates the mean EPP amplitude in the example vehicle-treated LEMS NMJ. **B.** Average of 10 traces from the same NMJ before (blue) and after (red) 30 min incubation in 50 μM GV-58 show a GV-58-induced widening of the EPP trace. **C.** Representative mEPP traces from the same NMJ before and after GV-58 application. **D.** The quantal content determined by measuring the peak (peak EPP amplitude divided by the average peak mEPP amplitude) was slightly, but significantly smaller following 50 μM olomoucine (Olom) application (left), but was significantly increased following 50 μM GV-58 application (right). **E.** The quantal content determined by measuring the area (EPP area divided by average mEPP area) was not significantly different following 50 μM olomoucine application (left), but was significantly increased following GV-58 application (right). The scatter plots in both **D** and **E** represent the variability between individual synapses studied. Dashed line indicates the mean of each population. Error bars indicate SEM; * indicates significance ( $p < 0.05$).

from the area (integral) under EPP and mEPP waveforms, the quantal content in the vehicle controls was 38.3 ± 12.7 (mean ± SD, n = 73 terminals), and was significantly increased to 65.6 ± 15.0 (mean ± SD, n = 73 terminals; $p < 0.05$, Student's paired *t* test; Figure 13E) following GV-58 application. The difference between the compound's effect on quantal content when measuring peak (~62% increase) compared with its effect on quantal content when measuring area (~92% increase) suggests that there is a broadening of the EPP waveform caused by the action of GV-58 on calcium channels (expected based on the GV-58-mediated slowing of calcium current deactivation). To further explore this possibility, we measured both the full-width at half-maximum (FWHM) and the 90 to 10% decay time before and after GV-58 application. Figure 13B shows an overlay of the average EPP amplitudes in a sample NMJ before (blue) and after (red) GV-58 application. The FWHM increased significantly from 3.39 ± 0.06 ms in the vehicle controls (n = 73 terminals) to 3.90 ± 0.07 ms following 50 μM GV-58 application (n = 73 terminals; $p < 0.05$, Student's paired *t* test). Similarly, the 90 to 10% decay time increased from 5.84 ± 0.12 ms in vehicle controls (n = 73 terminals) to 6.79 ± 0.11 ms following GV-58 application (n = 73 terminals; $p < 0.05$, Student's paired *t* test). This indicates that the effect of GV-58 cannot fully be appreciated by only observing changes in peak EPP amplitude.

Previous reports have shown an increase in neurotransmitter release following pharmacological block or knock-out of cdk5 (Fu et al., 2005; Kim and Ryan, 2010). To ensure that the observed effect of GV-58 on transmitter release was not due to inhibition of Cdks, we tested the effect of olomoucine on transmitter release at LEMS passive transfer mouse NMJs. Olomoucine is a compound that is structurally related to (*R*)-roscovitine and has potent Cdk inhibitory activity (Vesely et al., 1994), but no calcium channel activity (Buraei et al., 2005).

Application of 50 μM olomoucine caused a slight decrease in quantal content compared with vehicle controls when measuring quantal content from peak (35.7 ± 15.0, mean ± SD, n = 23 vs 33.4 ± 11.3, mean ± SD, n = 23, for vehicle controls and olomoucine, respectively; $p < 0.05$, Student's paired *t* test; Fig. 3D). The quantal content measured from area in vehicle controls (36.1 ± 14.3, mean ± SD, n = 23) did not significantly change after application of olomoucine (34.6 ± 11.2, mean ± SD, n = 23; $p = 0.16$, Student's paired *t* test; Figure 13E). Therefore, the effects of GV-58 on increasing action potential-evoked transmitter release at LEMS passive transfer NMJs appear to be due to effects on calcium channels rather than effects on Cdks.

In addition to analyzing the changes in quantal content and EPP kinetics, we also analyzed the effect of GV-58 on spontaneous transmitter release. Figure 13C shows sample mEPP traces recorded in the vehicle control and following 50 μM GV-58 application. The mEPP frequency was significantly increased from 3.27 ± 0.15 s−1 (n = 73) in vehicle controls to 10.45 ± 0.64 s−1 (n = 73) following application of 50 μM GV-58 ($p < 0.05$, Students paired *t* test). Furthermore, the mEPP amplitude did not significantly change following addition of GV-58 (mean change in amplitude following GV-58 = 1.00 ± 0.02, n = 73; $p = 0.86$, Student's one sample *t* test), consistent with a presynaptic locus for effects.

Finally, we determined the short-term plasticity characteristics of our LEMS model and the effect of GV-58 on these properties by eliciting trains of 10 stimuli at 50 Hz (Figure 14). We first compared the short-term plasticity characteristics of our LEMS passive transfer model NMJs to those of NMJs taken from mice that received control serum injections. In the control serum condition, there is almost no facilitation, and by the 10th EPP in the train there is a depression to ~66% of the first EPP. The trains of stimuli in the “aBC2” condition triggered EPPs that were generally erratic in size during any single train, but the overall average showed

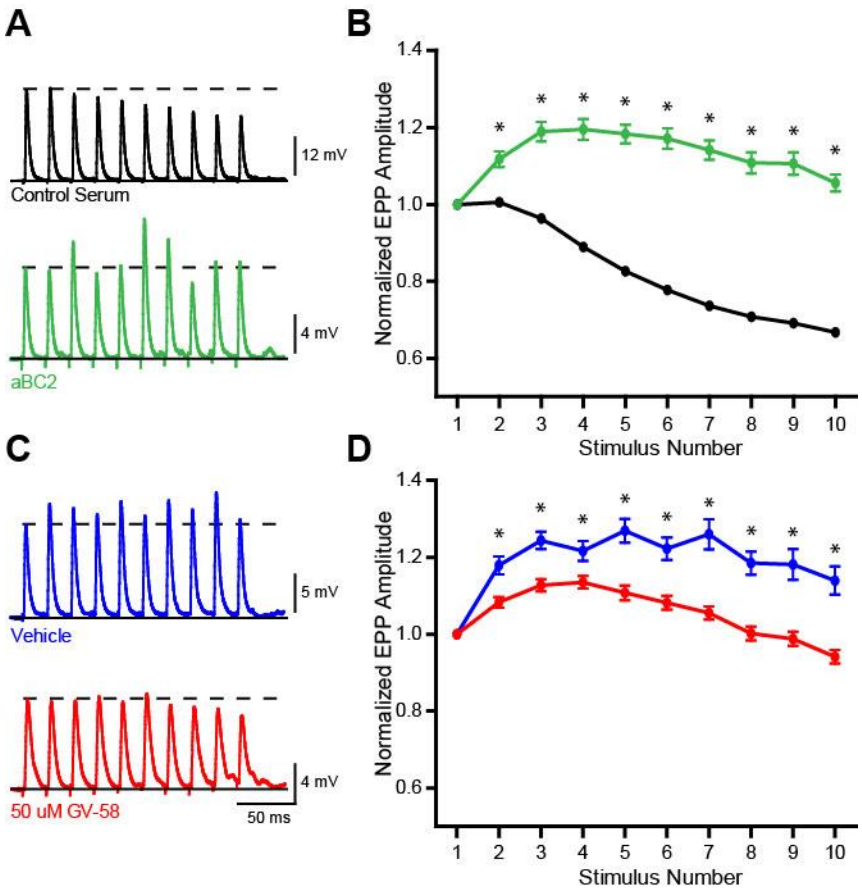


**Figure 14. Short-term plasticity during trains of stimuli.**

**A.** Representative EPPs evoked by 50 Hz stimuli recorded from terminals in control serum-injected mice (black) and aBC2 LEMS serum-injected mice (green). **B.** Plot of the average 50 Hz train data normalized to the amplitude of the first EPP of the train for the two conditions shown in **A**. **C,** Representative 50 Hz trains for aBC2 LEMS serum-injected mice in the presence of the DMSO vehicle (blue), and aBC2 LEMS serum-injected mice following application of 50 μM GV-58 (red). **D,** Plot of the average 50 Hz train data normalized to the amplitude of the first EPP of the train for the two conditions shown in **C**. The GV-58 condition was performed on the same set of NMJs as the vehicle condition following a 30 min. incubation in 50 μM GV-58. Representative traces in **A** and **C** were chosen to display the differences in short-term plasticity characteristics, rather than the differences in the first EPP's amplitude (which were quite variable; Figure 13), among the four conditions. Asterisks in **B** and **D** indicate a significant difference between the two normalized EPP amplitudes below each asterisk as determined by a Student's *t* test in **B** or a Student's paired t test in **D**. Error bars indicate SEM; * indicates significance ( $p < 0.05$).

facilitation throughout the 50 Hz train, with a peak facilitation of ~120% at EPP 4 and a small facilitation of ~105% remaining at the final EPP in the train. When both conditions are normalized to the first EPP of the respective train, the control serum condition (n = 41) is significantly different from the aBC2 condition (n = 52) at each EPP in the train following the first ($p < 0.05$, Student's *t* test; Figure 14A,B). We then compared the short-term plasticity characteristics before (0.05–0.1% DMSO vehicle) and after application of 50 μM GV-58 in our LEMS passive transfer model NMJs (Figure 14C,D). The "Vehicle" condition shows facilitation throughout, with a facilitation of ~113% remaining at the final EPP in the train. Following the application of 50 μM GV-58 in the same NMJs, there was a slight facilitation followed by depression to ~94% at the final EPP in the train. Furthermore, the "GV-58" condition was significantly different from the Vehicle condition at every EPP following the first when both conditions are normalized to the first EPP of the train ($p < 0.05$, Student's paired *t* test; Figure 14C,D).

## 3.4 DISCUSSION

We have shown that directly targeting presynaptic calcium channels using a novel agonist can partially restore the deficiency of transmitter release in a LEMS passive-transfer mouse model NMJ. By synthesizing and screening multiple analogs of (*R*)-roscovitine, we identified a compound (GV-58) that has both a reduced Cdk antagonist activity and an increased calcium channel agonist activity. Although further testing will be required to evaluate calcium channel agonists as viable treatment options for patients with LEMS, our work suggests that directly

targeting presynaptic calcium channels represents a new therapeutic paradigm for patients with LEMS.

### 3.4.1 GV-58 effects on transmitter release

Our novel calcium channel agonist GV-58 increases the amount of calcium influx through channels that open during an action potential, which in turn leads to an increase in the amount of transmitter released (Figure 13). This effect is not due to inhibition of Cdks, as the potent Cdk inhibitor olomoucine had no agonist effect on transmitter release (Figure 13D,E). When determining how such a calcium channel agonist would increase transmitter release at the mammalian NMJ, it is useful to consider the calcium-dependent mechanisms that normally regulate release at this synapse. The adult mouse NMJ has been shown to contain ~850 very small active zones (Ruiz et al., 2011; Chen et al., 2012), each of which contains approximately two docked synaptic vesicles (Nagwaney et al., 2009). Because the entire adult mouse ETA neuromuscular synapse releases ~100 vesicles normally following each action potential stimulus (Figure 12), the probability of release from each active zone is ~12% (assuming a homogeneous release probability across all active zones during low-frequency stimulation (Gaffield et al., 2009), although a heterogeneous distribution is also possible (Wyatt and Balice-Gordon, 2008)). There are an unknown number of calcium channels positioned with mouse NMJ active zones, but if there are relatively few present, and if they have a low probability of opening as has been shown at the frog NMJ (Luo et al., 2011), this may contribute significantly to the low probability of release from each active zone. Furthermore, the coupling between calcium channel opening and vesicle fusion in these active zones may also be very low (similar mechanisms appear to control release at the frog NMJ (Wachman et al., 2004; Luo et al., 2011; Tarr et al., 2013a)).

Under these conditions, a calcium channel agonist like GV-58 would be expected to increase the flux through a subset of open channels, increasing the probability of vesicle fusion at these sites.

Interestingly, some NMJs show more than a threefold increase in transmitter release after exposure to GV-58, whereas others show a very small effect (Figure 13D,E, scatter plots). There are several potential sources of variability in GV-58 effects on quantal content. First, during our relatively short (30–60 min) exposure, there may have been variable connective tissue barriers to diffusion, which may have resulted in different concentrations of GV-58 affecting particular NMJs within the muscle. It is also possible that the mix of calcium channels at LEMS model synapses is variable when compared between NMJs (even in the same muscle). Compensatory changes in calcium channel expression have been reported to include an upregulation of L-type calcium channel expression at the NMJ that might contribute to the triggering of release at these disease model synapses (Flink and Atchison, 2002), but L-type channels would not be sensitive to modulation by GV-58 (see Table 1).

We have also shown that GV-58 partially restores normal short-term plasticity characteristics in LEMS model mouse NMJs (Figure 14). One interesting observation is the lack of facilitation in the 50 Hz train in control serum NMJs compared with the large facilitation present in the 50 Hz train in LEMS serum-treated NMJs. If many calcium channels contribute to the release of a single vesicle within each active zone, as has been shown in multiple CNS synapses (Eggermann et al., 2012; Tarr et al., 2013a), then the large facilitation in the LEMS serum-treated NMJs would be caused by a smaller total intracellular calcium flux through fewer calcium channels at each active zone. GV-58 would then compensate by increasing the calcium influx through the remaining calcium channels at the active zone. If, however, the mouse NMJ functions as has been reported at the frog NMJ, there may be an approximately one-to-one

relationship between calcium channel opening and vesicle fusion (Luo et al., 2011; Tarr et al., 2013a). Under these conditions at the small, isolated active zones present at the mouse NMJ, an explanation for the increase in facilitation observed in the LEMS serum-treated NMJs is less straightforward. In this scenario, if the opening of one calcium channel normally contributes to the release of one vesicle (calcium channel − release site cooperativity = 1), then simply removing calcium channels (as a result of LEMS) should only reduce quantal content without affecting short-term plasticity because each release site that lost a calcium channel would simply drop out, with no change in the calcium flux at release sites that had a calcium channel opening. On the other hand, if there is a compensatory expression of other types of calcium channels in LEMS NMJs (Flink and Atchison, 2002), this may result in the insertion of calcium channels into sites further away from the vesicle and its release machinery (Urbano et al., 2003). This could lead to a calcium channel–release site coupling such that it might be required that more than one open calcium channel provide the flux that is necessary for the release of a single vesicle. Under these conditions, one would predict an increased facilitation during a 50 Hz train compared with control. GV-58 would then reverse this by increasing the calcium influx through each channel, thus increasing the likelihood that the flux through a single channel could trigger the release of a synaptic vesicle. Last, it is also possible that active zone structure and organization is disrupted in the LEMS passive transfer NMJ (Fukunaga et al., 1983). Disruption of active zone structure and organization could alter the normally one-to-one calcium channel-to-vesicle coupling, thus accounting for both the facilitation seen in the LEMS serum-treated NMJs and the partial restoration of short-term plasticity characteristics by GV-58 as described above. LEMS could induce active zone disorganization in this scenario by disrupting the interactions between calcium channels and active zone proteins following the autoimmune-mediated removal

of calcium channels. For example, previous work has shown that preventing the interaction between calcium channels and the active zone protein laminin β2 induces active zone disorganization similar to that seen in LEMS NMJs (Fukunaga et al., 1983; Nishimune et al., 2004; Chen et al., 2011).

### 3.4.2 New calcium channel agonists as potential therapeutics

There are few symptomatic treatment options for LEMS, and those that are available can sometimes be associated with unwanted side effects (Verschuuren et al., 2006; Oh et al., 2009; Titulaer et al., 2011a). The currently recommended symptomatic treatment option (DAP) works to increase transmitter release by broadening the action potential waveform to increase calcium influx (Verschuuren et al., 2006). Directly targeting the calcium channels involved in transmitter release at the NMJ could represent an alternative treatment option for LEMS patients. Additionally, a calcium channel agonist might be used in combination with DAP to exert synergistic effects on transmitter release when both are applied at concentrations that are lower than what is required for effects when either is given alone.

Before this study, the only known compound with agonist effects on the calcium channel subtypes involved with transmitter release at the NMJ was (*R*)-roscovitine (Yan et al., 2002; Buraei et al., 2005; Cho and Meriney, 2006). Our chemical modifications of (*R*)-roscovitine have led to the generation of GV-58, which represents a promising lead structure in the development of selective calcium channel agonists. Additional chemical modifications to further reduce Cdk activity would be useful, but given that these compounds compete with ATP for binding to Cdks (De Azevedo et al., 1997), the high cellular ATP concentrations (in the 1–10 mM range

(Maechler et al., 1998; Kennedy et al., 1999)) are expected to outcompete compounds that bind with affinities in the μM range.

In addition to the possibility of treating the muscle weakness associated with LEMS, a direct calcium channel agonist could also serve as a treatment option for other neuromuscular diseases characterized by muscle weakness. In particular, a calcium channel agonist would be expected to provide symptomatic relief for some of the congenital myasthenic syndromes (Schara et al., 2012), and perhaps myasthenia gravis caused by muscle-specific kinase autoantibodies (Mori et al., 2012; Morsch et al., 2013). The effects of GV-58 on animal models of other neuromuscular diseases remain to be examined. Of course, before treatment options can be considered further, off-target effects, toxicity, and blood–brain barrier penetrance will also need to be examined.

### 3.4.3 New calcium channel agonists as experimental tools

Independent of its therapeutic potential for treatment of diseases characterized by neuromuscular weakness, a selective and potent calcium channel agonist of the P/Q- and N-type calcium channels would serve as an important experimental tool for studying the basic properties of these calcium channel subtypes. Just as the L-type calcium channel agonists BayK 8644 and FPL64176 were important in studies of L-type channel gating, conductance, and kinetics (Hess et al., 1984; Zheng et al., 1991; Church and Stanley, 1996; Tavalin et al., 2004), an agonist of the P/Q- and N-type channels would be equally useful in the study of their properties. Furthermore, GV-58 may serve as a useful probe molecule in studies of the calcium control of chemical transmitter release. Even though (*R*)-roscovitine is an agonist of the P/Q- and N-type channel

subtypes, our novel compound GV-58 is more selective and potent than (*R*)-roscovitine, and thus likely to be more effective for studies on basic P/Q- and N-type calcium channel function.

# 4.0 CHAPTER THREE: COMPLETE REVERSAL OF LAMBERT-EATON MYASTHENIC SYNDROME SYNAPTIC IMPAIRMENT BY THE COMBINED USE OF A $K^+$ CHANNEL BLOCKER AND A CALCIUM CHANNEL AGONIST

***Preface***

Lambert–Eaton myasthenic syndrome (LEMS) is an autoimmune disorder in which a significant fraction of the presynaptic P/Q-type calcium channels critical to the triggering of neurotransmitter release at the neuromuscular junction (NMJ) are thought to be removed. There is no cure for LEMS, and the current most commonly used symptomatic treatment option is a potassium channel blocker [3,4-diaminopyridine (3,4-DAP)] that does not completely reverse symptoms and can have dose-limiting side-effects. We previously reported the development of a novel calcium channel agonist, GV-58, as a possible alternative treatment strategy for LEMS. In this study, we tested the hypothesis that the combination of GV-58 and 3,4-DAP will elicit a supra-additive increase in neurotransmitter release at LEMS model NMJs. First, we tested GV-58 in a cell survival assay to assess potential effects on cyclin-dependent kinases (Cdks) and showed that GV-58 did not affect cell survival at the relevant concentrations for calcium channel effects. Then, we examined the voltage dependence of GV-58 effects on calcium channels using patch clamp techniques; this showed the effects of GV-58 to be dependent upon calcium channel opening. Based on this mechanism, we predicted an interaction between 3,4-DAP and GV-58. We tested this hypothesis using a mouse passive transfer model of LEMS. Using intracellular

electrophysiological ex vivo recordings, we demonstrated that a combined application of 3,4-DAP plus GV-58 had a supra-additive effect that completely reversed the deficit in neurotransmitter release magnitude at LEMS model NMJs. This reversal contrasts with the less significant improvement observed with either compound alone. Our data indicate that a combination of 3,4-DAP and GV-58 represents a promising treatment option for LEMS and potentially for other disorders of the NMJ.

**The results of this chapter have been published in the *Journal of Physiology* in 2014, and the citation for this article is given below. Minor formatting changes and changes to the numbering of figures and tables have been made to preserve consistency with the rest of this dissertation document.**

**Tarr TB, Liang M, Valdomir G, Frasso M, Lacomis D, Reddel SW, Wipf P, Meriney SD (2014) Complete reversal of Lambert-Eaton myasthenic syndrome synaptic impairment by the combined use of a $K^+$ channel blocker and a $Ca^{2+}$ channel agonist. *J. Physiol.* 592:3687-3696**

## 4.1 INTRODUCTION

Lambert–Eaton myasthenic syndrome (LEMS) is an autoimmune disorder characterized by a presumed loss of a fraction of the presynaptic P/Q-type calcium channels required for action potential-evoked acetylcholine release at the neuromuscular junction (NMJ) (Lambert et al. 1956; Nagel et al. 1988; Vincent et al. 1989; Smith et al. 1995; Meriney et al. 1996). A reduction in the number of presynaptic P/Q-type calcium channels at the NMJ in LEMS is assumed on the basis of multiple lines of evidence, including the presence of antibodies to the P/Q-type calcium channel in sera of LEMS patients (Lennon et al. 1995; Motomura et al. 1997), a reduction in the number of active zone particles following passive transfer of LEMS to mice (Fukunaga et al. 1983) and a reduction in calcium current in various model systems following application of LEMS IgG (Lang et al. 1989; Meriney et al. 1996). A reduction in P/Q-type calcium channels results in a disruption of neuromuscular transmission that predominately causes limb weakness and areflexia that improve after a few seconds of sustained contraction of the weak muscle (Lambert et al. 1956; Titulaer et al. 2008). The electrophysiological correlates are a reduced quantal content [QC (magnitude of acetylcholine release)] and a reduction in the resulting compound muscle action potential (CMAP) (Lambert et al. 1956; Vincent et al. 1989; Titulaer et al. 2008). LEMS can occur as a primary autoimmune disease or as a paraneoplastic autoimmune disorder (most commonly triggered by small cell lung cancer in smokers) (Titulaer et al. 2011a). The most common treatment for LEMS is the potassium channel blocker 3,4-diaminopyridine (3,4-DAP), although pyridostigmine (which increases the persistence of acetylcholine in the synaptic cleft) or immunotherapies such as i.v. immunoglobulin, plasma exchange and

immunosuppression are also used in some cases (Lindquist & Stangel, 2011; Titulaer et al. 2011b). These therapies can often control the disease, but generally do not result in a return to complete normality (Sedehizadeh et al. 2012).

We previously reported the initial evaluation of our novel compound GV-58 as a calcium channel agonist that selectively affects P/Q- and N-type, but not L-type, calcium channels (Liang et al. 2012; Tarr et al. 2013). We developed GV-58 as a synthetic analogue of (*R*)-roscovitine, a trisubstituted purine derivative that is best known as an inhibitor of cyclin-dependent kinases (Cdks) (De Azevedo et al. 1997; Meijer et al. 1997). However, a previous study found that (*R*)-roscovitine also has unexpected calcium channel agonist activity (Yan et al. 2002). In order to develop a compound to selectively increase chemical transmitter release at diseased synapses, we sought to modify (*R*)-roscovitine with the goal of decreasing Cdk antagonist activity and enhancing calcium channel agonist activity (Liang et al. 2012). We selected GV-58 as our primary lead structure for further evaluation as it showed the most desirable characteristics as a potential treatment for neuromuscular disease, including a 22-fold reduction in Cdk inhibitory activity and a four-fold increase in calcium channel agonist effect (Liang et al. 2012; Tarr et al. 2013).

In the present study, we evaluated the effects of GV-58 on cell toxicity and survival in a cultured cell assay designed to reveal potential off-target effects on Cdks. Next, we characterized the voltage-dependent properties of the GV-58 effect on calcium channels, the results of which predicted that a combination treatment with 3,4-DAP would be supra-additive. We then tested the hypothesis that GV-58 would work in combination with 3,4-DAP to create a supra-additive effect at LEMS model mouse NMJs that would completely reverse the deficit in neurotransmitter release at the NMJ caused by the passive transfer of LEMS to mice. Lastly, we characterized the

effects of this novel treatment approach on short-term synaptic plasticity at NMJs in a LEMS model mouse.

## 4.2 METHODS

### 4.2.1 Ethical approval

Serum from LEMS patients was collected in line with the guidelines set forth by the University of Pittsburgh Institutional Review Board. Animal studies were performed according to protocols approved by the University of Pittsburgh Institutional Animal Care and Use Committee (IACUC).

### 4.2.2 Cell lines

For the evaluation of effects of GV-58 on P/Q-type channels, tsA-201 cells were transiently transfected with $Ca_v2.1$ in combination with $Ca_v\beta3$ and $Ca_v\alpha2\delta1$ (Addgene, Inc., Cambridge, MA, USA) using FuGENE 6 (Promega Corp., Madison, WI, USA). SH-SY5Y cells (a kind gift from Dr Susan G. Amara) were used to evaluate Cdk antagonist effects in the cell survival assay. All cells were maintained in Dulbecco's modified Eagle's medium (DMEM) supplemented with 10% (tsA-201) or 15% (SH-SY5Y) fetal bovine serum.

### 4.2.3 Cell survival assay

A cell survival assay using [3-(4,5-dimethylthiazol-2-yl)-5-(3-carboxymethoxyphenyl)-2-(4-sulfophenyl)-2H-tetrazolium, inner salt (MTS) (Ribas & Boix, 2004) in SH-SY5Y cells was used to test Cdk antagonist effects in the presence of physiological levels of ATP. SH-SY5Y is a cell line originating from a human neuroblastoma and has been used in previous studies that examine the effect of Cdk inhibition on apoptosis (Ribas & Boix, 2004; Ribas et al. 2006). Briefly, SH-SY5Y cells were first plated into 96 well clear-bottom plates 1 day prior to drug application. After 24 h of drug treatment, an MTS reagent (CellTiter 96 Kit; Promega Corp.) was added and absorbance at 490 nm was determined using an Infinite 200 PRO microplate reader (Tecan Trading AG, Männedorf, Switzerland). The absorbance values in the drug-treated wells were normalized to the absorbance values in wells containing the vehicle (0.05% DMSO). Background absorbance was determined in wells containing no cells and was subtracted from all values.

### 4.2.4 Whole-cell perforated patch clamp recordings

To assess the calcium channel agonist effects of GV-58, whole-cell currents through calcium channels were recorded using perforated patch methods as previously described (Tarr et al. 2013). The pipette solution consisted of 70 mm $Cs_2SO_4$, 60 mm CsCl, 1 mm $MgCl_2$ and 10 mm Hepes, at pH 7.4. The extracellular saline contained 130 mm choline chloride, 10 mm tetraethylammonium chloride (TEA-Cl), 2 mm $CaCl_2$, 1 mm $MgCl_2$ and 10 mm Hepes, at pH 7.4. All standard chemicals were obtained from Sigma-Aldrich Corp. (St Louis, MO, USA). Patch pipettes were fabricated from borosilicate glass and pulled to a resistance of ~1 MΩ.

Capacitive currents and passive membrane responses to voltage commands were subtracted from the data. A liquid junction potential of −11.7 mV was subtracted during recordings. Currents were activated by a depolarizing step from −100 mV to +20 mV, amplified by an Axopatch 200B amplifier, filtered at 5 kHz, and digitized at 10 kHz for subsequent analysis using pClamp 10 software (Molecular Devices, LLC, Sunnyvale, CA, USA). The tail current integral was measured before and after the application of a compound and the integral of each trace was normalized to its peak. All experiments were carried out at room temperature (22°C). GV-58 was bath-applied via a glass pipette in a ~0.5 ml static bath chamber during whole-cell recordings of calcium current.

### 4.2.5 LEMS passive transfer

To test GV-58 in a LEMS model NMJ, we utilized an established LEMS passive transfer mouse model (Fukunaga et al. 1983; Lang et al. 1984; Fukuoka et al. 1987; Smith et al. 1995; Xu et al. 1998; Flink & Atchison, 2002). Serum from patient aBC2 [calcium channel antibody titre: 3.2 fmol $L^{-1}$ (Tarr et al. 2013)] was used for all LEMS passive transfer models reported here and was collected using plasmapheresis. Control serum was obtained from the University of Pittsburgh Medical Center blood bank. The serum was filtered with a 0.22 μm filter prior to the injection protocol. Adult female CFW mice (16 mice aged 2–3 months at the beginning of passive transfer and weighing 25–32 g; Charles River Laboratories, Inc., Wilmington, MA, USA) received one i.p. injection of LEMS or control serum on day 1, and then an injection of 300 mg $kg^{-1}$ cyclophosphamide on day 2 to suppress the specific immune response to human IgG. This was followed by an i.p. injection of 1.5 ml LEMS or control serum once per day for 15–30 consecutive days. In all cases, experimenters were blinded to the injection conditions.

### 4.2.6 Intracellular recordings at mouse NMJs

Following the passive transfer protocol, mice were killed by $CO_2$ inhalation followed by thoracotomy in accordance with procedures approved by the University of Pittsburgh IACUC, and intracellular recordings to assess the LEMS-mediated deficit in transmitter release were made in the mouse epitrochleoanconeus (ETA) *ex vivo* nerve–muscle preparation as previously described (Tarr et al. 2013). The extracellular saline contained 150 mm NaCl, 5 mm KCl, 11 mm dextrose, 10 mm Hepes, 1 mm $MgCl_2$ and 2 mm $CaCl_2$ (pH 7.3–7.4). The nerve was stimulated with a suction electrode and muscle contractions were blocked by exposure to 1 μm μ-conotoxin GIIIB (Alomone Labs Ltd, Jerusalem, Israel) (Hong & Chang, 1989). Microelectrode recordings were performed using ~40–60 MΩ borosilicate electrodes filled with 3M potassium acetate. Spontaneous miniature synaptic events [miniature endplate potentials (mEPPs)] were collected for 1–2 min in each muscle fiber, and then 10–30 nerve-evoked synaptic events [endplate potentials (EPPs)] were collected with an inter-stimulus interval of 5 s. Each digitized point in each trace was corrected for non-linear summation (McLachlan & Martin, 1981). To calculate QC, the integral of signal under the average corrected EPP waveform was divided by the integral of signal under the average mEPP waveform recorded from each NMJ. This ratio calculates the average number of quanta that are released following each presynaptic action potential. To evaluate effects on short-term synaptic plasticity, a train of 10 EPPs with an inter-stimulus interval of 20 ms (50 Hz) was collected in each muscle fiber. In some recordings the protocol involved first performing vehicle (0.05% v/v DMSO) control recordings, then recording in the same muscle fibers after a 30–60 min incubation in either 50 μm GV-58 or 1.5 μm 3,4-DAP, and finally recording in the same muscle fibers again after a 30–60 min incubation in a combination of 50 μm GV-58 plus 1.5 μm 3,4-DAP. In other cases, we recorded only vehicle controls in a

group of muscle fibers prior to recording in the same muscle fibers following a 30–60 min incubation in a combination of 50 μm GV-58 plus 1.5 μm 3,4-DAP. There was no significant difference in QC between a sequential (vehicle→GV-58 or 3,4-DAP→GV-58 and 3,4-DAP; 104.60 ± 5.45, n = 41) and a non-sequential (vehicle→GV-58 plus 3,4-DAP; 106.00 ± 5.53, n = 22) application of drugs ($p$ = 0.86, Student's $t$ test). Similarly, there was no significant difference in short-term plasticity between a sequential (normalized 10th EPP: 0.725 ± 0.025, n = 45) and a non-sequential (normalized 10th EPP: 0.737 ± 0.024, n = 30) application of drugs ($p$ = 0.72, Student's $t$ test). Therefore, the data from both the sequential and non-sequential application protocols were pooled. Recordings made in 1.5 μm 3,4-DAP also contained the vehicle (0.05% v/v DMSO). A 3,4-DAP concentration of 1.5 μm was chosen because previous studies have reported that oral administration of 3,4-DAP to patients leads to peak serum levels of ~70–150 ng ml−1 (Aisen et al. 1995; Wirtz et al. 2009), which corresponds to a concentration of ~0.5–1.5 μm. We chose a GV-58 concentration of 50 μm because this concentration showed maximal agonist effect in patch clamp studies of calcium current (Liang et al. 2012; Tarr et al. 2013). Data were collected using an Axoclamp 900A and digitized at 10 kHz for subsequent analysis using pClamp 10 software.

### 4.2.7 Statistical analysis

Statistical analysis was performed using either GraphPad Prism Version 5.0 (GraphPad Software, Inc., La Jolla, CA, USA) or Origin 7 (OriginLab Corp., Northampton, MA, USA). Data are presented as the mean ± s.e.m. unless otherwise noted. The significance level was set at $p < 0.05$ for all statistical tests.

## 4.3 RESULTS

### 4.3.1 Reduced Cdk activity of GV-58

Our initial screens of GV-58 for Cdk antagonist activity were performed in low ATP levels (10 μm) (Liang et al. 2012; Tarr et al. 2013). However, because (*R*)-roscovitine and GV-58 inhibit Cdks by competing with ATP at the ATP binding site on Cdks (De Azevedo et al. 1997), we compared the Cdk inhibitory effects of (*R*)-roscovitine and GV-58 under physiological ATP conditions in a cell survival assay (Figure 15) (Ribas & Boix, 2004). Using this assay, we found an IC50 of 52.6 μm for (*R*)-roscovitine (n = 6 at each concentration), which is similar to previous results obtained in mammalian cell lines (Meijer et al. 1997; Ribas & Boix, 2004). Interestingly, GV-58 did not reduce cell survival at concentrations up to 50 μm, and caused only an 8% reduction in cell survival at 100 μm (n = 12 at each concentration; $p < 0.05$; one-sample *t* test), indicating that, in the presence of physiological levels of ATP in an in vitro assay, GV-58 does not inhibit Cdks in the concentration range used for calcium channel agonist effects (≤50 μm) (Figure 15).

### 4.3.2 Voltage-dependent effects of GV-58 on calcium channels

Previous studies with (*R*)-roscovitine have shown that it preferentially affects to calcium channels in the open conformation in order to induce agonist effects (Buraei et al. 2005). To test if GV-58 has a similar mechanism of action, we performed whole-cell patch clamp recordings on cell lines expressing P/Q-type calcium channels and gave square-step depolarizations to +20 mV of varying durations in the presence of 50 μm GV-58 (Figure 16A and B). A long, 100 ms

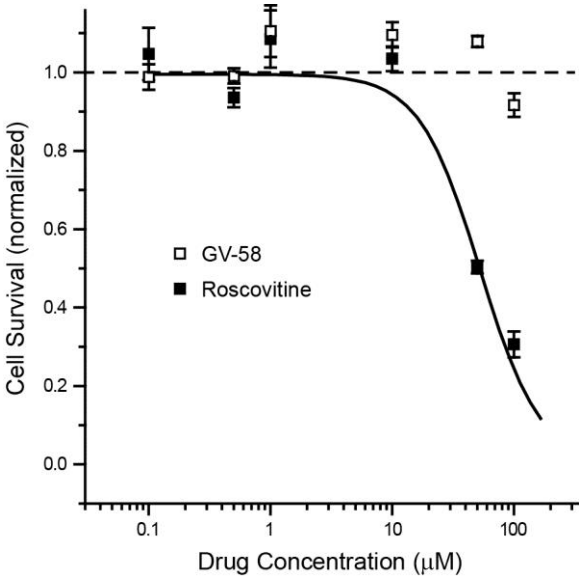


**Figure 15. GV-58 does not inhibit cell survival at concentrations required for calcium channel agonist effects.** Dose–response curve for inhibition of SH-SY5Y cell survival with (*R*)-roscovitine and GV-58 in an in vitro assay with physiological levels of ATP. Cell survival was measured at six different concentrations of (*R*)-roscovitine (n = 6 at each concentration) or GV-58 (n = 12 at each concentration). Data are normalized to values recorded in control cells and expressed as the mean ± S.E.M. for each concentration. The dotted line represents no change in cell survival. The (*R*)-roscovitine data are fit using the Hill equation for dose–response relationships.

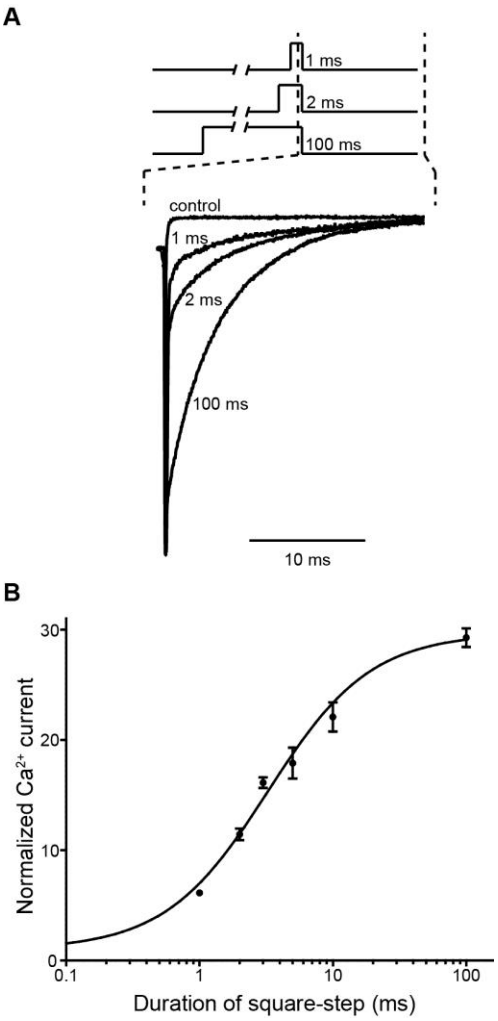


**Figure 16. GV-58 elicits calcium channel agonist effects by preferentially affecting the open conformation of the channel.**

**A.** representative traces for the voltage step to +20 mV for 1 ms, 2 ms and 100 ms (top) and the resultant calcium current traces (bottom) in the presence of 50 μM GV-58 (tail currents are shown starting at the end of the depolarizing step). A control trace in response to a 100 ms step prior to application of GV-58 is shown for comparison. The amplitude of each current trace is scaled to the amplitude of the control current trace to allow the comparison of decay kinetics. The dashed line indicates the portion of voltage traces (top) that correspond to the sample current traces (bottom). **B.** the calcium channel agonist effect of GV-58 at voltage steps to +20 mV of 1 ms, 2 ms, 3 ms, 5 ms, 10 ms and 100 ms duration (n = 3–9 for each duration). Each GV-58-modified tail current integral was first normalized to its peak and then normalized to the control current integral prior to GV-58 application. Data are expressed as the mean ± S.E.M. and fit using the Hill equation for dose–response relationships.

square-step resulted in a strong GV-58 agonist effect on the calcium channel tail current; therefore, in our analysis, all other square-step durations were normalized to this value. As the duration of the square-step was decreased, the magnitude of the GV-58 agonist effect also decreased. Nevertheless, GV-58 still elicited an approximately six-fold increase in the calcium channel tail current during very short duration square-steps of 1 ms (Figure 16B), which is similar to the half-width of a presynaptic action potential. Not only do these data suggest that GV-58 preferentially affects to calcium channels that are in open conformation, but they also support the notion that GV-58 can significantly increase calcium entry during physiological stimulus conditions.

### 4.3.3 Supra-additive effects of GV-58 plus 3,4-DAP on LEMS model NMJs

The patch clamp data presented in Figure 16 show that GV-58 has a greater effect when more calcium channels are open, which would occur when the depolarizing stimulus is longer in duration. Because 3,4-DAP induces the opening of more calcium channels by prolonging the duration of the presynaptic action potential (Kirsch & Narahashi, 1978), we sought to investigate the intriguing possibility that 3,4-DAP and GV-58 would interact to cause a supra-additive effect. To test this hypothesis, we performed intracellular microelectrode recordings on *ex vivo* nerve–muscle preparations taken from LEMS passive transfer model mice and measured the magnitude of acetylcholine released at the NMJ. The most sensitive method of quantifying the magnitude of acetylcholine released is to determine the QC. We determined the QC by first measuring the area under the average action potential-evoked EPP waveform and then dividing this value by the area under the average single vesicle release event (mEPP) waveform. Using this approach, we compared the QC among five experimental conditions: control serum NMJs;

LEMS NMJs in the vehicle (0.05% DMSO); LEMS NMJs exposed to 50 μm GV-58; LEMS NMJs exposed to 1.5 μm 3,4-DAP, and LEMS NMJs exposed to 50 μm GV-58 plus 1.5 μm 3,4-DAP (Figure 17). We chose to use a concentration of 1.5 μm 3,4-DAP because previous studies have reported the oral administration of 3,4-DAP in patients to lead to peak serum levels of ~70–150 ng $ml^{-1}$ (Aisen et al. 1995; Wirtz et al. 2009), which corresponds to a concentration of ~0.5–1.5 μm. NMJs taken from LEMS model mice showed significantly reduced QC (n = 63 terminals; QC 26.7 ± 1.4; EPP amplitude 10.18 ± 0.62 mV) compared with control serum-treated mouse NMJs (n = 41 terminals; QC 107.5 ± 3.6; EPP amplitude 34.62 ± 1.37 mV) ($p < 0.05$, one-way ANOVA with Tukey's *post hoc* test) (Tarr et al. 2013). After exposure to 50 μm GV-58, the QC in LEMS NMJs was significantly larger (n = 20 terminals; QC 48.4 ± 2.7; EPP amplitude 13.75 ± 1.244 mV) than the QC in vehicle controls ($p < 0.05$, one-way ANOVA with Tukey's *post hoc* test). In fact, this GV-58-mediated enhancement was very similar to the significant enhancement observed after exposing LEMS model NMJs to 1.5 μm 3,4-DAP (n = 21 terminals; QC 49.0 ± 4.4; EPP amplitude 17.94 ± 1.381 mV) ($p < 0.05$, one-way ANOVA with Tukey's *post hoc* test). Interestingly, when LEMS model NMJs were exposed to a combination of 50 μm GV-58 plus 1.5 μm 3,4-DAP, QC increased (n = 63 terminals; QC 105.1 ± 4.0; EPP amplitude 32.30 ± 1.85 mV) ($p < 0.05$, one-way ANOVA with Tukey's *post hoc* test) such that it was not significantly different from the QC measured from NMJs taken from control serum-treated mice ($p \geq 0.05$, one-way ANOVA with Tukey's *post hoc* test). These data indicate that the magnitude of transmitter release in LEMS model NMJs was completely restored to control levels under conditions of exposure to both GV-58 and 3,4-DAP (Figure 17B). The combination of these two drugs also slightly, but significantly, prolonged the duration of the EPP [full width at half-maximum 3.08 ± 0.05 ms and 3.84 ± 0.07 ms for control serum (n = 41 terminals) and 50 μm

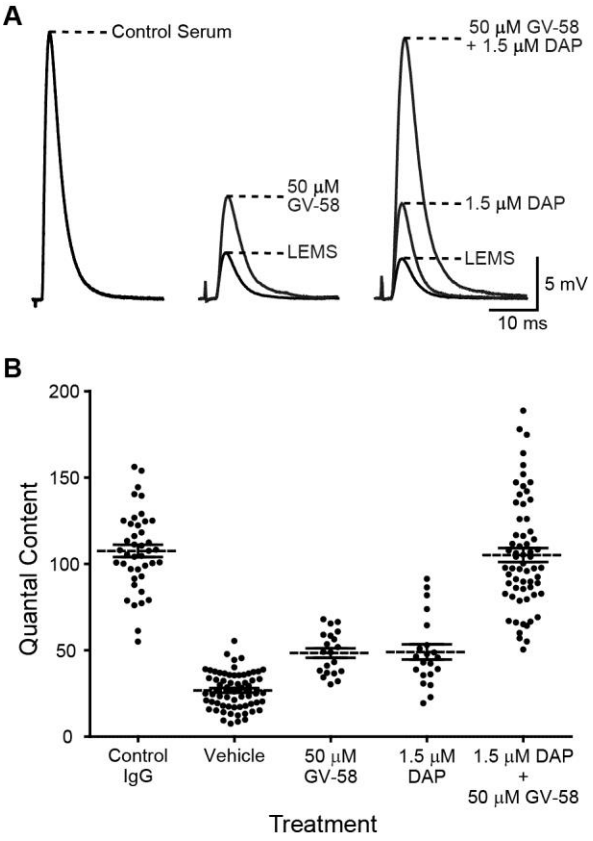


**Figure 17. The supra-additive effect of GV-58 plus 3,4-DAP completely reverses the deficit in the magnitude of neurotransmitter release.**

**A.** sample traces showing average endplate potential (EPP) amplitudes following exposure to the indicated conditions. Left: sample average EPP recorded from a neuromuscular junction (NMJ) in a control serum-treated mouse. Middle: sample average EPPs of a Lambert–Eaton myasthenic syndrome (LEMS) model NMJ before and after application of 50 µM GV-58. Right: sample average EPPs recorded from a LEMS model NMJ before drug application (LEMS), following application of 1.5 µM 3,4-DAP, and following application of 50 µM GV-58 plus 1.5 µM 3,4-DAP. **B.** quantal content for NMJs in each of the five conditions: NMJs from control serum-treated mice (n = 41); LEMS model NMJs in the presence of vehicle (n = 63); LEMS model NMJs following application of 50 µM GV-58 (n = 20); LEMS model NMJs following application of 1.5 µM 3,4-DAP (n = 21), and LEMS model NMJs following application of 50 µM GV-58 plus 1.5 µM 3,4-DAP (n = 63). Data are represented as the mean ± S.E.M.

GV-58 plus 1.5 μm 3,4-DAP (n = 63 terminals), respectively; $p < 0.05$, Student's independent-samples *t* test]. The potential impact of this small change in EPP duration on neuromuscular function in vivo is unknown.

### 4.3.4 Effects of GV-58 plus 3,4-DAP on short-term synaptic plasticity

In addition to measuring the properties of individual action potential-evoked events, we also measured and compared short-term synaptic plasticity characteristics among all conditions by eliciting a train of 10 stimuli at 50 Hz (Figure 18). In NMJs taken from mice injected with control patient serum, the magnitude of transmitter release did not change much during the first few stimuli in the train, and the 10th EPP in the train depressed to 66% of the first EPP (n = 41 terminals) (Tarr et al. 2013). By contrast, LEMS model NMJs showed strong facilitation throughout the train, with the 10th EPP showing facilitation to ~148% of the first EPP (n = 75 terminals). Both the 50 μm GV-58 condition (10th EPP at ~123% of the first EPP; n = 24 terminals) and the 1.5 μm 3,4-DAP condition (10th EPP at ~132% of the first EPP; n = 21 terminals) showed only a partial restoration of normal short-term plasticity characteristics. However, when the combination of 50 μm GV-58 plus 1.5 μm 3,4-DAP was applied, there was a near complete restoration of normal short-term plasticity characteristics, with a small amount of facilitation during the first few EPPs of the train and a depression at the 10th EPP to ~73% of the first EPP (n = 75 terminals) (Figure 18).

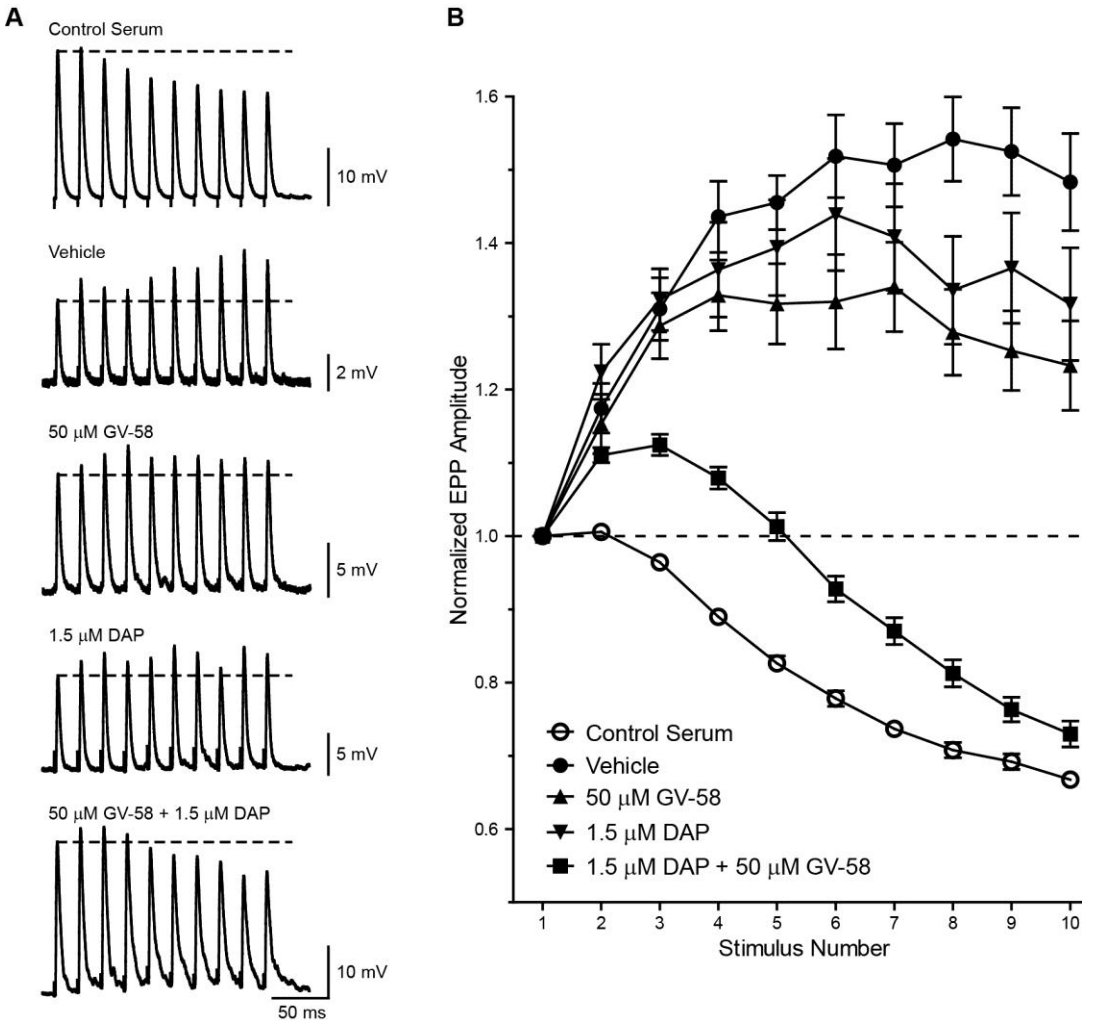


**Figure 18. The supra-additive effect of GV-58 plus 3,4-DAP elicits a near complete restoration of short-term synaptic plasticity characteristics.**

**A.** sample endplate potentials (EPPs) recorded from neuromuscular junctions (NMJs) in each of the five conditions during a 50 Hz train of 10 stimuli. Dashed lines indicate the amplitude of the first EPP in each train. **B.** average change in EPP amplitude during a 50 Hz stimulus train for NMJs from control serum-treated mice (n = 41), Lambert–Eaton myasthenic syndrome (LEMS) model NMJs in vehicle (n = 75), LEMS model NMJs after application of 50 μM GV-58 (n = 24), LEMS model NMJs following application of 1.5 μM 3,4-DAP (n = 21), and LEMS model NMJs following application of 50 μM GV-58 plus 1.5 μM 3,4-DAP (n = 75). Each EPP in the train is first normalized to the first EPP in the train before responses from many trials are averaged. The average normalized values are then plotted for each treatment condition. Data are represented as the mean ± S.E.M. The dashed line represents no change from the amplitude of the first EPP in the train.

## 4.4 DISCUSSION

The present study further evaluates the potential of GV-58 as a novel treatment for LEMS. In particular, we show that 50 μm GV-58 is not toxic to dividing cells in culture, suggesting that GV-58 is not an effective Cdk inhibitor under physiological ATP conditions at concentrations that show maximal effects on calcium channels. This is in contrast with findings of inhibitory effects of GV-58 at lower concentrations using a Cdk kinase assay with very low concentrations of ATP (Liang et al. 2012; Tarr et al. 2013). These data indicate that GV-58 competes with ATP at the ATP binding site on Cdks; therefore, given the high physiological levels of intracellular ATP (Maechler et al. 1998; Kennedy et al. 1999), these data mitigate the potential concern that Cdk inhibition will impede the development of optimized (R)-roscovitine analogues, such as GV-58, as potential therapeutics in LEMS.

Whereas either GV-58 or 3,4-DAP in isolation caused an increase of about 80% in the magnitude of transmitter release from LEMS model NMJs, the combination of GV-58 plus 3,4-DAP elicited an increase of approximately 300% in transmitter release magnitude, which is beyond that expected of a simple additive effect. This supra-additive effect is not surprising given the mechanistic actions of the two compounds. By blocking potassium channels, 3,4-DAP causes a broadening of the presynaptic action potential (Kirsch & Narahashi, 1978), which, in turn, leads to an increase in the number of open calcium channels per action potential. GV-58 is a calcium channel agonist that increases the amount of calcium influx by prolonging the duration for which calcium channels will remain open only after they have been induced to open by voltage depolarization. When both compounds are applied simultaneously, more calcium channels are opened as a result of the action of 3,4-DAP, and GV-58 can therefore elicit a greater increase in calcium influx than it can when applied alone because more open channels are

available. The interaction between these two compounds leads to a complete restoration of neurotransmitter release magnitude in LEMS model mouse NMJs (Figure 17). In addition, the combination of GV-58 and 3,4-DAP caused a small increase (~0.76 ms) in the duration of the EPP waveform. Although we cannot know how this might affect neuromuscular synaptic transmission, we do not believe it to be a major issue because the change is small.

The slight differences in short-term synaptic plasticity that persist in LEMS model NMJs treated with GV-58 plus 3,4-DAP may reflect several factors. Firstly, the combined effects of GV-58 and 3,4-DAP can completely restore transmitter release magnitude in LEMS model NMJs because both the probability of opening (3,4-DAP) and the flux of calcium (GV-58) through the reduced number of calcium channels that remain in the active zones of these LEMS model NMJs are enhanced. The enhanced calcium flux at the reduced number of calcium entry sites in these nerve terminals would be predicted to create a different spatial and temporal profile of presynaptic calcium concentration following each action potential, which may enhance the residual calcium effects that critically influence short-term synaptic plasticity. Secondly, previous freeze-fracture electron microscopic studies of LEMS active zones have revealed a disruption in the organization of presynaptic proteins (presumed to include calcium channels) (Fukunaga et al. 1983; Fukuoka et al. 1987; Nagel et al. 1988). If this disruption changes the spatial distance between the remaining presynaptic calcium channels and docked synaptic vesicles that are ready for release, this may also affect short-term synaptic plasticity at these synapses. The potential impact of both of these issues at LEMS model synapses will require further study.

Overall, our data show that exposure of LEMS model mouse NMJs to a combination of 3,4-DAP plus our novel calcium channel agonist (GV-58) completely reverses the deficit in

neurotransmitter release magnitude that underlies the neuromuscular weakness that is characteristic of LEMS NMJs. This effect of the two compounds is not simply additive, but is supra-additive based on the mechanism of action of each compound. These data lead us to propose a new combination treatment strategy for LEMS that should be explored further in pre-clinical evaluation, including in vivo animal studies and studies to determine factors such as off-target effects, toxicity and blood–brain barrier penetrance. Lastly, this treatment strategy may also prove beneficial for those with disorders that respond positively to 3,4-DAP treatment (Sedehizadeh et al. 2012), such as muscle-specific kinase (MuSK) myasthenia (Mori et al. 2012; Morsch et al. 2013), congenital myasthenic syndromes (Schara et al. 2012), botulism (Adler et al. 2012), and amyotrophic lateral sclerosis (Bertorini et al. 2011).

# 5.0 CHAPTER FOUR: BUILDING AN MCELL MODEL TO EXPLAIN DIFFERENCES IN RELEASE CHARACTERISTICS AND DRUG EFFECTS BETWEEN NORMAL AND LEMS NMJS

## 5.1 INTRODUCTION

In Lambert-Eaton myasthenic syndrome (LEMS), the normally reliable neuromuscular junction (NMJ) becomes unreliable due to an autoimmune-induced attack on the presynaptic motor nerve terminal, targeting predominately the presynaptic P/Q-type calcium channels responsible for neurotransmitter release. As a result of this attack, there is a reported reduction in the number of presynaptic calcium channels (Lennon et al., 1995; Meriney et al., 1996; O'Suilleabhain et al., 1998), which leads to reduced neurotransmitter release and therefore less reliable activation of the postsynaptic muscle fibers. Freeze fracture studies of mouse NMJs after LEMS passive transfer have also reported a disruption in the normally ordered array of active zone organization (Fukunaga et al., 1983; Nagel et al., 1988). Further, the presynaptic terminal appears to react to this attack by upregulating the expression of other calcium channel subtypes (Flink and Atchison, 2002), but despite this attempted homeostatic compensation, there still appears to be smaller presynaptic calcium current (Xu et al., 1998) and less neurotransmitter release. Therefore, at LEMS-modified synapses, it is hypothesized that there are fewer P/Q-type calcium

channels, a slight upregulation of other calcium channel types, and a disruption in active zone organization.

Given the alterations that likely exist at the LEMS-modified active zone, symptomatic treatment focuses on increasing calcium entry and transmitter output. The current common symptomatic treatment option for LEMS is 3,4-diaminopyridine (DAP) (Maddison, 2012; Sedehizadeh et al., 2012), a potassium channel blocker that prolongs the presynaptic action potential and increases the likelihood that calcium channels open in response to an action potential (Kirsch and Narahashi, 1978), thus increasing the probability of neurotransmitter release. Although DAP is modestly effective for most LEMS patients, there is a portion of LEMS patients who cannot get symptomatic relief from DAP because of dose-limiting side effects. Furthermore, even those that receive symptomatic relief report incomplete recovery (Sedehizadeh et al., 2012). Therefore, other treatment options would be beneficial for LEMS patients.

In Chapter 1 of this document, I have argued that there are two low-probability components in the process of neurotransmitter release at the mouse NMJ: the low probability that calcium channels open in response to a presynaptic action potential and the low probability that a vesicle will be released even when a nearby channel does open. The first low probability component basically means that there is a low probability that a ready-to-be-released vesicle will have an open channel in its vicinity. In LEMS, the low probability of release at the NMJ is exacerbated to pathological levels, so symptomatic treatment options should, in theory, target one or both of the low probability components of release. DAP increases the probability of channel opening during an action potential, so it targets the first low probability component of release. We previously described the synthesis of a novel calcium channel agonist that increases

the amount of calcium influx when channels do open (Tarr et al., 2013b). This compound (GV-58) targets the second low-probability component of release, the low probability that release occurs when a nearby channel does open, by increasing the amount of calcium influx through open channels. Both DAP and GV-58 increase neurotransmitter release in LEMS model NMJs, although neither alone can return release to control levels (Tarr et al., 2013b; Tarr et al., 2014). We showed that these two low-probability components are cooperative, such that targeting both with a combination of DAP and GV-58 leads to a supra-linear increase in neurotransmitter release in LEMS model NMJs (Tarr et al., 2014).

One minor, but interesting observation in these dual drug treated synapses is related to short-term plasticity characteristics. Even though a combination of DAP and GV-58 completely restored the magnitude of neurotransmitter release, short-term plasticity characteristics were only partially restored to control levels (Tarr et al., 2014). Considering this information, as well as the upregulation of other calcium channel subtypes (Xu et al., 1998; Flink and Atchison, 2002) and previous reports showing a disruption in active zone structure according to freeze-fracture EM (Fukunaga et al., 1983; Nagel et al., 1988), it is reasonable to hypothesize that the LEMS-mediated reduction in neurotransmitter release is more complex than a simple removal of P/Q-type calcium channels.

In order to help us understand the disconnect between full quantal content recovery and partial short-term plasticity recovery after GV-58 and DAP combination treatment in LEMS model mouse NMJs, we sought to build an MCell model of a LEMS active zone using our previously discussed MCell model of the mouse NMJ active zone as a starting point. The basic goal was to build a model of the mouse active zone in which neurotransmitter release was reduced by ~75% and the facilitation ratio of the 4$^{th}$ stimulus (EPP4 amplitude/EPP1 amplitude)

during 50 Hz trains was increased to ~1.3-1.4. The hypothesis was that a parameter search in the MCell model would lead to candidate mechanistic explanations for observed effects. In this study, we altered several model parameters that were consistent with previous experimental observations (number of calcium channels in the active zone, number of calcium channels outside of the active zone, and distance between channels and docked vesicles). By altering the number of channels in the active zone, we modeled a reduction in the number of P/Q-type channels that physically couple to docked synaptic vesicles via the synprint site (Rettig et al., 1996; Yokoyama et al., 2005). The addition of extra calcium channels outside of the active zone double rows was motivated by a desire to model the compensatory upregulation of L-type channels that would not be expected to associate directly with docked synaptic vesicles (due to their lack of a synprint sequence). Lastly, by altering the distance between channels and docked synaptic vesicles we could explore the impact of a disruption in active zone structure on synaptic function. After testing multiple configurations and combinations of these parameters, we found that the best match for the experimental data included a mixture of reduced active zone channels and increased channels outside of the active zone.

## 5.2 METHODS

### 5.2.1 Model geometry

All simulations were done using MCell 3.1 (Kerr et al., 2008) using our previously described MCell model of the mouse NMJ active zone (Ma, 2014), which was built by simply rearranging the organization of the active zone (specifically the calcium channels and their spatial

relationship with respect to the vesicles) of our previously validated frog NMJ active zone model (Dittrich et al., 2013; Ma et al., 2015). Therefore, it would be useful to describe the characteristics of our model to help with the interpretation of our data. The initial mouse model contained 6 active zones spaced ~500 nm from one another (Ruiz et al., 2011). Each of the active zones in the initial model contained 2 vesicles (50 nm in diameter) and 2 closely-associated calcium channels on either side of each vesicle for a total of 4 calcium channels per active zone (Figure 19A). The distance between the center of each channel and the center of its closely-associated vesicle was 30 nm. The bottom hemisphere of each vesicle contained meshes representing two types of calcium sensors, 40 of which represented synaptotagmin-like binding sensors and 16 of which represented a second binding sensor (termed "Y" binding sites) with a slower unbinding rate than the synaptotagmin-like sensor (Figure 19B; Table 1; (Ma et al., 2015)).

### 5.2.2 Kinetics of calcium channels and calcium binding

calcium channel kinetics were identical to those in our previous reports (Dittrich et al., 2013; Ma et al., 2015), and consisted of a 4 state model (3 closed states and 1 open state) as follows:

$$C_0 \underset{\beta}{\overset{3\alpha}{\leftrightarrow}} C_1 \underset{2\beta}{\overset{2\alpha}{\leftrightarrow}} C_2 \underset{3\beta}{\overset{\alpha}{\leftrightarrow}} O \overset{k}{\rightarrow} \mathrm{Ca}^{2+}$$

The voltage-dependent rate constants between states were computed based on experimentally measured action potential and whole-cell calcium current waveforms (Dittrich et al., 2013). The channel conductance (G) was 2.4 pS (Church and Stanley, 1996). Once a channel entered its conducting state, calcium ions could diffuse throughout the terminal and bind to either of the two calcium sensor binding sites or bind to static calcium buffer molecules, which were at a

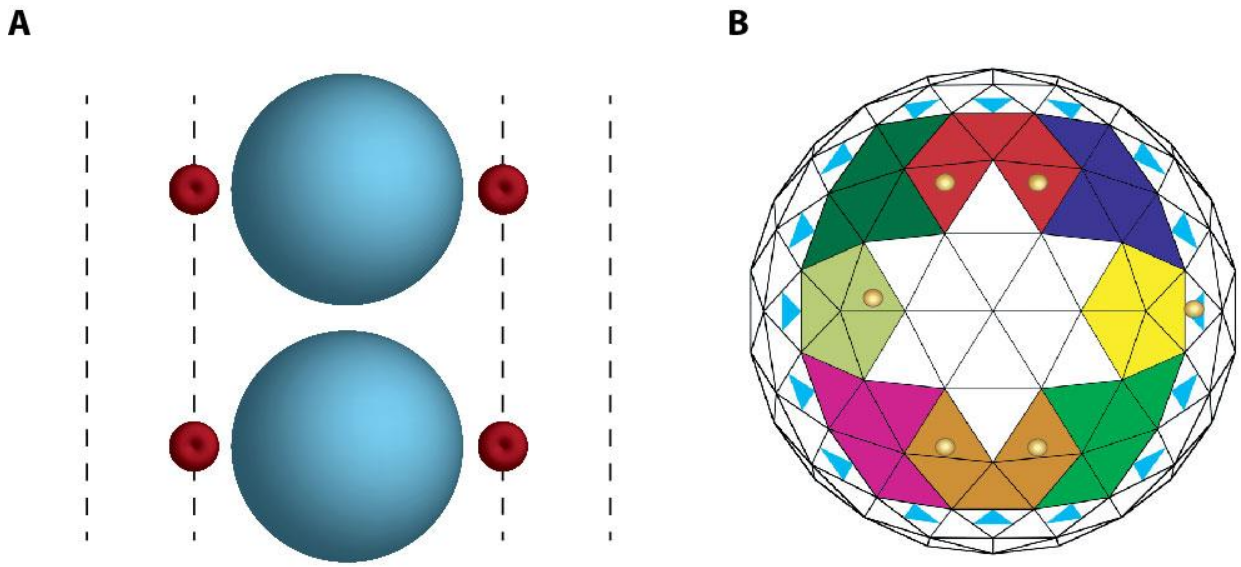


**Figure 19. MCell model of the mouse NMJ active zone.**

**A.** Initial configuration of the mouse NMJ active zone model as previously described (Ma, 2014). The two blue spheres represent docked vesicles, the red donuts represent P/Q-type calcium channels, and the dashed lines represent the approximate location of the rows of intramembranous particles observed in freeze-fracture EM (Fukunaga et al., 1983; Nagel et al., 1988). These schematic descriptors apply to Figures 19-24. **B.** Schematic of a vesicle and its calcium binding sites from our MCell model. The large colored triangular meshes represent synaptotagmin binding sites. Each color represents a different synaptotagmin with 5 binding sites each. The small blue triangles forming a ring around the outside of the synaptotagmin represent the Y binding sites. The small yellow spheres are calcium ions that have bound to either a synaptotagmin or a Y binding site. **B.** is adapted from Ma, 2014.

concentration of 2 mM in our model. The various rate constants, including the binding and unbinding rates for each of the calcium binding sites, as well as the diffusion coefficient for calcium, was identical to our previously described model (Ma et al., 2015).

### 5.2.3 Modeling of vesicle fusion

Vesicle fusion was modeled as previously reported (Ma et al., 2015). Briefly, the binding of calcium to either the synaptotagmin or Y binding sites reduced the free energy barrier for fusion, which was set at 40 kBT (Li et al., 2007a; Martens et al., 2007). Calcium binding to a synaptotagmin site reduced the free energy barrier by 9 kBT, and binding of calcium to the Y binding site reduced the free energy barrier by 11 kBT. Therefore, a vesicle had an increased probability to be released as more synaptotagmin and/or Y binding sites became "active" (synaptotagmin must bind 2 calcium ions simultaneously to become active while Y sites need only bind one calcium ion).

### 5.2.4 MCell simulations

We sought to build a LEMS active zone model by simply altering our previously described MCell model of the mouse NMJ active zone (Ma, 2014). The only features of the mouse NMJ active zone model that were altered in our parameter search were the number and organization of calcium channels in and around the active zone and the calcium-binding rate of the synaptotagmin-like synchronous release sensor site. Any change to the binding rate of the synchronous release sensor site was small and stayed within the range of previously reported values of $1 \times 10^8$ $M^{-1}s^{-1}$ and $4 \times 10^8$ $M^{-1}s^{-1}$ (Davis et al., 1999; Dittrich et al., 2013; Ma et al.,

2015). Changes to the number and organization/location of calcium channels were made in MCell's model description language (MDL) and then were verified using CellBlender. The simulations were run using a 4-pulse protocol with an interstimulus interval of 20 ms and a resting potential of -60 mV. The simulation time step was 10 ns to ensure accurate spatial sampling. At least 800 seeds of each configuration were run to determine that configuration's validity.

## 5.3 RESULTS

### 5.3.1 Building an accurate MCell model of the mouse NMJ active zone

Since our hypothesis is that LEMS-induced changes to the NMJ are more complex than a simple reduction of calcium channels in the active zone, we wanted to confirm that removing a significant portion of channels in the mouse NMJ active zone model did cause a LEMS-like phenotype. We have shown experimentally that a ~75-80% reduction in release due to 25 μM cadmium leads to facilitation (normalized to the first EPP in the train) of ~1.17 at the $4^{th}$ EPP in the train (Figure 6B). Similarly, a ~75-80% reduction in release due to 50 nM ω-agatoxin leads to a facilitation of ~1.25 at the $4^{th}$ EPP in the train (Figure 20B). When we reduced release in our mouse NMJ active zone model by a similar percent by removing 17 random calcium channels out of the total of 24 (our initial mouse NMJ active zone model contained 6 active zones with 4 calcium channels in each active zone; Figure 20A), the normalized release at the fourth stimulus in a 50 Hz train was only 0.90 (a mild depression; see Figure 20B), which was significantly less that the facilitation seen in LEMS or when blocking with ω-agatoxin (Figure 20B). This

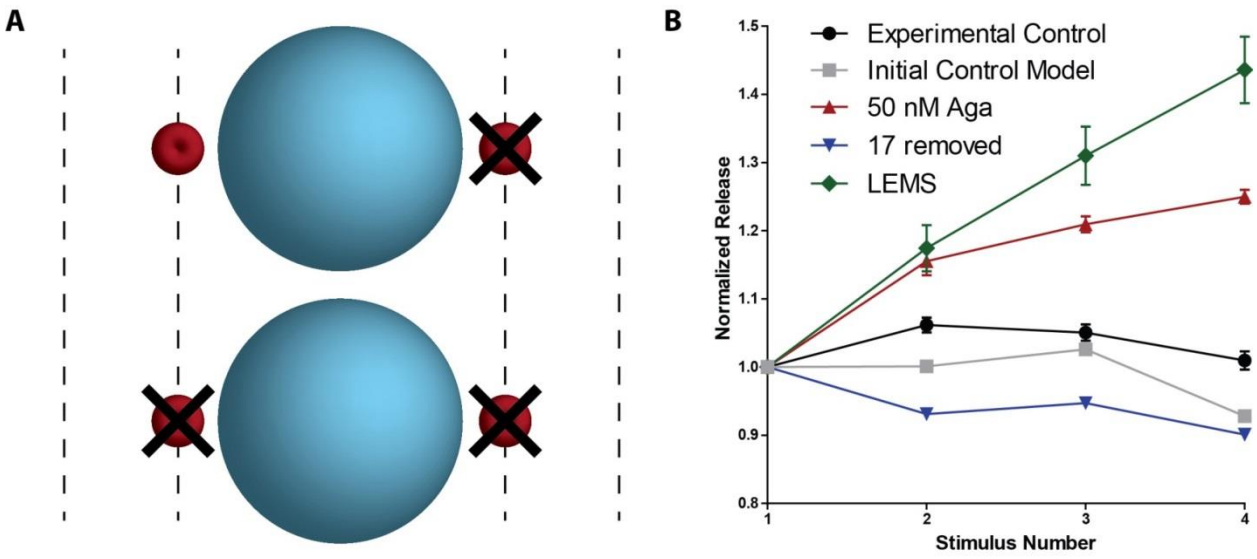


**Figure 20. Removing channels in model does not increase facilitation.**

**A.** Schematic of initial mouse NMJ active zone model with a portion of channels removed (represented by black Xs). **B.** Removing 17 (blue line) channels from the model (~75-80% reduction in release) did not increase facilitation to either Aga (red line) or LEMS (green line) levels.

indicated that before we continued to search for the right parameters for the LEMS model, the control model needed to be optimized.

We previously have shown that a simple rearrangement of the frog NMJ active zone model into the mouse NMJ active zone model closely matches the physiological characteristics of the mouse NMJ (Ma, 2014), although the short-term facilitation was slightly lower than the experimental results and this lower facilitation was even more apparent when removing a portion of the calcium channels (Figure 20B). Therefore, our next goal was to match more closely the facilitation in the control mouse NMJ before moving on to trying to create a LEMS-modified NMJ. We hypothesized that increasing the number of calcium channels, especially in the outer rows, could lead to greater facilitation because of a larger residual calcium effect. To test this hypothesis, we modeled multiple configurations that had an increase in the number of channels (Figures 21 and 22). We found that increasing the number of channels in the inner rows not only failed to increase facilitation to appropriate levels, but also increased the probability of release to much higher levels than those measured experimentally, even when we reduced the sensor binding rate 4-fold to $1.5 \times 10^8$ $M^{-1}s^{-1}$ (Figure 21B). Similarly, having 4 extra channels in the outer rows also increased probability of release beyond experimentally measured values and did not increase facilitation to appropriate levels (Figure 22B). However, having 2 extra channels in the outer row, either in a "diagonal" (2ch2rDg) or "middle" (2ch2rM) configuration, showed facilitation similar to that of our initial model (Figure 22B). Additionally, the probability of release with these two configurations was slightly higher than experimental values. Rather than continue to alter the number of channels in each active zone, we decided to alter the calcium-binding site binding rate because the initial mouse NMJ active zone model had a binding rate on the high end of reported literature values for synaptotagmin 1 ($4 \times 10^8$ $M^{-1}s^{-1}$ (Davis et al., 1999;

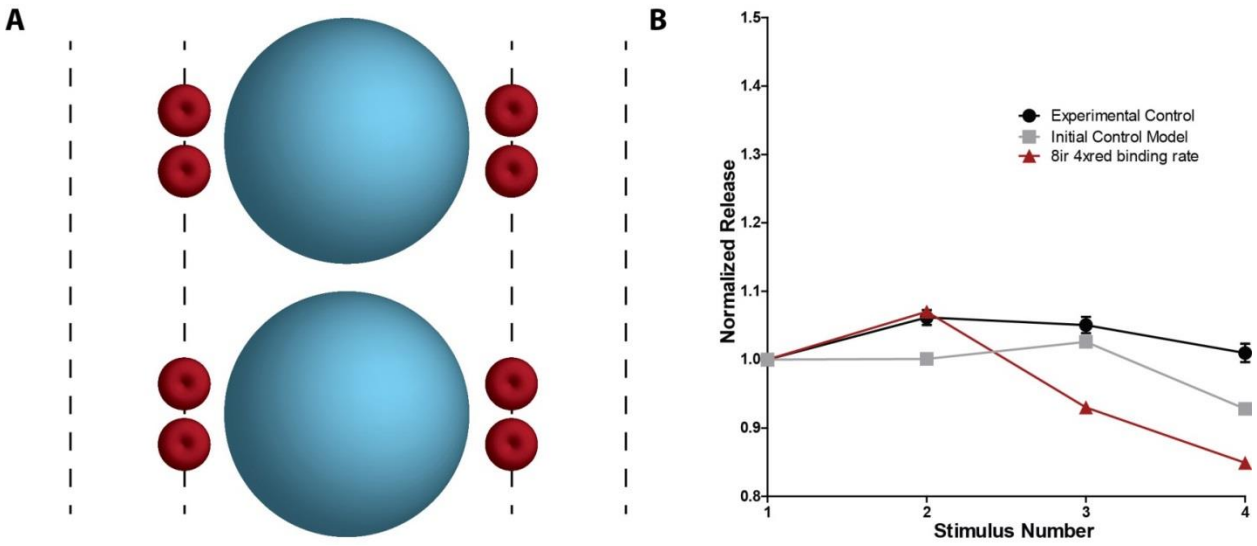


**Figure 21. Additional inner row channels cause too much release and depression.**

**A.** Schematic of mouse active zone model with 4 additional channels in the inner row. **B.** Although initially this model began to facilitate, depression became too extreme on the 3$^{rd}$ and 4$^{th}$ pulses.

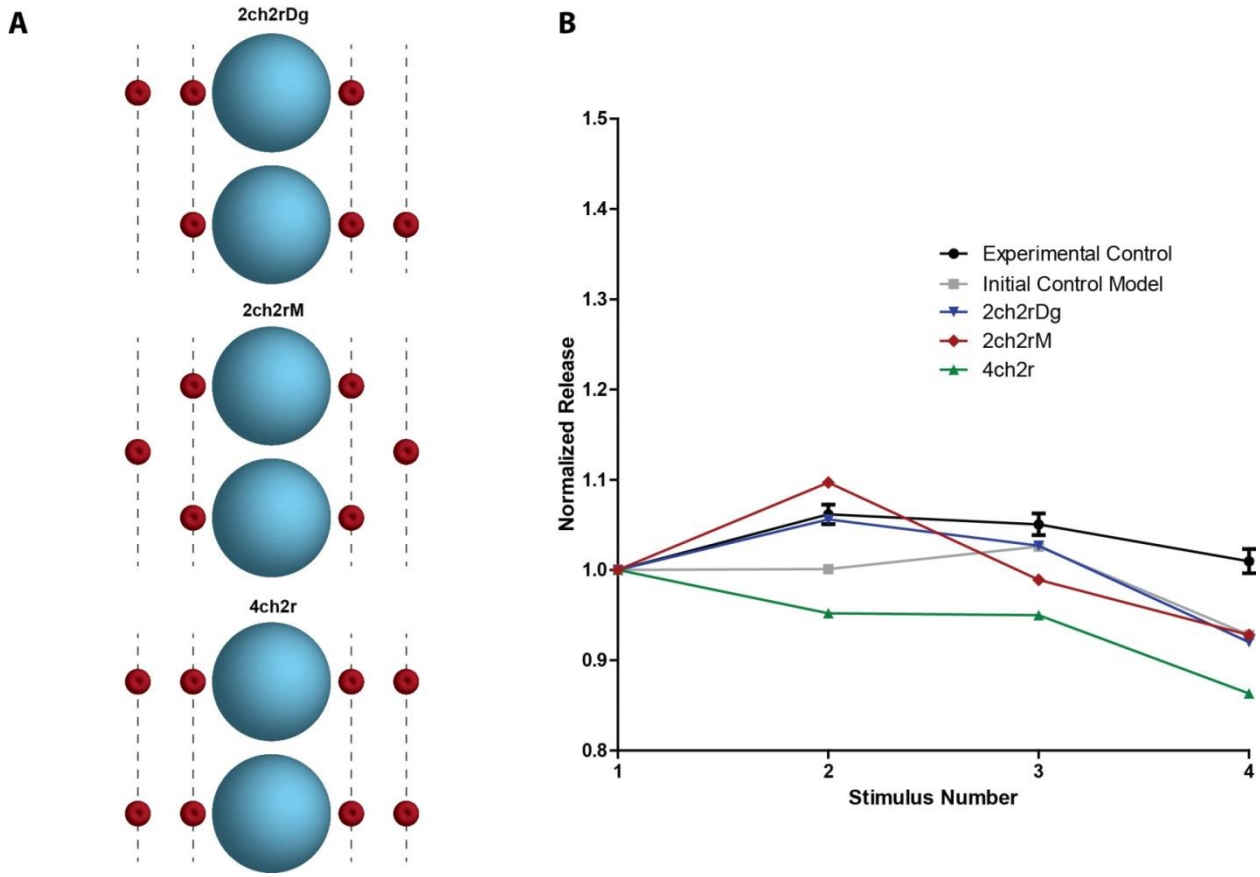


**Figure 22. Channels in the outer row lead to more facilitation.**

**A.** Different active zone configurations with extra channels in the second rows, including 2 channel diagonal (2ch2rDg, top), 2 channels middle (2ch2rM, middle) and 4 channels in line with the original 4 (bottom). **B.** Adding 2 channels to the outer rows either diagonally (blue line) or in the middle (red line) increased facilitation (diagonal slightly better at the 4$^{th}$ pulse), but adding 4 channels in the outer rows (green line) led to too much depression. **C**. Change the synaptotagmin binding rate to $1.5 \times 10^8$ $M^{-1}s^{-1}$ (blue line) increased facilitation to sufficiently match the experimental facilitation in control NMJs.

Dittrich et al., 2013; Ma et al., 2015)). We tried multiple binding rates in the 2ch2rDg configuration and found that a binding rate of $1.5 \times 10^8$ $M^{-1}s^{-1}$ had a probability of release within the experimental range and a slight decrease in depression at the 4th stimulus to 0.99 (Figure 22C), which was reasonably close to our control NMJ experimental faciliation value of ~1 at the $4^{th}$ stimulus (Figure 6). We decided to move forward with this configuration (2ch2rDg, kon = $1.5 \times 10^8$ $M^{-1}s^{-1}$) as our control mouse NMJ active zone model.

### 5.3.2 LEMS-induced active zone changes involve more than a reduction in calcium channel number

As previously mentioned, experimentally removing calcium channels with a blocker does not result in LEMS-like facilitation (Figure 6B). Previous reports have shown that there is an upregulation of other calcium channels subtypes, mainly the L-type channel, in LEMS (Xu et al., 1998; Flink and Atchison, 2002). Since the L-type channel does not have the synprint site, it is likely that these channels are inserted into the membrane outside of the active zone. We decided to model this possibility by adding channels outside of the double row of intramembranous particles in our mouse NMJ active zone while simultaneously removing a portion of channels from the two double rows within the active zone (which represent the LEMS-targeted P/Q-type calcium channels). Clearly there are innumerable configurations we could model, so we decided to test first the effect of adding channels 20 nm further out compared to the outer rows of the two double rows of particles. In essence, this would be similar to have two “triple rows” of intramembranous particles on either side of the two vesicles. This is obviously completely arbitrary, but we knew that modeling this type of configuration would inform us about the necessary distance that a channel must be relative to the vesicles in order for the channel to

contribute calcium ions towards the release of a vesicle. We started with two configurations, which were 2 channels located in the middle of the "third rows" and four channels located in parallel to the 4 channels of the inner row (Figure 23). As a reminder, these models with "third row" channels had a lower number of channels in the original double rows. The reasoning behind fewer channels in the original double rows is that the channels in the original double rows represent the P/Q-type calcium channels that are lost in LEMS, and the channels we added in the "third rows" represent L-type channels that are upregulated in LEMS. The addition of only one channel in the middle of each of the "third rows" did increase facilitation, although not to the level of LEMS model NMJs (Figure 23A). However, 4 channels in the "third rows" (2 in each "third row") produced too much release during a single action potential and less facilitation than produced when channels were removed from our 2ch2rDg control model (Figure 23B).

As adding 2 channels in the "third rows" increased facilitation but not to the level of facilitation seen in LEMS model NMJs, we knew we must consider a different configuration. Rather than changing the number of channels, we instead decided to shift the remaining channels further away from the vesicles by 10 nm (Figure 24). This was once again an arbitrary change, but it would at least inform us about the effect of moving all the remaining channels as opposed to continuously adding channels that are far away from the vesicles. This manipulation of the active zone actually led to too little release in single pulses and very little facilitation. It seems as though release is very sensitive to the movement of the channels closest active zone channels away from the vesicles.

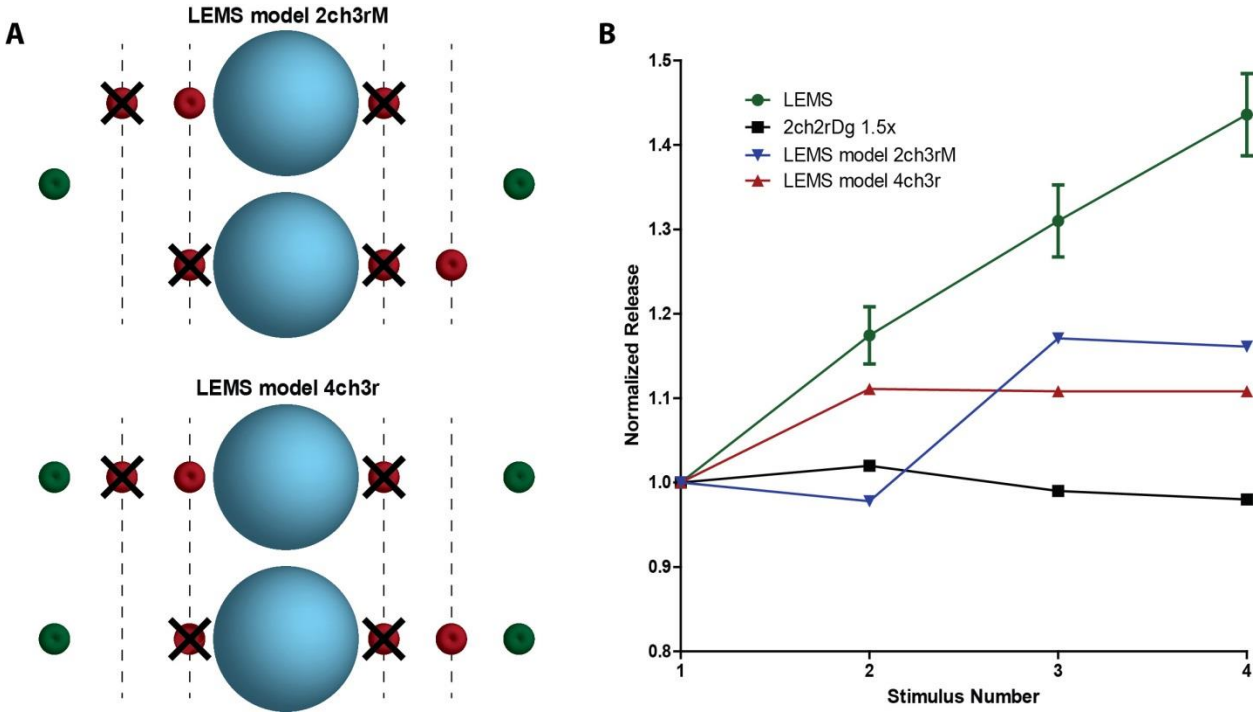


**Figure 23. Adding channels outside the active zone almost produces LEMS facilitation.**

**A.** Active zone schematic showing LEMS active zones with extra channels (presumably L-type, green donuts) being added outside of the normal active zone space while also removing a portion (18 out of 24) of the channels. **B.** Both 4 (red line) and 2 (blue line) extra channels outside the active zone increased facilitation, but neither made it to the level of LEMS experimental measurements (green line).

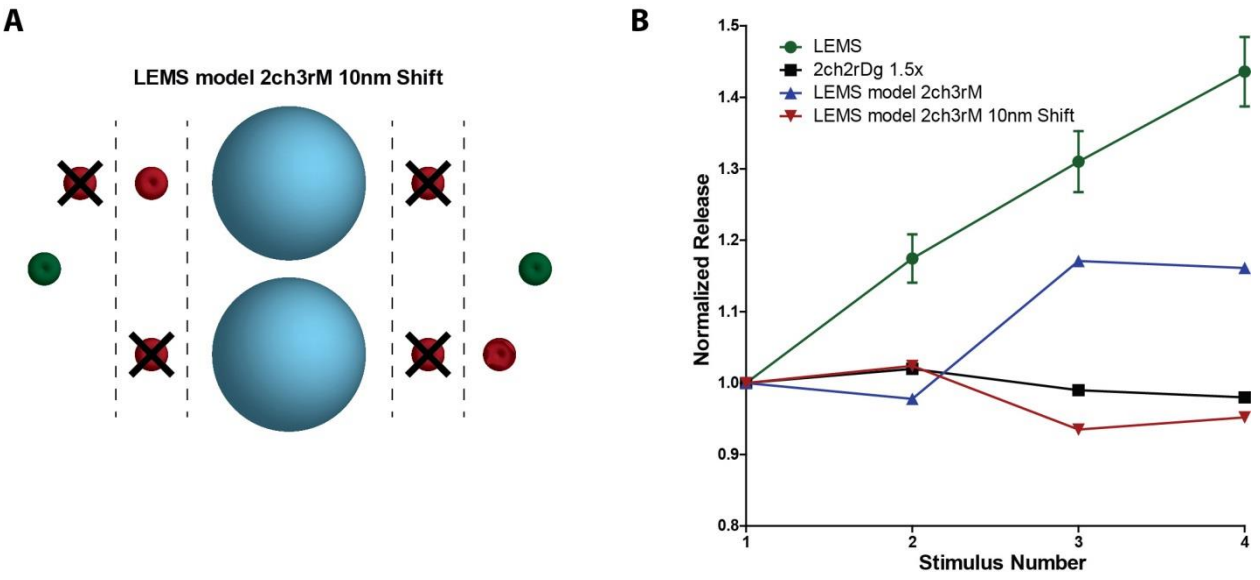


**Figure 24. Shifting all remaining channels does not mimic LEMS physiology.**

**A.** Diagram showing LEMS model from Figure 23A (top) that had its remaining channels shifted 10 nm away from the vesicles (18 channels are still being removed, black Xs). **B.** The shifted LEMS model (red line) led to even less facilitation than the control (no channels removed) model (black line).

## 5.4 DISCUSSION

### 5.4.1 Extra channels in the outer rows of the double rows of active zone protein positions leads to more facilitation in the control model

Here we have performed a parameter search with the hope of making an MCell model of the mouse NMJ that recapitulates the physiological characteristics of LEMS model mouse NMJs. Our MCell model of the mouse NMJ active zone was built by simply rearranging our previously validated frog NMJ active zone model without changing any of the parameters of the elements in the model, but until now we have not optimized the mouse NMJ active zone model to closely match the physiological characteristics of the mouse NMJ. Nonetheless, short-term plasticity characteristics were reasonably close when we initially made the mouse NMJ active zone model using this simple rearrangement. We attempted to match LEMS characteristics by removing a portion of calcium channels from our model such that release matched the amount of release measured experimentally in LEMS model NMJs (Figure 20). However, when we removed 17 out of the 24 channels (6 active zones with 4 channels in each), which reduced release by ~70-75% and thus matched the reduction we see in LEMS NMJs (Figure 17B), we actually only saw slight depression during a 4-pulse train at 50 Hz. Not only did this not match the strong facilitation to ~1.4 seen in LEMS NMJs (Figure 18), it also failed to match the slight facilitation (~1.2) we observed when we blocked ~75% of release in a control synapse with a channel blocker (Figure 20B). Although our initial mouse NMJ active zone model closely matched many parameters measured experimentally at the mouse NMJ (Ma, 2014), we needed to optimize the model to match more closely the experimentally measured short-term plasticity before we continued our parameter search for a LEMS MCell model.

Our original mouse NMJ active zone model lacked the appropriate amount of facilitation, so we began to make changes to the calcium channel configuration within active zones with the hope of increasing facilitation. We assumed a reasonable first step would be to add channels and thus increase the possibility of having calcium from one stimulus in the train remain bound within the active zone and affect release during a future stimulus in the train. We wanted to increase facilitation without having much effect on the probability of release during a single action potential, so we thought that having channels further away in the second rows of the double rows of intramembranous particles would be ideal for this. As expected, adding channels further away did increase facilitation (Figure 22), although not quite to the level we expected. Additionally, adding these channels in the outer rows on each side also increased the probability of release slightly. In contrast, adding more channels to the inner row seemed out of the question since facilitation was not improved and the probability of release was much too high. Fortunately for our models with extra channels in the outer rows, we could reduce the probability of release but still retain the desired short-term plasticity characteristics by slightly reducing the synaptotagmin binding rate (to a value still within the range of reported values). Of course, there was a limit to the number of channels we could add to the outer rows if we wanted to stay within our constraints. Having 2 extra channels seemed to be a reasonable fit, so we went forward with this model. This initial portion of the parameter search informed us that both the probability of release and short-term plasticity is greatly affected by the number of channels that are tightly coupled to the vesicle (in the inner rows), whereas short-term plasticity seems to be more affected than the probability of release by the number of channels further away or loosely coupled to the vesicle (in the outer rows). However, both parameters are less sensitive to changes in the number of channels in the outer row compared to changes in the number of channels in the

inner rows. We can't say with certainty that no configuration that increases the number of channels in the inner rows could increase facilitation, but the model seemed too sensitive to changes in the inner row channels to be of interest to us in our parameter search.

### 5.4.2 Extra channels outside of the active zone approaches LEMS-like facilitation

After our determination of a satisfactory control mouse NMJ active zone model (2ch2rDg; Figure 22), we once again attempted to build a model with output that matched experimentally measured values in LEMS NMJs. We noticed early on in our parameter search that simply removing channels does not increase facilitation much at all. We know that blocking a significant portion of calcium channels leads to facilitation (~1.1-1.25; Figure 6A and 20), but not to the level of LEMS facilitation (~1.4-1.5; Figure 18). Rather than attempting to match the facilitation observed with channel block, we proceeded to explore configurations that might match LEMS facilitation first. We know that other subtypes of calcium channels, especially L-type, are upregulated in LEMS (Xu et al., 1998; Flink and Atchison, 2002) and we also know that there seems to be a partial disorganization of active zone particles as a result of LEMS (Fukunaga et al., 1983; Nagel et al., 1988). Since L-type channels do not have a synprint site (although see (Wiser et al., 1999)), it is reasonable to hypothesize that L-type channels are being inserted into the terminal membrane outside of the active zones, and this may result in the greatly increased facilitation observed in LEMS NMJs. We tested this idea by adding channels 20 nm away from the outer rows of the two double rows of intramembranous particles (Figure 23), while still removing channels from the original inner and outer rows to mimic removal of P/Q-type channel reduction. As expected, adding channels in these "third rows" increased facilitation, although adding too many channels blunted the increase in facilitation (Figure 22). Interestingly,

we still could not reach LEMS facilitation levels using this approach. Therefore, the last configuration we tried was a 10 nm shift of all the remaining channels (Figure 24). Surprisingly, there was little or no facilitation in this configuration, although the steep reduction in the probability of release was not surprising. It is possible that the probability of release was reduced so much that significant facilitation was not possible. In any case, we abandoned this model and the idea of shifting all remaining channels since baseline release seemed to be especially sensitive to this manipulation. Even though we didn't match the LEMS facilitation completely, we made some basic observations about the relationship between active zone organization and synaptic function using our MCell mouse NMJ active zone model. Because we could not completely match the LEMS parameters, we hypothesize that factors other than the calcium channel number and organization play a role in LEMS pathophysiology (see General Discussion). Nevertheless, it is clear that active zone structure and organization play a critical role in determining the function at both normal and LEMS model NMJs.

# 6.0 GENERAL DISCUSSION

## 6.1 VESICLES HAVE AN AVERAGE LOW PROBABILITY OF RELEASE AT THE NMJ

In Chapter 1, I presented evidence that suggested that the mouse NMJ is built with hundreds or thousands of unreliable single-vesicle release sites (Figure 25). On average, the mouse NMJ releases a small number of quanta, relative to the total number of active zones, in response to a single presynaptic action potential. Our evidence suggests that the average probability of release per active zone is only ~0.1, and assuming two vesicles per active zone, the average probability of release per individual vesicle is only ~0.05. Therefore, any individual vesicle is not likely to be released in response to a presynaptic action potential if we assume functional homogeneity across all active zones.

Although we have assumed homogeneity across all active zones, many reports at other synapses, as well as at the mouse NMJ, suggest there are functional and structural differences among active zones within an individual terminal. For example, there is evidence concerning active zone heterogeneity at multiple CNS synapses, including the calyx of Held (Sheng et al., 2012) and small bouton synapses (Holderith et al., 2012; Scimemi and Diamond, 2012). Interestingly, there is evidence suggesting that some active zones control spontaneous miniature release while others control action-potential evoked release at CNS small bouton synapses

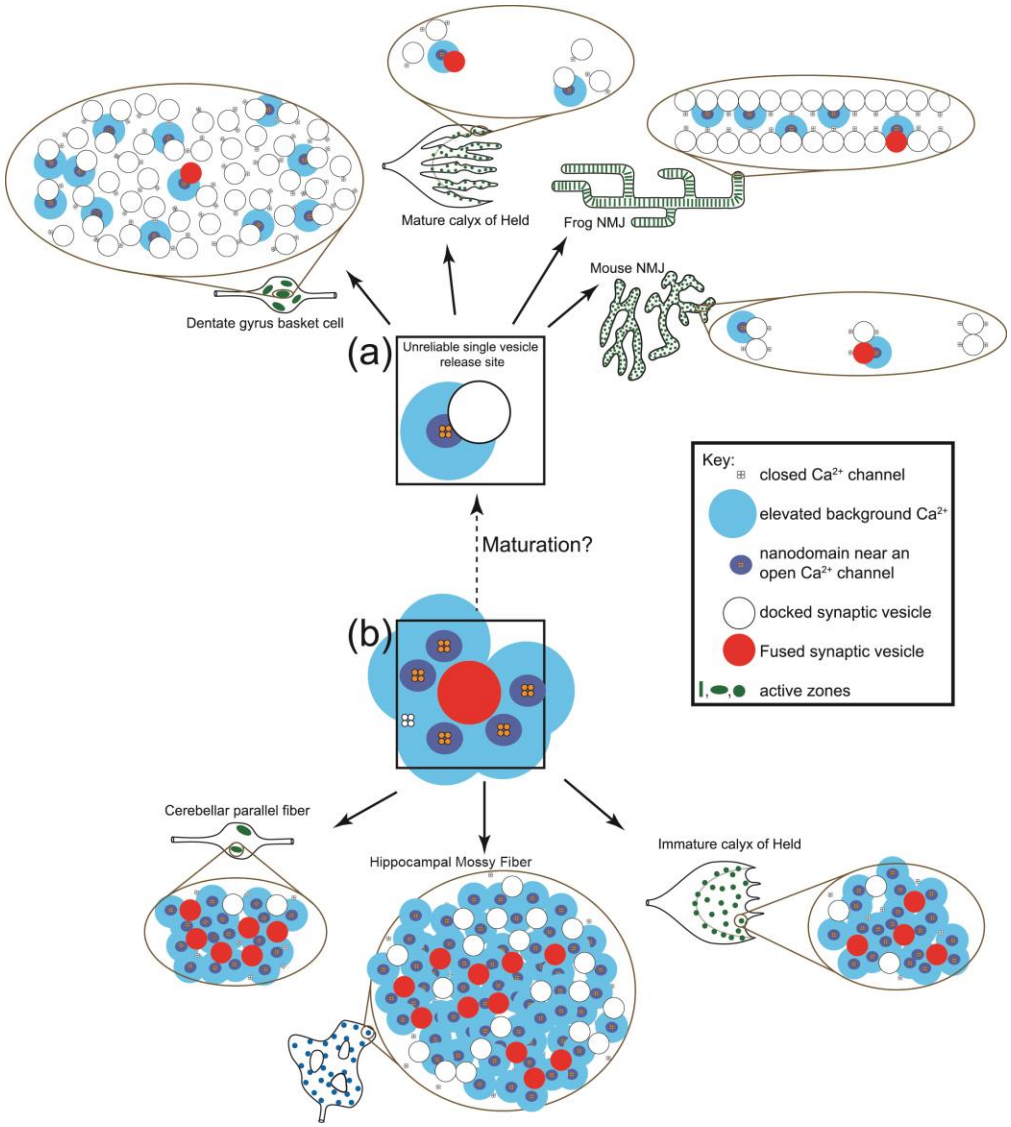


**Figure 25. Hypothetical model based on the unreliable single vesicle release site as a building block of mature synapses.**

Synaptic elements [calcium channels and synaptic vesicles] are depicted at the time of action potential invasion of the nerve terminal. **a.** Recent data have led to a model for synaptic assembly based on unreliable single vesicle release sites. These comprise a synaptic vesicle, sparse numbers of closely associated calcium channels that each open with a low probability during an action potential stimulus, and vesicle fusion that is triggered by the nanodomain of calcium flux from as few as one tightly associated calcium channel (dark-blue regions near the mouth of an open channel). Low release probability synapses can be constructed using a small number of these basic building blocks within a few active zones. By contrast, large and reliable synapses can be constructed using large

numbers of the same unreliable single vesicle release site within hundreds of active zones. Variation in the number and size of active zones in these larger synapses, and the number and spatial organization of the unreliable single vesicle release sites within the active zones, likely contributes to differences in synaptic properties. The top half of the figure shows representative examples of synapses that appear to be constructed in this manner [i.e., dentate gyrus basket cell boutons, mature calyx of Held synapses, frog neuromuscular junction (NMJ), and mouse NMJ]. **b.** By contrast, some central nervous system (CNS) synapses appear to be assembled with a large number of presynaptic calcium channels that are loosely coupled to synaptic vesicles and open with a relatively high probability in response to an action potential stimulus. Vesicle fusion at these synapses is triggered by the microdomain of calcium that is created by the flux through many loosely coupled calcium channels, essentially increasing background calcium in the active zone region (light-blue regions). The bottom half of the figure shows representative examples of synapses that appear to be constructed in this manner (i.e., boutons of cerebellar parallel fibers and immature calyx of Held synapses). Evidence also suggests that, during development, some synapses initially assembled using microdomain-coupled vesicle release sites may mature into synapses that use unreliable single vesicle release sites (Fedchyshyn and Wang, 2005; Yang and Wang, 2006; Wang et al., 2009). Figure reproduced from Tarr et al. (2013a)

(Kavalali, 2015). Importantly, there is also evidence that active zone heterogeneity exists at the NMJ of both frog and mouse. At the frog NMJ, multiple reports have presented evidence for heterogeneous release along the length of the frog NMJ presynaptic terminal (D'Alonzo and Grinnell, 1985; Bennett et al., 1986; Zefirov et al., 1995). By using either multiple intracellular or multiple extracellular electrodes positioned at different sites along the frog NMJ presynaptic terminal, these studies showed that there is heterogeneity in the evoked release profile along the axis of the terminal, such that release sites closest to the first contact point of the axon have a higher probability of release than those sites that are located at the end of the terminal branches (D'Alonzo and Grinnell, 1985; Bennett et al., 1986; Zefirov et al., 1995). Additionally, spontaneous miniature transmitter release seem to have a much more consistent release profile across release sites (Zefirov et al., 1995). It is important to note that these studies looked at evoked release in a low-calcium/high-magnesium solution in order to reduce quantal content to an average of ~1. These earlier studies required a single release event because multiple release events with each action potential stimulus would contaminate the signal and make it difficult to localize release sites. However, although the low-calcium/high-magnesium solution uncovered a clear heterogeneity across active zones, it is not clear that physiological levels of calcium and magnesium show the same heterogeneity. For instance, in low-calcium/high-magnesium, it is likely that only the most tightly coupled single-vesicle release sites (a vesicle and its associated calcium channel/s) would be able to be triggered for release. However, there may also be single-vesicle release sites in which the associated channel/s are too far away to trigger release in low-calcium/high-magnesium, but can participate in action potential-triggered transmitter release in physiological saline (normal levels of calcium and magnesium). So despite a structural heterogeneity (channel-vesicle distances differing slightly), the consequent functional difference

may be so subtle in normal conditions that it can be considered mostly irrelevant. Even if the functional heterogeneity may not be easily detectable under physiological conditions, based on previous reports in low-calcium/high-magnesium saline, there are likely to be differences among active zones at the frog NMJ. Furthermore, even if this heterogeneity extends to physiological conditions, our unreliable single-vesicle release site hypothesis may still hold true. Even in low-calcium/high-magnesium, it was suggested that a great proportion of the terminal (60-90%) is mostly uniform with respect to probability of release (D'Alonzo and Grinnell, 1985). Therefore, the majority of the terminal may show a relatively uniform low probability of release in physiological ion levels, with distal portions of terminals may having an even lower probability of release.

There have also been reports of active zone heterogeneity at the mouse NMJ. Experiments using the pH-sensitive fluorescent indicator synaptopHluorin (spH), which is the vesicle-associated protein synaptobrevin fused to a pH-sensitive pHluorin (Miesenbock et al., 1998), have indicated that there may be heterogeneous release across the mouse NMJ presynaptic terminal (Tabares et al., 2007; Wyatt and Balice-Gordon, 2008). The pHluorin portion of this molecule, which is highly fluorescent at neutral pH but much less fluorescent in acidic pH, is located in the lumen of the vesicle (pH ~5). When a vesicle fuses to the terminal membrane, the pHluorin is exposed to a more neutral pH and increases its fluorescence. Therefore, sites of neurotransmitter release can be visualized as spots of increased fluorescence. Two previous studies showed that there was a heterogeneous fluorescence profile, or “hot spots” of release, across the terminal during high-frequency trains of stimuli (10-100 Hz) (Tabares et al., 2007; Wyatt and Balice-Gordon, 2008). There are some caveats to these studies, however. First, although synaptobrevin is a vesicle-associated protein, a portion of the total measured

synaptobrevin exists in the terminal membrane (Takamori et al., 2006; Mutch et al., 2011), which increases the background fluorescence and reduces the signal-to-noise ratio of spH. Secondly, because of the high background fluorescence of spH, these studies used high-frequency trains of action potentials so that the signal was clear and noticeable above background (although one study mentioned they found similar results at low-frequency stimulation but did not show the data (Tabares et al., 2007)). Therefore, it is not clear if the same heterogeneous profile of release exists when the terminal functions following single action potential stimuli. In support of this idea, a more recent report using spH found that a heterogeneous release profile across the mouse NMJ terminal was not apparent during low-frequency action potential stimuli (Gaffield et al., 2009). This discrepancy does not diminish the possible importance of heterogeneity across active zones during high-frequency trains of stimuli.

Binomial analyses of release at the mouse NMJ have also suggested heterogeneity in function across active zones (Wang et al., 2010). By altering the extracellular calcium concentration and observing the effect on both quantal content and the variance in quantal content of individual NMJs (variance could be observed because voltage-clamp was used), it was determined that there are a relatively small number of release sites (~70) that have a high probability of release (~0.9) in physiological levels of calcium (Wang et al., 2010). Even in 5 mM calcium, the estimate for the number of release sites was still less than 100 (Wang et al., 2010). These findings are striking in light of the hundreds to thousands of active zones measured immunohistochemically (Figure 2A) and the relative lack of short-term depression seen during high-frequency trains of stimuli (Figure 3C). One would imagine there would be significant depression at a synapse that had release sites with a high probability of release, unless there was an unusually fast refilling of docked vesicles. It is important to note that the term “release site” in

this functional analysis has no defined or confirmed structural correlate. Therefore, a release site in a binomial analysis could be a single-vesicle release site, an active zone consisting of two vesicles, or possibly even a group of active zones totaling tens or even hundreds of vesicles. Interestingly, just as in classical quantal analysis (Katz, 1969), one must assume a homogeneous probability of release across active zones when using a binomial analysis (Redman, 1990; Zucker and Regehr, 2002), although it was argued that this assumption of a homogeneous probability of release had little effect on the results based on statistical simulations (Wang et al., 2010). In the end, this type of analysis can be difficult to interpret because the manipulation of one of the binomial parameters (probability of release) by altering extracellular calcium could in theory alter the other binomial parameter (number of release sites).

Ultimately, newer, higher resolution techniques will be needed to explore the possible functional heterogeneity across active zones of the mouse NMJ. One way in which this could be achieved is an extension of the spH imaging technique discussed above. Although functional imaging of spH is a powerful technique, the low signal-to-noise ratio is a problem if we want the resolution to look for active zone heterogeneity in action-potential evoked release of single quanta. One technique that possibly has the resolution to distinguish single vesicle release events is functional imaging using a better conjugate: the vesicle-associated synaptophysin protein conjugated to 4 pH-sensitive pHluorin molecules (synaptophysin-pHluorin 4x; sypH 4x). This particular construct has been shown to have sufficient signal-to-noise ratio to discern individual release events (Zhu et al., 2009). Another optical quantal analysis technique that may have the signal-to-noise level necessary in order for one to observe individual release events is the use of the genetic calcium sensor GCamP to detect the postsynaptic calcium influx through local transmitter activated receptor clusters that result from each quantum of transmitter released.

GCamP indicators have been utilized at the Drosophila NMJ to detect spatially distinct spontaneous miniature and evoked release events, and it has been found that there is functional heterogeneity across release sites at this synapse (Melom et al., 2013; Peled et al., 2014). One possibility is to conjugate a GCamP indicator to the postsynaptic NMJ scaffolding protein rapsyn, similar to the way in which GFP has been conjugated to rapsyn to observe postsynaptic structural changes (Bruneau and Akaaboune, 2010). In any case, it seems as though some type of optical quantal analysis method would be ideal for the detailed study of heterogeneous release across active zones.

Although there is evidence for active zone heterogeneity at the mouse NMJ, I believe our unreliable single-vesicle release site hypothesis still seems plausible. In fact, I hypothesize that both active zone heterogeneity and our unreliable single-vesicle release site hypothesis can coexist. It is very likely that there are different populations of active zones at the mouse NMJ that have different roles (e.g. spontaneous vs evoked release), but likely some large portion of these active zones rarely release a vesicle on average because they contain only two vesicles with a low probability of release.

## 6.2 TWO LOW-PROBABILITY COMPONENTS OF RELEASE

If we believe the active zones of the mammalian NMJ, or at least a substantial portion of these active zones, have a low probability of release on average, we may next wonder what components of the release process lead to this average low probability of release. Two particular possibilities are the probability that a calcium channel opens in response to a presynaptic action potential and the probability that a vesicle is released when a nearby calcium channel does open.

As an initial comparison, we can consider the more heavily studied frog NMJ. In fact, our lab has performed experiments at the frog NMJ that explore both the probability of opening for a presynaptic calcium channel during an action potential and the probability that a vesicle fuses even when a nearby channel does open (Luo et al., 2011; Luo et al., 2015). These experiments showed that the N-type channels controlling release at the frog NMJ have a relatively low probability of opening during an action potential (~0.2 (Luo et al., 2011)), and that vesicles rarely release even when a nearby channel does open (Luo et al., 2015). These two low probability components can explain, at least in part, the average low probability of release per vesicle at the frog NMJ (~0.017). We have not yet performed the necessary experiments in the mouse NMJ to determine with confidence the average number of calcium channels per active zone or their probability of opening during an action potential. However, we do have indirect evidence that suggests the mouse NMJ functions similarly to the frog NMJ with respect to these two low-probability components of release. First, 50 nM ω-agatoxin reduced both transmitter release and presynaptic calcium influx by a similar degree (Figure 4), indicating that there is a linear or near-linear relationship between calcium influx and transmitter release. If the relationship is linear, then only a single channel normally contributes to the release of a vesicle. Even if it is only near-linear, it is likely that the majority of the calcium ions contributing to a release event come from a single nearby channel, with the remaining small number of ions being contributed by neighboring channels (Luo et al., 2015). This near linearity is seen in the frog NMJ, where the calcium channel-release site relationship falls between 1st and 2nd order (Luo et al., 2015). Our frog NMJ MCell model suggested that this was due to a single channel contributing most of the calcium ions for release (Luo et al., 2015). Furthermore, our mouse NMJ active zone model also predicted a near-linear relationship between changes in calcium

entry and changes in transmitter release when channels were removed from the active zone (Ma, 2014), thus supporting our data using ω-agatoxin. Finally, in paired-pulse experiments, cadmium did not elicit a significant increase in paired-pulse facilitation at the mouse NMJ (Figure 5A), which indicates that a small number of calcium channel likely contribute to each release event (Scimemi and Diamond, 2012). All of these data suggest that there are a small number of channels contributing to the release of a vesicle on average. The most likely explanation for very few channels opening during an action potential at any one active zone could be a small number of channels per active zone, a low probability of channel opening during an action potential, or both. Our MCell modeling of both the frog and mouse NMJ active zones has suggested that there is low probability of release when only one or very few channels open near a vesicle, even when one of these channels is tightly coupled to the vesicle (Dittrich et al., 2013; Ma, 2014). However, this is only our hypothesis and we do not currently have direct evidence for this at the mouse NMJ.

An additional piece of evidence that supports the hypothesis that a small number of calcium channels open at an active zone during an action potential at the mouse NMJ is the relative absence of both short-term facilitation and short-term depression during high frequency trains of action potentials (Figure 3). Short-term depression is unlikely to occur at a synapse in which the number of ready-to-be-released vesicles is high and the likelihood of a vesicle being near an open channel, and releasing during any one stimulation, is low. The small amount of short-term facilitation, however, is somewhat more complex to explain. One would imagine that a small number of open channels per action potential and an abundance of docked vesicles would lead to little vesicle depletion and a good chance for residual calcium to facilitate release during subsequent stimuli. In fact, this is the case at the frog NMJ (Feng, 1940; Eccles et al., 1941;

Feng, 1941; Braun and Schmidt, 1966; Braun et al., 1966; Mallart and Martin, 1967). The important difference to remember is that the mouse NMJ built with hundreds of small, punctate active zones with only ~2 docked vesicles (Nagwaney et al., 2009). The active zones are far enough away from each other (~500 nm on average (Ruiz et al., 2011)) that they can be considered to be mostly independent of one another. In other words, it is very unlikely that calcium influx from the opening of a calcium channel in one active zone could affect release of a vesicle in a neighboring active zone. Individual active zones are also relatively far apart at the frog NMJ. However, unlike the frog NMJ, there is very little chance that residual calcium can affect release at the very small active zones of the mouse NMJ. With a small number of calcium channels per active zone and a low probability of opening during an action potential, it is very unlikely that a single active zone would have an open calcium channel in two consecutive action potentials. So, unlike the frog NMJ, there is very little calcium channel domain overlap at active zones of the mouse NMJ. Furthermore, pushing the synapse to facilitate by reducing calcium influx with blockers (cadmium or ω-agatoxin) only could increase facilitation to ~1.2 during a train of 10 action potentials at 50 Hz (Figure 6), an amount of facilitation that still falls below the average magnitude of facilitation in the frog NMJ under control conditions (Ma et al., 2015). Our MCell models also predicts this result by showing that during trains of action potentials, residual calcium from previous stimuli has a smaller effect at the mouse NMJ compared to the frog NMJ (Figure 9). If there were many channels contributing to release on average, we would expect to see much stronger short-term plasticity characteristics at the mouse NMJ, and this is not the case.

## 6.3 TARGETING THE TWO LOW-PROBABILITY COMPONENTS OF RELEASE IN THE TREATMENT OF LEMS

Given our hypothesis that there are two low-probability components of release at the mammalian NMJ, we should be able to target these two components to increase the amount of neurotransmitter release, which could be helpful in diseases that affect the NMJ. One such disease, LEMS, leads to a removal of a portion of the P/Q-type calcium channels involved in transmitter release, thus reducing the amount of release (Lennon et al., 1995; Meriney et al., 1996). Although there is an upregulation of other subtypes, including the L-type channel (Xu et al., 1998; Flink and Atchison, 2002), there are still fewer overall channels compared to the normal state (Smith et al., 1995), especially within the active zone. With fewer channels, the probability of a channel opening near a vesicle becomes even lower. Additionally, there is evidence that active zone structure is disrupted in LEMS, with the intramembranous particles becoming partially disorganized (Fukunaga et al., 1983; Nagel et al., 1988). This likely means the remaining calcium channels are farther away from the vesicles on average, so the probability of release when a nearby calcium channel does open is also lower because the calcium ions have to diffuse a greater distance to reach the vesicle-associated sensor for release. Therefore, in LEMS, I hypothesize that one or possibly both of the two normally low-probability components of release become even lower. Although the channels' probability of opening likely wouldn't change, there would be a lower probability that an active zone has an open channel because there are fewer channels overall. The probability of release when a channel does open could also be reduced if the normal active zone organization is disrupted. In theory, symptomatic treatment options targeting either or both of these low-probability components of release should increase transmitter release and help alleviate symptoms in LEMS patients.

The current common symptomatic treatment option for LEMS, DAP, does in fact target one of these low-probability components of release, specifically the low probability that a calcium channel will open in an active zone (or near a docked vesicle if the active zones are disrupted). DAP is a potassium channel blocker that widens the presynaptic action potential by prolonging the repolarization phase of the action potential (Kirsch and Narahashi, 1978). Like potassium channels, calcium channels are relatively slow to open (Hille, 2001), so calcium influx occurs during the repolarization phase of the action potential. By prolonging the action potential, DAP increases the amount of time that the terminal is in a depolarized state, which leads to an increased probability that a calcium channel will open in an active zone (or near a docked vesicle) during an action potential. With more calcium channels open, there is an increase in neurotransmitter release (Figure 17 (Tarr et al., 2014)). However, DAP alone does not completely reverse the LEMS-induced reduction in transmitter release, and its actions on potassium channels elsewhere in the periphery can lead to dose-limiting side effects (Sedehizadeh et al., 2012).

Given the limits on the use of DAP clinically, we began synthesizing compounds to target the other low-probability component of release: the low probability that a vesicle will release even when a nearby calcium channel does open. The obvious way to achieve this would be to increase the amount of calcium influx when a calcium channel does open. Although there are many types of calcium channel antagonists, calcium channel agonists are in shorter supply, and almost all of these affect the L-type channel (Hille, 2001). Fortunately, the Cdk antagonist (*R*)-roscovitine was found to have $Ca_v2$ calcium channel agonist effects independent of its Cdk antagonist effects (Yan et al., 2002). Furthermore, our lab has shown that it increases transmitter release at the frog NMJ (Cho and Meriney, 2006). Specifically, (*R*)-roscovitine increases the

mean open time, or the amount of time that the channel stays in the open state after it has been activated by depolarization (DeStefino et al., 2010). Importantly, (*R*)-roscovitine does not open calcium channels independent of a voltage change, but rather requires that the channel is in the open state to elicit its agonist effects (DeStefino et al., 2010). In pursuit of a more selective calcium channel agonist, we developed novel roscovitine analog compounds in the hope of removing Cdk antagonist activity while retaining calcium channel agonist activity. Not only did we achieve this with our compound GV-58, but we were also able to increase both the potency and efficacy of the calcium channel agonist activity (Figure 11 (Tarr et al., 2013b)). We found that GV-58 increases transmitter release in LEMS model NMJs to a similar extent as DAP, which indicates that there is a low probability of vesicle release even when a nearby channel does open (at least in LEMS model NMJs; Figure 17 (Tarr et al., 2014)).

Since our hypothesized two low-probability components of release are sequential, increasing the probability of both components simultaneously should lead to a non-linear increase in transmitter release. That the components are sequential is important because increasing the probability of the first (calcium channels opening) will allow a greater increase in the probability of the second (release when a channel does open). In other words, vesicle fusion when a nearby channel does open first requires a nearby channel to actually open. Therefore, increasing the number of open channels will increase the likelihood of an open channel agonist like GV-58 affecting a channel. As expected, when we treated LEMS model NMJs with a combination of DAP and GV-58, there was a supralinear increase in transmitter release. The increase was so great that the magnitude of transmitter release was completely restored to control levels (Figure 17 (Tarr et al., 2014)). This effect of GV-58 plus DAP supports our hypothesis that there are two low-probability components of release at the mouse NMJ, at least in the LEMS

model NMJ. It is worth noting that we have also done preliminary experiments in which GV-58 is applied to control mouse NMJs, and we see a significant increase in transmitter release under these conditions as well (data not shown). This at least provides some additional evidence to support a low probability of release even when a channel does open, although future experiments are still necessary to determine how low this probability is.

## 6.4 ACTIVE ZONE ORGANIZATION PLAYS AN IMPORTANT ROLE IN LEMS PATHOPHYSIOLOGY

Although it is fairly well accepted that LEMS leads to a reduction in the number of presynaptic P/Q-type calcium channels (Lennon et al., 1995; Meriney et al., 1996), it is also evident that the LEMS-induced changes in neurotransmitter release are more complex than a simple reduction in channel number. Specifically, the short-term plasticity characteristics are much different than expected with only a reduction in channel number. Considering that physiological stimuli at the NMJ are bursts of high-frequency action potentials (Hennig and Lomo, 1985), a greater understanding of the LEMS effects on short-term plasticity would greatly benefit future therapeutic approaches for LEMS and other disease of the NMJ.

The particular property of LEMS model NMJs that cannot be matched to a model with a simple calcium channel reduction is the large increase in short-term facilitation. LEMS model NMJs greatly increase facilitation during trains of high-frequency activity (~1.4-1.5 at 50 Hz; Figure 18). When the number of calcium channels is reduced by applying a blocker, facilitation only reaches ~1.2-fold(Figure 6, 20). The difference in facilitation is evident despite the fact that quantal content is reduced to a similar extent in both cases. Furthermore, our MCell model

cannot recapitulate the facilitation in LEMS model NMJs when the number of channels is reduced so that release in response to a single action potential matches that of LEMS model NMJs (Figure 20). Therefore, the LEMS-induced active zone changes extend beyond a simple reduction in the number of channels. Two pieces of evidence support this hypothesis. First, freeze-fracture EM has shown a partial disruption in active zone particles, some of which are presumed to be calcium channels (Fukunaga et al., 1983; Nagel et al., 1988). This evidence seems to suggest that active zones break up or disorganize, which would mean the average coupling distance between calcium channels and vesicles may increase in LEMS. Second, although release is usually reduced to ~25-50% of control in LEMS passive transfer model NMJs (Figure 13, 17), the amount of presynaptic calcium current has been measured to be about 75% of control (Smith et al., 1995; Xu et al., 1998). This finding is interesting in light of the hypothesized linear calcium channel-release site relationship in normal mouse NMJs (see Chapter 1). It seems as though the LEMS-induced changes have converted the mouse NMJ from a nanodomain-like release configuration to a microdomain-like release situation (Eggermann et al., 2012; Tarr et al., 2013a). In other words, the control mouse NMJ only needs one or very few calcium channels on average to contribute ions to cause release, the LEMS model NMJ needs many open channels to lead to vesicle release. If this is the case, it is likely because the channels are no longer tightly coupled to the vesicles, so a single channel opening will very rarely trigger release in LEMS NMJs.

With all of this in mind, in Chapter 4 we took advantage of our MCell model mouse NMJ and ran a parameter search to help determine what properties of active zone structure and function lead to an increase in short-term facilitation. We knew that active zone organization played a critical role in short-term plasticity properties because a simple rearrangement of the

organization frog NMJ active zone model (large facilitation) into the organization of the mouse NMJ active zone led to almost no facilitation (Figure 8 (Ma, 2014)). Specifically, the only changes were the relationship between the organization of calcium channels with respect to the vesicles and the overall size of the active zones. Using this knowledge, we attempted multiple calcium channel configurations in our mouse NMJ active zone model first to better match the control short-term plasticity and then to attempt to match the facilitation in LEMS NMJs. We found that adding some channels in the outer rows of the double rows of intramembranous particles increased facilitation (Figure 22). Once we better matched the control short-term plasticity, we used this new mouse NMJ active zone model for our attempts to match LEMS short-term plasticity (while also matching the decrease in quantal content observed in LEMS). Ultimately, we were unable to recreate the LEMS short-term facilitation in our MCell model, but we did learn valuable information about how the positioning of channels can affect transmitter release. Perhaps the most obvious conclusion is that distance matters, especially when there are very few channels. A mere 10 nm shift of the remaining channels away from the vesicles drastically reduced the probability of release and did very little to increase facilitation (Figure 24). The lack of an increase in facilitation was surprising, but the probability of release was so low that it is possible that facilitation was not possible because calcium ions could not ever reach the calcium binding sites associated with a single vesicle on two consecutive stimuli. A second important conclusion from our parameter search is that introducing channels farther away from the vesicles does increase facilitation, although not quite as much as we expected (Figure 22 and 23). Of course, there are many different configurations that we have not yet tested, but the inability to push facilitation beyond ~1.2 was still unexpected. Perhaps the most important point to remember is that we only altered the configuration and number of channels in our LEMS

MCell models, and there is reason to think that other changes occur in LEMS. For example, there is evidence that some LEMS patients have antibodies to other presynaptic proteins, such as synaptotagmin and M1 muscarinic acetylcholine receptors (Takamori, 2008). If the primary isoform of synaptotagmin is removed in LEMS, then the upregulation of other isoforms with different binding and unbinding kinetics could certainly lead to effects of short-term facilitation. This could be tested in the future by altering the number of synaptotagmin molecules per vesicle and/or their kinetic rates. M1 muscarinic receptors have been shown to play a modulatory role in transmitter release at the mammalian NMJ (Santafe et al., 2003; Santafe et al., 2006), and affecting these receptors could easily alter short-term plasticity. Effects other than those on calcium channel number and organization are likely a missing link in our LEMS MCell models and will need to be further explored in the future. However, despite our inability to perfectly match the LEMS physiology in our model, we have been able to show that calcium channel number and organization within an active zone are certainly critical factors modulating functional characteristics at the NMJ and synapses in general.

## 6.5 DO UNRELIABLE SINGLE-VESICLE RELEASE SITES PLAY A ROLE IN THE CNS?

It is important to consider if our unreliable single-vesicle release site hypothesis can be applied to synapses in the CNS as well. Several CNS synapses share similar requirements of reliability and strength with the NMJ. One such system that has been studied extensively is the calyx of Held synapse, which has become a popular model system due to the accessibility of its presynaptic terminal to direct electrophysiological manipulation (Forsythe, 1994; Borst et al.,

1995). Studies of the mature rat calyx of Held (~P14 or older, which is considered mature for this synapse as it corresponds to the onset of hearing (Taschenberger et al., 2002; Fedchyshyn and Wang, 2005)) have shown that the synapse has about 700 active zones, each with an average of three docked synaptic vesicles (Taschenberger et al., 2002). The probability of vesicle fusion at each of these single vesicle release sites appears to be very low (~0.13) (Taschenberger et al., 2002). Additionally, the calcium channel-release site relationship follows a power law with an exponent of less than 3 (Fedchyshyn and Wang, 2005; Kochubey et al., 2009), which indicates that only a small number of channels contribute to release. Finally, it has been shown that the mature calyx of Held has a very fast action potential waveform, leading to the recruitment of only a small fraction of calcium channels upon action potential invasion into the terminal (Taschenberger and von Gersdorff, 2000; Yang and Wang, 2006). These findings demonstrate that the mechanisms that govern synaptic vesicle release at the calyx of Held are similar to those found at the NMJ, namely single vesicle release sites with a low vesicle release probability triggered by calcium from a small number of closely-associated open calcium channels (Figure 25).

Interestingly, this situation is quite different from what emerged based on earlier studies performed in slice preparations of the immature calyx of Held (~P10 or younger). These immature calyx synapses have roughly the same number of total docked vesicles as their mature counterparts but only about half as many active zones, and thus, about twice as many docked vesicles per active zone as the mature calyx (Satzler et al., 2002; Taschenberger et al., 2002). Patch-clamp recordings of calcium current showed that a single action potential-like waveform could activate a calcium current that is about 70% of the maximum achievable with a prolonged waveform (Borst and Sakmann, 1998). Furthermore, experiments to determine the calcium

channel-release site relationship found a power relationship with an exponent of about 3-5 (Borst and Sakmann, 1999; Fedchyshyn and Wang, 2005), which indicates that calcium flux through many calcium channels triggers the release of a single vesicle (Figure 1). In support of this conclusion, experiments show that the slow calcium buffer EGTA has similar effects on release as the fast buffer BAPTA (Meinrenken et al., 2002; Fedchyshyn and Wang, 2005). Thus, it appears that as these synapses mature there is a transition from microdomain coupling in immature synapses to unreliable single vesicle release sites controlled by nanodomain coupling in adult synapses (Figure 25). Further, narrowing of the action potential during development and maturation at this synapse may attenuate calcium influx, but the switch from microdomain to nanodomain coupling may effectively boost synaptic efficacy and counteract the action potential narrowing effect (Wang et al., 2009).

Studies at other large CNS synapses have also provided results that are reminiscent of the mechanisms employed at the NMJ. One such synapse is the dentate gyrus basket cell-granule cell (BC-GC) synapse, which is a synapse known for high temporal fidelity and reliable spiking (Jonas et al., 2004). This synapse is estimated to contain three to seven active zones, and each active zone appears to have a release probability of ~0.5 and an estimated releasable vesicle pool size at each active zone of around 50 (Kraushaar and Jonas, 2000). Thus, the probability of release per vesicle is very low. Ultrastructural analysis and modeling data show a very short distance between the calcium channels and the calcium sensor (~10-20 nm) (Bucurenciu et al., 2008), which suggests nanodomain coupling between presynaptic calcium channels and vesicle release sites. This is supported further by experiments with exogenous chelators, which show that release is inhibited by the fast calcium chelator BAPTA, but not by the slow calcium chelator EGTA (Bucurenciu et al., 2008). Finally, determination of the calcium channel-release

site relationship, coupled with computer modeling, indicate that only a few calcium channels are involved in the release of each vesicle (Bucurenciu et al., 2010). With its large pool of releasable vesicles, a low probability of release per vesicle, and tight coupling between calcium channels and vesicle release sites, the reliable BC-GC synapse appears to be built from unreliable single vesicle release sites in a fashion similar to the NMJ.

Another large, multi-active zone synapse that has been studied extensively is the hippocampal mossy fiber synapse between dentate gyrus granule cells and CA3 pyramidal cells. This is a large synapse known for high temporal fidelity and reliable spiking (Henze et al., 2002), and is often used in studies of synaptic plasticity (Henze et al., 2000; Nicoll and Schmitz, 2005; Rollenhagen and Lubke, 2010). The mossy fiber synapse is characterized by an average of about 30 active zones (Chicurel and Harris, 1992; Acsady et al., 1998; Rollenhagen et al., 2007), and with an estimated readily releasable pool of about 1400 vesicles (Hallermann et al., 2003), each active zone has ~46 single vesicle release sites. Under low-frequency stimulation conditions, the release probability per active zone is quite low (<0.3) (Lawrence et al., 2004). Consequently, the release probability per vesicle is substantially lower. However, in contrast to the NMJ, there appears to be a large number of presynaptic calcium channels at the mossy fiber synapse (Li et al., 2007b), and these calcium channels appear to be efficiently activated by a single action potential (Bischofberger et al., 2002); action potential waveforms were shown to open ~80% of the maximal current that could be activated with a long square depolarization (Bischofberger et al., 2002). Thus, calcium channels open with a high probability during an action potential, and the flux through many calcium channels may be required to trigger the release of a single vesicle. This is reminiscent of the situation in the immature calyx of Held. In fact, the hippocampal mossy fiber synapse is usually studied in acute hippocampal slices from relatively young rats,

and may indeed be a relatively immature synapse. The synapse itself forms along the axon of the dentate granule neuron, which is one of only a few neurons in the CNS that continues to be born in adult animals from a proliferation zone near the dentate gyrus (Kempermann et al., 1998; von Bohlen Und Halbach, 2007; von Bohlen und Halbach, 2011). The dentate granule cells are likely to turn over constantly and reform mossy fiber synapses (Faulkner et al., 2008), perhaps in response to plasticity associated with learning and memory (Schinder and Gage, 2004; Marin-Burgin et al., 2012). Therefore, it is possible that even in the adult animal this synapse retains some immature features (including the organization of single vesicle release sites). We will have to await further studies to gain additional insight into this issue.

Based on the available data from synapses of both the PNS and CNS, we suggest that a functionally heterogeneous population of synapses can be built via assembly and spatial organization of varying numbers of a basic unit: the low probability (unreliable) single vesicle release site. In this view, smaller unreliable synapses are characterized by only a few unreliable single vesicle release sites whereas the reliability of larger synapses derives from assembling a large number of them. Beyond that, the spatial organization of single vesicle release sites in individual active zones offers even more functional diversity. Therefore, one way in which synapses can be built to be reliable or unreliable is by varying the number and spatial organization of these unreliable building blocks.

Why should the fundamental unit of transmitter release be unreliable? While the answer to this question is not yet fully understood, several hypotheses have been advanced. At small CNS synapses that only contain one or a few active zones, only a small total number of unreliable single vesicle release sites will be present, rendering the synapses unreliable. Small CNS synapses have been reported to be highly unreliable for many years (see (Zador, 1998) for

example), although the magnitude of unreliability may be temperature-dependent (Hardingham and Larkman, 1998). At CNS synapses that often fire in bursts, unreliable synapses offer a broader dynamic range of transmitter release and do not result in vesicle depletion during normal activity patterns, which are properties important for information processing in the brain (Goda and Sudhof, 1997). Similarly, the use of unreliable single vesicle release sites within large synapses that may contain hundreds or thousands of these units creates synapses that on the whole release enough transmitter to reliably activate postsynaptic cells. Yet, these synapses do not fatigue with continued or tonic use because only a small percentage of the available release sites are used with each action potential. This conservation of resources may be a major reason why NMJs do not show significant short-term depression during short trains of action potential activity – an important quality that underlies function at this synapse. Thus, as a basic unit, an unreliable release site provides significantly more flexibility than a high fidelity site in assembling synapses with a large range of properties and characteristics.

The assembly of unreliable single vesicle release sites into active zones could be accomplished via active zone precursor vesicles (or small dense core vesicles) that contain a collection of pre-assembled presynaptic plasma membrane-associated active zone proteins, as have been shown to exist in developing neurons in vitro (Zhai et al., 2001; Sorra et al., 2006). After these release site components are inserted into the active zone region of the nerve terminal, calcium channels may associate with them in a manner carefully regulated by intracellular biochemical events that control whether microdomain or nanodomain coupling to vesicle release will occur. Differential regulation of calcium channel coupling to vesicle release sites as synapses mature may then explain why some immature synapses appear to use microdomain coupling, whereas mature synapses often use nanodomain coupling (at some synapses, like

cultured frog NMJs, nanodomain coupling may be present even at early developmental stages; (Yazejian et al., 1997; Yazejian et al., 2000)). The development of nanodomain coupling at mature vesicle release sites in the CNS may involve alterations in protein-protein interactions between release site proteins and calcium channels (see for example (Han et al., 2011; Kaeser et al., 2011)) and/or changes in the phosphorylation state of some of these proteins, which may modulate the probability of calcium channel opening during an action potential (see for example (Bezprozvanny et al., 1995; Atlas, 2001; Yokoyama et al., 2005; Keith et al., 2007; Pozzi et al., 2008; Yang et al., 2010)). Active zones initially assembled in a microdomain fashion could gradually reduce the number of vesicles associated calcium channels during development, morphing into low-probability single-vesicle release sites with nanodomain coupling once mature. Consistent with this hypothesis, there is evidence at some synapses that the probability of release decreases as synapses mature (Taschenberger and von Gersdorff, 2000; Taschenberger et al., 2002; Feldmeyer and Radnikow, 2009; Golshani et al., 2009; Rochefort et al., 2009; Crins et al., 2011; Eggermann et al., 2012).

Although our hypothesized low-probability single-vesicle release site mechanism for regulating transmitter release may not act at all synapses, integration of numerous findings over the past few years suggests it as a fundamental principle of synapse assembly in a number of well-studied synapses. This realization has spawned many interesting and challenging new research questions that will prompt investigators to strive to elucidate additional details of the presynaptic mechanisms that control chemical transmitter release. An important set of synapses that requires further investigation is the large heterogeneous population of small cortical bouton-like synapses. Previous studies have shown that transmitter release from these small CNS synapses is often unreliable (Goda and Sudhof, 1997). In studies performed to date, significant

variability exists when measuring the average calcium influx in response to a single action potential among different boutons of a single presynaptic neuron (Koester and Sakmann, 2000). However, when studying the variability in calcium influx at a single bouton, some have reported a high degree of variability (consistent with a low probability of calcium channel opening following action potential stimuli; (Frenguelli and Malinow, 1996)), while others have observed a homogeneous calcium influx with repeated stimulus trials (consistent with either a large number of calcium channels and/or a high probability of calcium channel opening following action potential stimuli; (Koester and Sakmann, 2000)). Additional studies will be required to better understand calcium channel number and function at this diverse set of synapses. Another interesting set of synapses are the specialized ribbon sensory synapses. Ribbon synapses are unique synapses that release large amounts of transmitter over extended periods of time in response to graded potentials. A number of studies suggest that single vesicle release sites at ribbon synapses employ nanodomain control of vesicle fusion (Brandt et al., 2005; Goutman and Glowatzki, 2007; Jarsky et al., 2010; Bartoletti et al., 2011).

Finally, while I have focused my discussion on the ways in which different types of synapses may be assembled by varying the number and spatial organization of unreliable single vesicle release sites, many other factors undoubtedly contribute to shaping active zone function. The roles of synaptic vesicle pools, as well as potential molecular heterogeneity in synaptic vesicle protein constituents, active zone components, and presynaptic calcium channel subunits (Frank et al., 2009; Mutch et al., 2011; Raingo et al., 2012), require additional study.

# APPENDIX A

## SYNTHESIS AND BIOLOGICAL EVALUATION OF A SELECTIVE N- AND P/Q-TYPE CALCIUM CHANNEL AGONIST

### *Preface*

The acute effect of the potent cyclin-dependent kinase (cdk) inhibitor (*R*)-roscovitine on calcium channels inspired the development of structural analogues as a potential treatment for motor nerve terminal dysfunction. On the basis of a versatile chlorinated purine scaffold, we have synthesized ca. 20 derivatives and characterized their N-type calcium channel agonist action. Agents that showed strong agonist effects were also characterized in a kinase panel for their off-target effects. Among several novel compounds with diminished cdk activity, we identified a new lead structure with a 4-fold improved N-type calcium channel agonist effect and a 22-fold decreased cdk2 activity as compared to (*R*)-roscovitine. This compound was selective for agonist activity on N- and P/Q-type over L-type calcium channels.

**The results in this appendix have been published in the journal *ACS Medicinal Chemistry Letters* in 2012, and the citation for this article is given below. My contribution to this work was testing the novel analogs for calcium channel agonist activity using whole-cell perforated patch clamp recordings and helping with the writing and preparing of the manuscript. Minor formatting changes and changes to the numbering of figures and tables have been made to preserve consistency with the rest of this dissertation document.**

**Reprinted with permission from:**

**Liang M, Tarr TB, Bravo-Altamirano K, Valdomir G, Rensch G, Swanson L, DeStefino NR, Mazzarisi CM, Olszewski RA, Wilson GM, Meriney SD, Wipf P (2012) Synthesis and Biological Evaluation of a Selective N- and P/Q-Type Calcium Channel Agonist. *ACS Med. Chem. Lett.* 3: 985-90**

Chemical communication in the nervous system is tightly regulated by the flux of calcium ions through certain subtypes of voltage-gated channels. A decrease in calcium flux at synapses can cause neurological diseases. Lambert–Eaton myasthenic syndrome (LEMS) is a neurological autoimmune disorder characterized by an autoimmune reduction of presynaptic P/Q-type ($Ca_v2.1$) calcium channels at the neuromuscular junction and a partial compensatory up-regulation of N-type ($Ca_v2.2$), L-type ($Ca_v1$), and R-type ($Ca_v2.3$) channels (Motomura et al., 1997; Urbano et al., 2008). N-type and P/Q-type channels appear to be the most relevant for the control of transmitter release as they selectively bind directly to and colocalize with transmitter release sites (Seagar et al., 1999). The result is an overall calcium channel reduction at transmitter release sites that results in muscle weakness and is associated with compromised motor function. This disease is estimated to affect 1:100000 individuals in the United States (Lindquist and Stangel, 2011); however, the true incidence of LEMS remains unknown as it is often undiagnosed in patients (Sanders, 2003). Current treatment strategies are very limited, and those available are indirect and sometimes associated with undesirable side effects.

Selective calcium channel agonists that increase the ion flux through N- and P/Q-type calcium channels represent attractive potential therapeutics for LEMS and other neuromuscular diseases; however, to date, no such agonists have been identified. While (*R*)-roscovitine was originally developed as a cyclin-dependent kinase (cdk) inhibitor (Meijer and Raymond, 2003; Meijer et al., 2007), several laboratories have subsequently demonstrated that it is also a potent agonist for N- and P/Q-type calcium channels (Yan et al., 2002; Buraei et al., 2005; Cho and Meriney, 2006; DeStefino et al., 2010), showing a concentration required for 50% efficacy ($EC_{50}$) = 28–41 μM (Buraei and Elmslie, 2008). N- and P/Q-type channels are the two major subtypes that regulate chemical transmitter release in the nervous system (Sheng et al., 1998).

The development of a potent agonist for N- and P/Q-type calcium channels could have a significant impact on the treatment of LEMS as well as other neurological diseases. Furthermore, the availability of a more potent N- and P/Q-selective agonist would be useful as an experimental tool to facilitate the study of calcium channel gating and regulation of cellular events. Accordingly, we embarked on developing analogues of (*R*)-roscovitine with decreased cdk activity and increased selectivity for these subsets of voltage-gated calcium channels.

At the onset of our work, very little was known about structural modifications of (*R*)-roscovitine pertaining to its calcium channel modulating properties (Otyepka et al., 2000). As summarized in Figure 1, the available literature activity data on roscovitine analogues disclosed only three similarly potent N-type calcium channel agonists among 12 structural analogues. We used a four-zone approach to analyze the literature results and to guide our initial round of medicinal chemistry structure–activity relationship (SAR) studies. In particular, zone 1, the core region, had only been superficially probed in the inactive analogues 1 and 2, which, however, differ too greatly from the purine scaffold of roscovitine to allow for any conclusions regarding the influence of core scaffold variations (Buraei and Elmslie, 2008). Interestingly, translocation of the nitrogen atom in pyrazolo[1,5-*a*]-1,3,5-triazine 3 (Bettayeb et al., 2008b; Oumata et al., 2008; Popowycz et al., 2009), however, retained N-type calcium channel agonist activity and confirmed that at least conservative modifications were tolerable (Meriney, S.D., unpublished results). The literature data on zone 2 analogues were similarly very limited, as shown for compounds 4, 5, and 6 [e.g., (*R*)-olomoucine II] (Cho and Meriney, 2006; Buraei and Elmslie, 2008). The former two trisubstituted *N*-6 amine analogues were devoid of any activity, suggesting that a hydrogen atom was required at *N*-6. Because the phenol group in 6 was able to substitute for roscovitine's benzene ring in zone 2 with minimal loss of activity, we concluded

that zone 2 was amenable to further modifications. In contrast, analogues 7 (Buraei and Elmslie, 2008), 8 (e.g., bohemine) (Buraei and Elmslie, 2008), and 9 [e.g., (*S*)-roscovitine] (Cho and Meriney, 2006; Buraei and Elmslie, 2008) demonstrated that zone 3 was critical for the desired N-type calcium channel agonist activity. It was also noteworthy and encouraging for the robustness of the SAR that upon the seemingly minor modification of an inversion of configuration in zone 3 in 9, the activity dropped ca. 14-fold.

Because the literature data did not present any analogues of roscovitine with exclusive zone 4 modifications, the conclusions that could be drawn regarding the combined zone 3/4 alterations shown in Figure 1 were ambiguous. The *N*-9 methylated compound 10 (e.g., olomoucine) and (dimethylamino)olomoucine 11 were devoid of any activity (Buraei and Elmslie, 2008), but this deficiency could also be attributed to the lack of appropriate functionality in the zone 3 side chain. Similarly, iso-olomoucine 12 (Buraei and Elmslie, 2008) was inactive either due to the shift in substitution in the imidazole ring, the lack of a 2-propyl group in zone 4, or, most likely, once again the absence of the (*R*)-2-amino-1-butanol side-chain at *C*-2 in zone 3.

In summary, the available literature information on the roscovitine activity profile as it pertained to N-type calcium channel agonism/antagonism was very limited, and the combination of all previously observed effects did not yet allow for a rational second generation lead design and development. On the basis of the lack of activity resulting from minor modifications in zone 3 and the absence of significant SAR data from zone 1 scaffold alterations, we focused our studies on interrogating the purine scaffold further by variations of substituents in zones 2 and 4. Accordingly, for this first round of systematic SAR studies, we decided to retain the purine backbone as well as the (*R*)-2-amino-1-butanol side chain at *C*-2.

The synthetic strategy used for SAR investigations toward selective N-type calcium channel agonists based on purines 13 is summarized in Scheme 1. Starting with the commercially available 2,6-dichloropurine 14 (Oumata et al., 2008), *N*-9 alkylation of the purine with primary alkyl halides would lead to intermediate 15. Preferential nucleophilic aromatic substitution ($S_NAr$) reaction at the more reactive *C*-6 position followed by displacement of the *C*-2 chloride in 16 with primary amines would provide target analogues 13 (Wipf and George, 2010).

Zone 4 modifications $R^1$ were readily achieved by subjecting dichloropurine **14** to deprotonation in DMSO in the presence of a mild base such as potassium carbonate, followed by the addition of alkyl bromides or iodides at 16–18 °C. Primary alkyl halides ($R^1$ = Me, Pr) provided a similar yield (64–78%) to the secondary alkyl halide ($R^1$ = *i*-Pr, 65%). Microwave irradiation at 120 °C for 20 min in *n*-BuOH and triethylamine in the presence of various aryl- and alkylamines converted intermediates **15** to the *C*-6 aminated purines **16** in moderate-to-good yields (52–95%). Finally, aminolysis at *C*-2 under forcing conditions (heating neat in a sealed flask at 170 °C in the presence of the $R^3$-amine for 8–15 h) introduced the (*R*)-2-amino-1-butanol side chain to give target molecules **13** in variable yields (25–93%) (Oumata et al., 2009).

Table 1 presents an overview of the synthetic analogues prepared using this pathway, as well as their N-type calcium channel agonist and cdk2 kinase inhibitory properties. While most of the new derivatives were ineffective at enhancing N-type calcium channel activity, an encouraging result was obtained with **13d**, which showed a ca. 2-fold increased agonism and a 22-fold decreased cdk2 kinase activity versus the standard, (*R*)-roscovitine. We attributed the decreased kinase activity of **13d** to the replacement of the *i*-propyl side chain at $R^1$ with the more flexible *n*-propyl group, a hypothesis that was supported by the similarly decreased cdk2 activity

of **13g**. In addition, previous docking and experimental studies of roscovitine–cdk2 interactions also convey the significant effect of *N*-9 substituents on active site binding (Otyepka et al., 2000).

The preference of the $R^1$ group for the branched *i*-propyl with regard to cdk2 activity is quite pronounced, as shown for the methylated **13k**, which also reduced the kinase activity ca. 8-fold. Unfortunately, all larger substituents introduced at this position ablated the agonist activity or decreased compound solubility to the extent that we were unable to measure activities (results not shown). We were hoping to use the $R^2$ substituent in zone 2 to gain further channel selectivity, but unfortunately, all modifications of the benzyl group at this site, including the *cyclo*-propylmethyl group in **13g**, led to complete loss of N-type calcium channel activity. These negative results were hard to predict, given the dearth of information about zone 2 modifications prior to our work (Figure 1).

The first group at $R^2$ that proved to be an effective mimic of the benzyl group in roscovitine was the methylthiophenyl-substituted **13u**. This compound had almost 3-fold improved N-type calcium channel agonism, even though it was still a low nanomolar cdk2 inhibitor. Because **13u** was substituted with an *i*-propyl group at $R^1$, we speculated that replacing this group with methyl or *n*-propyl while maintaining the methylthiophenyl group at $R^2$ should give us reduced kinase inhibitory properties analogous to **13d**, **13g**, and **13k**. Indeed, this turned out to be the case. Both **13w** and **13x** had an $EC_{50} \approx 3$ μM against cdk2, but the $R^1$ = methyl substitution in **13w** also decreased the channel activity ca. 3-fold versus **13u**. In contrast, **13x** proved to be a considerably more potent N-type calcium channel agonist with an $EC_{50} = 7.2$ μM for N-type channels. The effects of small changes in the $R^1$ substitution on the N-channel affinity are quite remarkable. For **13x**, we also examined agonist effects on P/Q-type ($EC_{50} = 8.8 \pm 1.1$

μM) and L-type calcium channels ($EC_{50}$ > 100 μM). Accordingly, **13x** showed selectivity for N- and P/Q-type over L-type calcium channels. Furthermore, we profiled **13x** against cdk1, cdk5, mitogen-activated protein kinase 1 (MAPK1), and myosin light chain kinase (MLCK) kinase targets and found inhibitory effects with $EC_{50}$ = 20.56 ± 0.96, 3.03 ± 0.32, >20, and >20 μM, respectively, further illustrating the quite favorable low-activity kinase profile of this lead structure. In light of the large cellular ATP concentrations (in the 1–10 mM range) (Kemp et al., 2007), single-digit micromolar activities of **13x** against some kinases are likely readily compensated for in vivo and are therefore not considered significant impediments from possible therapeutic applications of **13x** as N/P/Q-type calcium channel agonist in LEMS.

In parallel to our synthetic studies, docking analyses to the cdk2/roscovitine complex were used to analyze structural parameters for interactions with (*R*)-roscovitine analogues and to lay the groundwork for future second generation SAR studies. The MVD algorithm for docking combines an algorithm for cavity detection in the 3D structure of the target protein with an optimization algorithm that evaluates different poses for the protein–ligand complex. Because the crystal structure of cdk2 (PDB ID: 3DDQ) (Bettayeb et al., 2008a) contains (*R*)-roscovitine bound to the active site, it was possible to identify critical residues surrounding the binding pocket. The MolDock scoring function was in combination with the MolDock SE search algorithm and Tabu clustering (Thompson et al., 2009). A search space volume of 25 Å radius encompassing the (*R*)-roscovitine binding domain was chosen for docking, and the ligands and catalytic pocket residues were allowed to be flexible during the simulation. Each ligand was docked iteratively into the chosen cavity in 10 independent runs, each of which consisted of 1500 steps. Poses generated from each run were subjected to Tabu clustering whereby the lowest energy pose below an energy threshold of 100 was generated as output. Thus, there were 10

poses per ligand ranked by energy. The lowest energy pose of the 10 poses per ligand was selected for visual inspection.

For validation purposes, docking was first applied to(*R*)-roscovitine, and the docked pose was computed to be very close to the position of the ligand in the X-ray structure (i.e., RMSD = 0.27 Å). The binding free energy, as estimated by the MolDock Score (arbitrary units) was −140, which indicated a strong interaction with cdk2 binding site. The same protocol was then applied to all (*R*)-roscovitine analogues. The docking studies demonstrated that analogues **13d**, **13g**, **13k**, **13w**, and **13x** bound with a MolDock Score value between −127 and −143 and in a different orientation, less favorable than (*R*)-roscovitine. Compound **13u** bound similarly to (*R*)-roscovitinewith a MolDock Score of −142 (Figures 2 and 3). These results are consistent with the experimental data that show this compound to retain cdk2 activity, while **13d**, **13g**, **13k**, **13w**, and **13x** displayed reduced cdk2 activities.

In summary, in ca. 20 synthetic analogues, we were able to generate a new lead structure **13x** with a 4-fold improved N-type calcium channel agonist efficacy and a 22-fold decreased cdk2 activity as compared to (*R*)-roscovitine. The SAR followed a logical trend, with small structural changes at $R^1$ greatly influencing the cdk2 activity. Replacing the benzyl group at $R^2$ with bioisosteric functions mostly led to compounds lacking N-type calcium channel activity, with the notable exception of the 5-methylthiophene group, which considerably increased the desired agonism. Molecular docking studies were used to predict and analyze the structural trends leading to reduced cdk2 activity. We are now studying the in vivo effects of **13x** as well as further improving its N- and P/Q-type calcium channel activity profile. The long-term goal of our program is to develop selective voltage-gated N- and P/Q-type calcium channel agonists for the therapy of LEMS and other neurological diseases. The potential side effects of a use-

dependent N- and P/Q-type calcium channel agonist that enhances calcium flux through calcium channels that are normally activated by action potential activity are expected to be few and manageable (assuming it does not cross the blood–brain barrier). This expectation is based on extensive clinical literature that uses an indirect method of achieving a similar outcome with potassium channel blockers such as 3,4-diaminopyridine (DAP) (Oh et al., 2009; Titulaer et al., 2011a). DAP prolongs the duration of the presynaptic action potential, and this indirectly increases the activation of all voltage-gated calcium channels in the peripheral nervous system. DAP is generally well tolerated by LEMS patients (Oh et al., 2009; Titulaer et al., 2011a), with many of the side effects reported likely due to either broadening of action potentials in all neurons or the nonselective indirect effect of increasing calcium flux through all voltage-gated channels. On the basis of these previous reports, selective use-dependent N- and P/Q-type calcium channel agonists are predicted to be well tolerated.

***Experimental Procedures***

For the synthesis of **15**, **16**, and **13**, see the ***Supporting Information*** below. Biological evaluations of the effects of (*R*)-roscovitine derivatives on N-type calcium channels were initially performed using a tsA201 cell line (Lin et al., 2004) that stably expresses all of the subunits of the N-type calcium channel splice variant predominantly present in mammalian brain and spinal cord: $Ca_v2.2$ rn$\alpha_{1B\text{-}c}$ ($Ca_v$ 2.2 e[24a,Δ31a]), $Ca_v\beta_3$, and $Ca_v\alpha_2\delta_1$. For subsequent evaluation of effects on N-, P/Q-, or L-type channels, tsA-201 cells were transiently transfected with $Ca_v2.2$, $Ca_v2.1$, or $Ca_v1.3$, in combination with $Ca_v\beta_3$ and $Ca_v\alpha_2\delta_1$ (Addgene, Cambridge, MA) using FuGENE 6 (Promega, Madison, WI). All cells were maintained in DMEM supplemented with 10% fetal bovine serum. For the stable cell line expressing N-type channels,

25 μg/mL zeocin, 5 μg/mL blasticidin, and 25 μg/mL hygromycin were added as selection agents.

To assess the biological effects of (*R*)-roscovitine derivatives, whole-cell currents through calcium channels were recorded using perforated patch methods as previously described (White et al., 1997; Yazejian et al., 1997; Cho and Meriney, 2006). Briefly, the pipet solution consisted of 70 nM $Cs_2SO_4$, 60 mM CsCl, 1 mM $MgCl_2$, and 10 mM 4-(2-hydroxyethyl)-1-piperazineethanesulfonic acid (HEPES) at pH 7.4. Cultured cells were bathed in a saline composed of 130 mM choline chloride (ChCl), 10 mM tetraethylammonium chloride (TEA-Cl), 2 mM $CaCl_2$, 1 mM $MgCl_2$, and 10 mM HEPES at pH 7.4. Patch pipettes were fabricated from borosilicate glass, and capacitive currents and passive membrane responses to voltage commands were subtracted from the data. Currents were amplified by an Axopatch 200B amplifier, filtered at 5 kHz, and digitized at 10 kHz for subsequent analysis using pClamp software (Axon Instruments/Molecular Devices, Sunnyvale, CA). A liquid junction potential of −11.3 mV was subtracted during recordings. To measure effects on calcium channel tail currents, the tail current integral was measured before and after application of a derivative, with the integral of each trace being normalized to its peak. All experiments were carried out at room temperature (22 °C). All (*R*)-roscovitine derivatives were dissolved in DMSO as a 100 mM stock and stored at −20 °C. For whole-cell recordings, (*R*)-roscovitine derivatives were diluted on the day of use into saline at a final concentration of 1–100 μM, and were bath-applied via a glass pipet in a ~0.5 mL static bath chamber. Control recordings performed with 0.1–1% DMSO alone added to the drug delivery pipet solution revealed no significant effects on whole-cell calcium currents. All other salts and chemicals were obtained from Sigma-Aldrich Chemical Company (St. Louis, MO).

Cdk1 cyclinB(h), cdk2 cyclinA(h), cdk5 p35(h), MAPK1(h), and MLCK(h) inhibitory activities were determined by Millipore UK Ltd. at 0.2, 2, and 20 μM agent concentration, with roscovitine as the positive control.

Flexible docking studies were performed using Molegro Virtual Docker (MVD, University of Aarhus, Denmark) to evaluate if the analogues bound to the (*R*)-roscovitine binding site of cdk2 (Bettayeb et al., 2008a). The basis of these docking studies was a new hybrid search algorithm, that is, a guided differential evolution (DE), which combines DE optimization with a cavity prediction algorithm, which is dynamically used during the docking process. Briefly, all individual ligands were initialized, evaluated, and scored ($E_{score}$/MolDock Score) according to the fitness function, which is the sum of the intermolecular interaction energy between the ligand and the protein and the intramolecular interaction energy of the ligand: $E_{score} = E_{inter} + E_{intra}$, with $E_{inter}$ being the ligand–protein interaction energy and $E_{intra}$ being the internal energy of the ligand (Thompson et al., 2009).

$E_{PLP}$ is a piecewise linear potential using two different sets of parameters: one set for approximating the steric van der Waals term between atoms and the other stronger potential for hydrogen bonds. $E_{clash}$ assigns a penalty of 1000 if the distance between two atoms (more than two bonds apart) is less than 2.0 Å. Thus, the $E_{clash}$ term punishes infeasible ligand conformations.

Offspring were created using a weighted difference of the parent solutions, which were randomly selected from the population. If, and only if, the offspring was more fit, it would replace the parent. Otherwise, the parent survived and was passed on to the next generation, representing an iteration of the algorithm. The search process was terminated when the number of fitness evaluations exceeded the maximum number of evaluations permitted.

***Supporting Information***

Experimental procedures, assay results, and spectral data for new compounds. This material is available free of charge via the Internet at http://pubs.acs.org.

## BIBLIOGRAPHY

(2001) Literature review of the usefulness of repetitive nerve stimulation and single fiber EMG in the electrodiagnostic evaluation of patients with suspected myasthenia gravis or Lambert-Eaton myasthenic syndrome. Muscle Nerve 24:1239-1247.

Acsady L, Kamondi A, Sik A, Freund T, Buzsaki G (1998) GABAergic cells are the major postsynaptic targets of mossy fibers in the rat hippocampus. J Neurosci 18:3386-3403.

Antoine JC, Camdessanche JP (2013) Treatment options in paraneoplastic disorders of the peripheral nervous system. Current treatment options in neurology 15:210-223.

Atlas D (2001) Functional and physical coupling of voltage-sensitive calcium channels with exocytotic proteins: ramifications for the secretion mechanism. J Neurochem 77:972-985.

Bain PG, Motomura M, Newsom-Davis J, Misbah SA, Chapel HM, Lee ML, Vincent A, Lang B (1996) Effects of intravenous immunoglobulin on muscle weakness and calcium-channel autoantibodies in the Lambert-Eaton myasthenic syndrome. Neurology 47:678-683.

Bartoletti TM, Jackman SL, Babai N, Mercer AJ, Kramer RH, Thoreson WB (2011) Release from the cone ribbon synapse under bright light conditions can be controlled by the opening of only a few Ca(2+) channels. J Neurophysiol 106:2922-2935.

Bennett MR (1996) Neuromuscular transmission at an active zone: the secretosome hypothesis. J Neurocytol 25:869-891.

Bennett MR, Farnell L, Gibson WG (2000) The probability of quantal secretion near a single calcium channel of an active zone. Biophys J 78:2201-2221.

Bennett MR, Gibson WG, Robinson J (1997) Probabilistic secretion of quanta and the synaptosecretosome hypothesis: evoked release at active zones of varicosities, boutons, and endplates. Biophys J 73:1815-1829.

Bennett MR, Jones P, Lavidis NA (1986) The probability of quantal secretion along visualized terminal branches at amphibian (Bufo marinus) neuromuscular synapses. J Physiol 379:257-274.

Bettayeb K, Oumata N, Echalier A, Ferandin Y, Endicott JA, Galons H, Meijer L (2008a) CR8, a potent and selective, roscovitine-derived inhibitor of cyclin-dependent kinases. Oncogene 27:5797-5807.

Bettayeb K, Sallam H, Ferandin Y, Popowycz F, Fournet G, Hassan M, Echalier A, Bernard P, Endicott J, Joseph B, Meijer L (2008b) N-&-N, a new class of cell death-inducing kinase inhibitors derived from the purine roscovitine. Mol Cancer Ther 7:2713-2724.

Bezanilla F (2000) The voltage sensor in voltage-dependent ion channels. Physiol Rev 80:555-592.

Bezprozvanny I, Scheller RH, Tsien RW (1995) Functional impact of syntaxin on gating of N-type and Q-type calcium channels. Nature 378:623-626.

Bird SJ (1992) Clinical and electrophysiologic improvement in Lambert-Eaton syndrome with intravenous immunoglobulin therapy. Neurology 42:1422-1423.

Bischofberger J, Geiger JR, Jonas P (2002) Timing and efficacy of $Ca^{2+}$ channel activation in hippocampal mossy fiber boutons. J Neurosci 22:10593-10602.

Bollmann JH, Sakmann B (2005) Control of synaptic strength and timing by the release-site $Ca^{2+}$ signal. Nat Neurosci 8:426-434.

Borst JG, Helmchen F, Sakmann B (1995) Pre- and postsynaptic whole-cell recordings in the medial nucleus of the trapezoid body of the rat. J Physiol 489 ( Pt 3):825-840.

Borst JG, Sakmann B (1998) Calcium current during a single action potential in a large presynaptic terminal of the rat brainstem. J Physiol 506 ( Pt 1):143-157.

Borst JG, Sakmann B (1999) Effect of changes in action potential shape on calcium currents and transmitter release in a calyx-type synapse of the rat auditory brainstem. Philos Trans R Soc Lond B Biol Sci 354:347-355.

Bradley SA, Lyons PR, Slater CR (1989) The epitrochleoanconeus muscle (ETA) of the mouse: a useful muscle for the study of motor innervation. J Physiol 415:3P.

Brandt A, Khimich D, Moser T (2005) Few CaV1.3 channels regulate the exocytosis of a synaptic vesicle at the hair cell ribbon synapse. J Neurosci 25:11577-11585.

Braun M, Schmidt RF (1966) Potential changes recorded from the frog motor nerve terminal during its activation. Pflugers Arch Gesamte Physiol Menschen Tiere 287:56-80.

Braun M, Schmidt RF, Zimmermann M (1966) Facilitation at the frog neuromuscular junction during and after repetitive stimulation. Pflugers Arch Gesamte Physiol Menschen Tiere 287:41-55.

Bruneau EG, Akaaboune M (2010) Dynamics of the rapsyn scaffolding protein at the neuromuscular junction of live mice. J Neurosci 30:614-619.

Bucurenciu I, Bischofberger J, Jonas P (2010) A small number of open $Ca^{2+}$ channels trigger transmitter release at a central GABAergic synapse. Nat Neurosci 13:19-21.

Bucurenciu I, Kulik A, Schwaller B, Frotscher M, Jonas P (2008) Nanodomain coupling between $Ca^{2+}$ channels and $Ca^{2+}$ sensors promotes fast and efficient transmitter release at a cortical GABAergic synapse. Neuron 57:536-545.

Buraei Z, Anghelescu M, Elmslie KS (2005) Slowed N-type calcium channel (CaV2.2) deactivation by the cyclin-dependent kinase inhibitor roscovitine. Biophys J 89:1681-1691.

Buraei Z, Elmslie KS (2008) The separation of antagonist from agonist effects of trisubstituted purines on CaV2.2 (N-type) channels. J Neurochem 105:1450-1461.

Catterall WA (2011) Voltage-gated calcium channels. Cold Spring Harb Perspect Biol 3:a003947.

Chapman ER (2002) Synaptotagmin: a Ca(2+) sensor that triggers exocytosis? Nat Rev Mol Cell Biol 3:498-508.

Chen J, Billings SE, Nishimune H (2011) Calcium channels link the muscle-derived synapse organizer laminin beta2 to Bassoon and CAST/Erc2 to organize presynaptic active zones. J Neurosci 31:512-525.

Chen J, Mizushige T, Nishimune H (2012) Active zone density is conserved during synaptic growth but impaired in aged mice. J Comp Neurol 520:434-452.

Chicurel ME, Harris KM (1992) Three-dimensional analysis of the structure and composition of CA3 branched dendritic spines and their synaptic relationships with mossy fiber boutons in the rat hippocampus. J Comp Neurol 325:169-182.

Cho S, Meriney SD (2006) The effects of presynaptic calcium channel modulation by roscovitine on transmitter release at the adult frog neuromuscular junction. Eur J Neurosci 23:3200-3208.

Chow RH (1991) Cadmium block of squid calcium currents. Macroscopic data and a kinetic model. J Gen Physiol 98:751-770.

Church PJ, Stanley EF (1996) Single L-type calcium channel conductance with physiological levels of calcium in chick ciliary ganglion neurons. J Physiol 496 ( Pt 1):59-68.

Crins TT, Rusu SI, Rodriguez-Contreras A, Borst JG (2011) Developmental changes in short-term plasticity at the rat calyx of Held synapse. J Neurosci 31:11706-11717.

D'Alonzo AJ, Grinnell AD (1985) Profiles of evoked release along the length of frog motor nerve terminals. J Physiol 359:235-258.

Davis AF, Bai J, Fasshauer D, Wolowick MJ, Lewis JL, Chapman ER (1999) Kinetics of synaptotagmin responses to $Ca^{2+}$ and assembly with the core SNARE complex onto membranes. Neuron 24:363-376.

De Azevedo WF, Leclerc S, Meijer L, Havlicek L, Strnad M, Kim SH (1997) Inhibition of cyclin-dependent kinases by purine analogues: crystal structure of human cdk2 complexed with roscovitine. Eur J Biochem 243:518-526.

DeStefino NR, Pilato AA, Dittrich M, Cherry SV, Cho S, Stiles JR, Meriney SD (2010) (R)-roscovitine prolongs the mean open time of unitary N-type calcium channel currents. Neuroscience 167:838-849.

Dittrich M, Pattillo JM, King JD, Cho S, Stiles JR, Meriney SD (2013) An excess-calcium-binding-site model predicts neurotransmitter release at the neuromuscular junction. Biophys J 104:2751-2763.

Dodge FA, Jr., Rahamimoff R (1967) Co-operative action of calcium ions in transmitter release at the neuromuscular junction. J Physiol 193:419-432.

Eccles JC, Katz B, Kuffler SW (1941) Nature of the 'end-plate potential' in curarized muscle. J Neurophysiol 4:362-387.

Eggermann E, Bucurenciu I, Goswami SP, Jonas P (2012) Nanodomain coupling between Ca(2) channels and sensors of exocytosis at fast mammalian synapses. Nat Rev Neurosci 13:7-21.

Ellisman MH, Rash JE, Staehelin LA, Porter KR (1976) Studies of excitable membranes. II. A comparison of specializations at neuromuscular junctions and nonjunctional sarcolemmas of mammalian fast and slow twitch muscle fibers. J Cell Biol 68:752-774.

Faulkner RL, Jang MH, Liu XB, Duan X, Sailor KA, Kim JY, Ge S, Jones EG, Ming GL, Song H, Cheng HJ (2008) Development of hippocampal mossy fiber synaptic outputs by new neurons in the adult brain. Proc Natl Acad Sci U S A 105:14157-14162.

Fedchyshyn MJ, Wang LY (2005) Developmental transformation of the release modality at the calyx of Held synapse. J Neurosci 25:4131-4140.

Feldmeyer D, Radnikow G (2009) Developmental alterations in the functional properties of excitatory neocortical synapses. J Physiol 587:1889-1896.

Feng TP (1940) Studies on the neuromuscular junction. XVIII. The local potentials around N-M junctions induced by single and multiple volleys. Chin J Physiol 15:367-404.

Feng TP (1941) Studies on the neuromuscular junction. XXVI. The changes of the end-plate potential during and after prolonged stimulation. Chin J Physiol 16:341-372.

Flink MT, Atchison WD (2002) Passive transfer of Lambert-Eaton syndrome to mice induces dihydropyridine sensitivity of neuromuscular transmission. J Physiol 543:567-576.

Forsythe ID (1994) Direct patch recording from identified presynaptic terminals mediating glutamatergic EPSCs in the rat CNS, in vitro. J Physiol 479 ( Pt 3):381-387.

Frank T, Khimich D, Neef A, Moser T (2009) Mechanisms contributing to synaptic $Ca^{2+}$ signals and their heterogeneity in hair cells. Proc Natl Acad Sci U S A 106:4483-4488.

Frenguelli BG, Malinow R (1996) Fluctuations in intracellular calcium responses to action potentials in single en passage presynaptic boutons of layer V neurons in neocortical slices. Learn Mem 3:150-159.

Fu AK, Ip FC, Fu WY, Cheung J, Wang JH, Yung WH, Ip NY (2005) Aberrant motor axon projection, acetylcholine receptor clustering, and neurotransmission in cyclin-dependent kinase 5 null mice. Proc Natl Acad Sci U S A 102:15224-15229.

Fukunaga H, Engel AG, Lang B, Newsom-Davis J, Vincent A (1983) Passive transfer of Lambert-Eaton myasthenic syndrome with IgG from man to mouse depletes the presynaptic membrane active zones. Proc Natl Acad Sci U S A 80:7636-7640.

Fukuoka T, Engel AG, Lang B, Newsom-Davis J, Vincent A (1987) Lambert-Eaton myasthenic syndrome: II. Immunoelectron microscopy localization of IgG at the mouse motor end-plate. Ann Neurol 22:200-211.

Gaffield MA, Tabares L, Betz WJ (2009) The spatial pattern of exocytosis and post-exocytic mobility of synaptopHluorin in mouse motor nerve terminals. J Physiol 587:1187-1200.

Goda Y, Sudhof TC (1997) Calcium regulation of neurotransmitter release: reliably unreliable? Curr Opin Cell Biol 9:513-518.

Golshani P, Goncalves JT, Khoshkhoo S, Mostany R, Smirnakis S, Portera-Cailliau C (2009) Internally mediated developmental desynchronization of neocortical network activity. J Neurosci 29:10890-10899.

Goutman JD, Glowatzki E (2007) Time course and calcium dependence of transmitter release at a single ribbon synapse. Proc Natl Acad Sci U S A 104:16341-16346.

Govind CK, Pearce J (2003) Active zones and receptor surfaces of freeze-fractured crayfish phasic and tonic motor synapses. J Neurocytol 32:39-51.

Grinnell AD (1995) Dynamics of nerve-muscle interaction in developing and mature neuromuscular junctions. Physiol Rev 75:789-834.

Hallermann S, Pawlu C, Jonas P, Heckmann M (2003) A large pool of releasable vesicles in a cortical glutamatergic synapse. Proc Natl Acad Sci U S A 100:8975-8980.

Han X, Wang CT, Bai J, Chapman ER, Jackson MB (2004) Transmembrane segments of syntaxin line the fusion pore of $Ca^{2+}$-triggered exocytosis. Science 304:289-292.

Han Y, Kaeser PS, Sudhof TC, Schneggenburger R (2011) RIM determines Ca(2)+ channel density and vesicle docking at the presynaptic active zone. Neuron 69:304-316.

Hardingham NR, Larkman AU (1998) Rapid report: the reliability of excitatory synaptic transmission in slices of rat visual cortex in vitro is temperature dependent. J Physiol 507 ( Pt 1):249-256.

Harlow ML, Ress D, Stoschek A, Marshall RM, McMahan UJ (2001) The architecture of active zone material at the frog's neuromuscular junction. Nature 409:479-484.

Hennig R, Lomo T (1985) Firing patterns of motor units in normal rats. Nature 314:164-166.

Henze DA, McMahon DB, Harris KM, Barrionuevo G (2002) Giant miniature EPSCs at the hippocampal mossy fiber to CA3 pyramidal cell synapse are monoquantal. J Neurophysiol 87:15-29.

Henze DA, Urban NN, Barrionuevo G (2000) The multifarious hippocampal mossy fiber pathway: a review. Neuroscience 98:407-427.

Hess P, Lansman JB, Tsien RW (1984) Different modes of Ca channel gating behaviour favoured by dihydropyridine Ca agonists and antagonists. Nature 311:538-544.

Heuser JE, Reese TS, Dennis MJ, Jan Y, Jan L, Evans L (1979) Synaptic vesicle exocytosis captured by quick freezing and correlated with quantal transmitter release. J Cell Biol 81:275-300.

Heuser JE, Reese TS, Landis DM (1974) Functional changes in frog neuromuscular junctions studied with freeze-fracture. J Neurocytol 3:109-131.

Hille B (2001). Ion channels of excitable membranes. Sunderland, Mass., Sinauer.

Holderith N, Lorincz A, Katona G, Rozsa B, Kulik A, Watanabe M, Nusser Z (2012) Release probability of hippocampal glutamatergic terminals scales with the size of the active zone. Nat Neurosci 15:988-997.

Hong SJ, Chang CC (1989) Use of geographutoxin II (mu-conotoxin) for the study of neuromuscular transmission in mouse. Br J Pharmacol 97:934-940.

Jarsky T, Tian M, Singer JH (2010) Nanodomain control of exocytosis is responsible for the signaling capability of a retinal ribbon synapse. J Neurosci 30:11885-11895.

Jenkinson DH (1957) The nature of the antagonism between calcium and magnesium ions at the neuromuscular junction. J Physiol 138:434-444.

Johnston I, Lang B, Leys K, Newsom-Davis J (1994) Heterogeneity of calcium channel autoantibodies detected using a small-cell lung cancer line derived from a Lambert-Eaton myasthenic syndrome patient. Neurology 44:334-338.

Jonas P, Bischofberger J, Fricker D, Miles R (2004) Interneuron Diversity series: Fast in, fast out--temporal and spatial signal processing in hippocampal interneurons. Trends Neurosci 27:30-40.

Kaeser PS, Deng L, Wang Y, Dulubova I, Liu X, Rizo J, Sudhof TC (2011) RIM proteins tether $Ca^{2+}$ channels to presynaptic active zones via a direct PDZ-domain interaction. Cell 144:282-295.

Katz B (1969). The release of neural transmitter substances. Liverpool, Liverpool Univ. Press.

Katz B, Miledi R (1979) Estimates of quantal content during 'chemical potentiation' of transmitter release. Proc R Soc Lond B Biol Sci 205:369-378.

Katz E, Ferro PA, Weisz G, Uchitel OD (1996) Calcium channels involved in synaptic transmission at the mature and regenerating mouse neuromuscular junction. J Physiol 497 ( Pt 3):687-697.

Kavalali ET (2015) The mechanisms and functions of spontaneous neurotransmitter release. Nat Rev Neurosci 16:5-16.

Keith RK, Poage RE, Yokoyama CT, Catterall WA, Meriney SD (2007) Bidirectional modulation of transmitter release by calcium channel/syntaxin interactions in vivo. J Neurosci 27:265-269.

Kemp GJ, Meyerspeer M, Moser E (2007) Absolute quantification of phosphorus metabolite concentrations in human muscle in vivo by 31P MRS: a quantitative review. NMR Biomed 20:555-565.

Kempermann G, Kuhn HG, Gage FH (1998) Experience-induced neurogenesis in the senescent dentate gyrus. J Neurosci 18:3206-3212.

Kennedy HJ, Pouli AE, Ainscow EK, Jouaville LS, Rizzuto R, Rutter GA (1999) Glucose generates sub-plasma membrane ATP microdomains in single islet beta-cells. Potential role for strategically located mitochondria. J Biol Chem 274:13281-13291.

Keogh M, Sedehizadeh S, Maddison P (2011) Treatment for Lambert-Eaton myasthenic syndrome. The Cochrane database of systematic reviews:CD003279.

Kerr RA, Bartol TM, Kaminsky B, Dittrich M, Chang JC, Baden SB, Sejnowski TJ, Stiles JR (2008) Fast Monte Carlo Simulation Methods for Biological Reaction-Diffusion Systems in Solution and on Surfaces. SIAM J Sci Comput 30:3126.

Kim SH, Ryan TA (2010) CDK5 serves as a major control point in neurotransmitter release. Neuron 67:797-809.

Kirsch GE, Narahashi T (1978) 3,4-diaminopyridine. A potent new potassium channel blocker. Biophys J 22:507-512.

Kochubey O, Han Y, Schneggenburger R (2009) Developmental regulation of the intracellular $Ca^{2+}$ sensitivity of vesicle fusion and $Ca^{2+}$-secretion coupling at the rat calyx of Held. J Physiol 587:3009-3023.

Koester HJ, Sakmann B (2000) Calcium dynamics associated with action potentials in single nerve terminals of pyramidal cells in layer 2/3 of the young rat neocortex. J Physiol 529 Pt 3:625-646.

Kraushaar U, Jonas P (2000) Efficacy and stability of quantal GABA release at a hippocampal interneuron-principal neuron synapse. J Neurosci 20:5594-5607.

Lambert EH, Eaton LM, Rooke ED (1956) Defect of neuromuscular conduction associated with malignant neoplasms. Am. J. Physiol. 187:612-613.

Lang B, Molenaar PC, Newsom-Davis J, Vincent A (1984) Passive transfer of Lambert-Eaton myasthenic syndrome in mice: decreased rates of resting and evoked release of acetylcholine from skeletal muscle. J Neurochem 42:658-662.

Lansman JB, Hess P, Tsien RW (1986) Blockade of current through single calcium channels by $Cd^{2+}$, $Mg^{2+}$, and $Ca^{2+}$. Voltage and concentration dependence of calcium entry into the pore. J Gen Physiol 88:321-347.

Lawrence JJ, Grinspan ZM, McBain CJ (2004) Quantal transmission at mossy fibre targets in the CA3 region of the rat hippocampus. J Physiol 554:175-193.

Lennon VA, Kryzer TJ, Griesmann GE, O'Suilleabhain PE, Windebank AJ, Woppmann A, Miljanich GP, Lambert EH (1995) Calcium-channel antibodies in the Lambert-Eaton syndrome and other paraneoplastic syndromes. The New England journal of medicine 332:1467-1474.

Li F, Pincet F, Perez E, Eng WS, Melia TJ, Rothman JE, Tareste D (2007a) Energetics and dynamics of SNAREpin folding across lipid bilayers. Nat Struct Mol Biol 14:890-896.

Li L, Bischofberger J, Jonas P (2007b) Differential gating and recruitment of P/Q-, N-, and R-type $Ca^{2+}$ channels in hippocampal mossy fiber boutons. J Neurosci 27:13420-13429.

Liang M, Tarr TB, Bravo-Altamirano K, Valdomir G, Rensch G, Swanson L, DeStefino NR, Mazzarisi CM, Olszewski RA, Wilson GM, Meriney SD, Wipf P (2012) Synthesis and Biological Evaluation of a Selective N- and P/Q-Type Calcium Channel Agonist. Acs Med Chem Lett 3:985-990.

Lin Y, McDonough SI, Lipscombe D (2004) Alternative splicing in the voltage-sensing region of N-Type CaV2.2 channels modulates channel kinetics. J Neurophysiol 92:2820-2830.

Lindquist S, Stangel M (2011) Update on treatment options for Lambert-Eaton myasthenic syndrome: focus on use of amifampridine. Neuropsychiatric disease and treatment 7:341-349.

Llinas R, Blinks JR, Nicholson C (1972) Calcium transient in presynaptic terminal of squid giant synapse: detection with aequorin. Science 176:1127-1129.

Llinas R, Nicholson C (1975) Calcium role in depolarization-secretion coupling: an aequorin study in squid giant synapse. Proc Natl Acad Sci U S A 72:187-190.

Llinas R, Sugimori M, Silver RB (1992) Microdomains of high calcium concentration in a presynaptic terminal. Science 256:677-679.

Llinas R, Sugimori M, Simon SM (1982) Transmission by presynaptic spike-like depolarization in the squid giant synapse. Proc Natl Acad Sci U S A 79:2415-2419.

Luo F, Dittrich M, Cho S, Stiles JR, Meriney SD (2015) Transmitter release is evoked with low probability predominately by calcium flux through single channel openings at the frog neuromuscular junction. J Neurophysiol 113:2480-2489.

Luo F, Dittrich M, Stiles JR, Meriney SD (2011) Single-pixel optical fluctuation analysis of calcium channel function in active zones of motor nerve terminals. J Neurosci 31:11268-11281.

Ma J (2014). Quantitative simulation of synaptic vesicle release at the neuromuscular junction (Doctoral Dissertation).

Ma J, Kelly L, Ingram J, Price TJ, Meriney SD, Dittrich M (2015) New insights into short-term synaptic facilitation at the frog neuromuscular junction. J Neurophysiol 113:71-87.

Maddison P (2012) Treatment in Lambert-Eaton myasthenic syndrome. Ann N Y Acad Sci 1275:78-84.

Maddison P, Lang B, Mills K, Newsom-Davis J (2001) Long term outcome in Lambert-Eaton myasthenic syndrome without lung cancer. Journal of neurology, neurosurgery, and psychiatry 70:212-217.

Maechler P, Wang H, Wollheim CB (1998) Continuous monitoring of ATP levels in living insulin secreting cells expressing cytosolic firefly luciferase. FEBS Lett 422:328-332.

Mallart A, Martin AR (1967) An analysis of facilitation of transmitter release at the neuromuscular junction of the frog. J Physiol 193:679-694.

Marin-Burgin A, Mongiat LA, Pardi MB, Schinder AF (2012) Unique Processing During a Period of High Excitation/Inhibition Balance in Adult-Born Neurons. Science.

Martens S, Kozlov MM, McMahon HT (2007) How synaptotagmin promotes membrane fusion. Science 316:1205-1208.

Mason WP, Graus F, Lang B, Honnorat J, Delattre JY, Valldeoriola F, Antoine JC, Rosenblum MK, Rosenfeld MR, Newsom-Davis J, Posner JB, Dalmau J (1997) Small-cell lung cancer, paraneoplastic cerebellar degeneration and the Lambert-Eaton myasthenic syndrome. Brain 120 ( Pt 8):1279-1300.

Mato S, Robbe D, Puente N, Grandes P, Manzoni OJ (2005) Presynaptic homeostatic plasticity rescues long-term depression after chronic Delta 9-tetrahydrocannabinol exposure. J Neurosci 25:11619-11627.

McLachlan EM, Martin AR (1981) Non-linear summation of end-plate potentials in the frog and mouse. J Physiol 311:307-324.

Meijer L, Bettayeb K, Galons H (2007). (*R*)-Roscovitine (cyc202, seliciclib). Inhibitors of Cyclin-Dependent Kinases as Anti-Tumor Agents. P. J. Smith and E. W. Yue. Boca Raton, CRC/Taylor & Francis**:** 187-225.

Meijer L, Borgne A, Mulner O, Chong JP, Blow JJ, Inagaki N, Inagaki M, Delcros JG, Moulinoux JP (1997) Biochemical and cellular effects of roscovitine, a potent and selective inhibitor of the cyclin-dependent kinases cdc2, cdk2 and cdk5. Eur J Biochem 243:527-536.

Meijer L, Raymond E (2003) Roscovitine and other purines as kinase inhibitors. From starfish oocytes to clinical trials. Acc Chem Res 36:417-425.

Meinrenken CJ, Borst JG, Sakmann B (2002) Calcium secretion coupling at calyx of held governed by nonuniform channel-vesicle topography. J Neurosci 22:1648-1667.

Melom JE, Akbergenova Y, Gavornik JP, Littleton JT (2013) Spontaneous and evoked release are independently regulated at individual active zones. J Neurosci 33:17253-17263.

Meriney SD, Dittrich M (2013) Organization and function of transmitter release sites at the neuromuscular junction. J Physiol 591:3159-3165.

Meriney SD, Hulsizer SC, Lennon VA, Grinnell AD (1996) Lambert-Eaton myasthenic syndrome immunoglobulins react with multiple types of calcium channels in small-cell lung carcinoma. Ann Neurol 40:739-749.

Miesenbock G, De Angelis DA, Rothman JE (1998) Visualizing secretion and synaptic transmission with pH-sensitive green fluorescent proteins. Nature 394:192-195.

Mintz IM, Venema VJ, Swiderek KM, Lee TD, Bean BP, Adams ME (1992) P-type calcium channels blocked by the spider toxin omega-Aga-IVA. Nature 355:827-829.

Miralles F, Solsona C (1998) 3,4-Diaminopyridine-induced impairment in frog motor nerve terminal response to high frequency stimulation. Brain Res 789:239-244.

Mori S, Kishi M, Kubo S, Akiyoshi T, Yamada S, Miyazaki T, Konishi T, Maruyama N, Shigemoto K (2012) 3,4-Diaminopyridine improves neuromuscular transmission in a MuSK antibody-induced mouse model of myasthenia gravis. J Neuroimmunol 245:75-78.

Morsch M, Reddel SW, Ghazanfari N, Toyka KV, Phillips WD (2013) Pyridostigmine but not 3,4-diaminopyridine exacerbates ACh receptor loss and myasthenia induced in mice by muscle-specific kinase autoantibody. J Physiol 591:2747-2762.

Motomura M, Lang B, Johnston I, Palace J, Vincent A, Newsom-Davis J (1997) Incidence of serum anti-P/O-type and anti-N-type calcium channel autoantibodies in the Lambert-Eaton myasthenic syndrome. Journal of the neurological sciences 147:35-42.

Msghina M, Millar AG, Charlton MP, Govind CK, Atwood HL (1999) Calcium entry related to active zones and differences in transmitter release at phasic and tonic synapses. J Neurosci 19:8419-8434.

Muchnik S, Losavio AS, Vidal A, Cura L, Mazia C (1997) Long-term follow-up of Lambert-Eaton syndrome treated with intravenous immunoglobulin. Muscle Nerve 20:674-678.

Mutch SA, Kensel-Hammes P, Gadd JC, Fujimoto BS, Allen RW, Schiro PG, Lorenz RM, Kuyper CL, Kuo JS, Bajjalieh SM, Chiu DT (2011) Protein quantification at the single vesicle level reveals that a subset of synaptic vesicle proteins are trafficked with high precision. J Neurosci 31:1461-1470.

Nagel A, Engel AG, Lang B, Newsom-Davis J, Fukuoka T (1988) Lambert-Eaton myasthenic syndrome IgG depletes presynaptic membrane active zone particles by antigenic modulation. Ann Neurol 24:552-558.

Nagwaney S, Harlow ML, Jung JH, Szule JA, Ress D, Xu J, Marshall RM, McMahan UJ (2009) Macromolecular connections of active zone material to docked synaptic vesicles and

presynaptic membrane at neuromuscular junctions of mouse. J Comp Neurol 513:457-468.

Nakao YK, Motomura M, Fukudome T, Fukuda T, Shiraishi H, Yoshimura T, Tsujihata M, Eguchi K (2002) Seronegative Lambert-Eaton myasthenic syndrome: study of 110 Japanese patients. Neurology 59:1773-1775.

Naraghi M, Neher E (1997) Linearized buffered $Ca^{2+}$ diffusion in microdomains and its implications for calculation of [$Ca^{2+}$] at the mouth of a calcium channel. J Neurosci 17:6961-6973.

Neher E, Sakaba T (2008) Multiple roles of calcium ions in the regulation of neurotransmitter release. Neuron 59:861-872.

Newcomb R, Szoke B, Palma A, Wang G, Chen X, Hopkins W, Cong R, Miller J, Urge L, Tarczy-Hornoch K, Loo JA, Dooley DJ, Nadasdi L, Tsien RW, Lemos J, Miljanich G (1998) Selective peptide antagonist of the class E calcium channel from the venom of the tarantula Hysterocrates gigas. Biochemistry 37:15353-15362.

Newsom-Davis J, Murray NM (1984) Plasma exchange and immunosuppressive drug treatment in the Lambert-Eaton myasthenic syndrome. Neurology 34:480-485.

Nicoll RA, Schmitz D (2005) Synaptic plasticity at hippocampal mossy fibre synapses. Nat Rev Neurosci 6:863-876.

Nishimune H, Sanes JR, Carlson SS (2004) A synaptic laminin-calcium channel interaction organizes active zones in motor nerve terminals. Nature 432:580-587.

O'Connor VM, Shamotienko O, Grishin E, Betz H (1993) On the structure of the 'synaptosecretosome'. Evidence for a neurexin/synaptotagmin/syntaxin/$Ca^{2+}$ channel complex. FEBS Lett 326:255-260.

O'Neill JH, Murray NM, Newsom-Davis J (1988) The Lambert-Eaton myasthenic syndrome. A review of 50 cases. Brain 111 ( Pt 3):577-596.

O'Suilleabhain P, Low PA, Lennon VA (1998) Autonomic dysfunction in the Lambert-Eaton myasthenic syndrome: serologic and clinical correlates. Neurology 50:88-93.

Oh SJ, Claussen GG, Hatanaka Y, Morgan MB (2009) 3,4-Diaminopyridine is more effective than placebo in a randomized, double-blind, cross-over drug study in LEMS. Muscle Nerve 40:795-800.

Oh SJ, Hatanaka Y, Claussen GC, Sher E (2007) Electrophysiological differences in seropositive and seronegative Lambert-Eaton myasthenic syndrome. Muscle Nerve 35:178-183.

Oh SJ, Kurokawa K, Claussen GC, Ryan HF, Jr. (2005) Electrophysiological diagnostic criteria of Lambert-Eaton myasthenic syndrome. Muscle Nerve 32:515-520.

Olivera BM, McIntosh JM, Cruz LJ, Luque FA, Gray WR (1984) Purification and sequence of a presynaptic peptide toxin from Conus geographus venom. Biochemistry 23:5087-5090.

Otyepka M, Krystof V, Havlicek L, Siglerova V, Strnad M, Koca J (2000) Docking-based development of purine-like inhibitors of cyclin-dependent kinase-2. J Med Chem 43:2506-2513.

Oumata N, Bettayeb K, Ferandin Y, Demange L, Lopez-Giral A, Goddard ML, Myrianthopoulos V, Mikros E, Flajolet M, Greengard P, Meijer L, Galons H (2008) Roscovitine-derived, dual-specificity inhibitors of cyclin-dependent kinases and casein kinases 1. J Med Chem 51:5229-5242.

Oumata N, Ferandin Y, Meijer L, Galons H (2009) Practical synthesis of roscovitine and CR8. Org Process Res Dev 13:641-644.

Palace J, Newsom-Davis J, Lecky B (1998) A randomized double-blind trial of prednisolone alone or with azathioprine in myasthenia gravis. Myasthenia Gravis Study Group. Neurology 50:1778-1783.

Parnas I, Atwood HL (1966) Phasic and tonic neuromuscular systems in the abdominal extensor muscles of the crayfish and rock lobster. Comp Biochem Physiol 18:701-723.

Pawson PA, Grinnell AD, Wolowske B (1998) Quantitative freeze-fracture analysis of the frog neuromuscular junction synapse--I. Naturally occurring variability in active zone structure. J Neurocytol 27:361-377.

Peled Einat S, Newman Zachary L, Isacoff Ehud Y (2014) Evoked and Spontaneous Transmission Favored by Distinct Sets of Synapses. Current Biology 24:484-493.

Popowycz F, Fournet G, Schneider C, Bettayeb K, Ferandin Y, Lamigeon C, Tirado OM, Mateo-Lozano S, Notario V, Colas P, Bernard P, Meijer L, Joseph B (2009) Pyrazolo[1,5-a]-1,3,5-triazine as a purine bioisostere: access to potent cyclin-dependent kinase inhibitor (R)-roscovitine analogue. J Med Chem 52:655-663.

Pozzi D, Condliffe S, Bozzi Y, Chikhladze M, Grumelli C, Proux-Gillardeaux V, Takahashi M, Franceschetti S, Verderio C, Matteoli M (2008) Activity-dependent phosphorylation of Ser187 is required for SNAP-25-negative modulation of neuronal voltage-gated calcium channels. Proc Natl Acad Sci U S A 105:323-328.

Raingo J, Khvotchev M, Liu P, Darios F, Li YC, Ramirez DM, Adachi M, Lemieux P, Toth K, Davletov B, Kavalali ET (2012) VAMP4 directs synaptic vesicles to a pool that selectively maintains asynchronous neurotransmission. Nat Neurosci 15:738-745.

Redman S (1990) Quantal analysis of synaptic potentials in neurons of the central nervous system. Physiol Rev 70:165-198.

Rettig J, Sheng ZH, Kim DK, Hodson CD, Snutch TP, Catterall WA (1996) Isoform-specific interaction of the alpha1A subunits of brain $Ca^{2+}$ channels with the presynaptic proteins syntaxin and SNAP-25. Proc Natl Acad Sci U S A 93:7363-7368.

Rizzoli SO, Betz WJ (2005) Synaptic vesicle pools. Nat Rev Neurosci 6:57-69.

Roberts A, Perera S, Lang B, Vincent A, Newsom-Davis J (1985) Paraneoplastic myasthenic syndrome IgG inhibits $45Ca^{2+}$ flux in a human small cell carcinoma line. Nature 317:737-739.

Rochefort NL, Garaschuk O, Milos RI, Narushima M, Marandi N, Pichler B, Kovalchuk Y, Konnerth A (2009) Sparsification of neuronal activity in the visual cortex at eye-opening. Proc Natl Acad Sci U S A 106:15049-15054.

Rogozhin AA, Pang KK, Bukharaeva E, Young C, Slater CR (2008) Recovery of mouse neuromuscular junctions from single and repeated injections of botulinum neurotoxin A. J Physiol 586:3163-3182.

Rollenhagen A, Lubke JH (2010) The mossy fiber bouton: the "common" or the "unique" synapse? Front Synaptic Neurosci 2:2.

Rollenhagen A, Satzler K, Rodriguez EP, Jonas P, Frotscher M, Lubke JH (2007) Structural determinants of transmission at large hippocampal mossy fiber synapses. J Neurosci 27:10434-10444.

Ruiz R, Cano R, Casanas JJ, Gaffield MA, Betz WJ, Tabares L (2011) Active zones and the readily releasable pool of synaptic vesicles at the neuromuscular junction of the mouse. J Neurosci 31:2000-2008.

Rusakov DA (2006) $Ca^{2+}$-dependent mechanisms of presynaptic control at central synapses. Neuroscientist 12:317-326.

Sabatini BL, Svoboda K (2000) Analysis of calcium channels in single spines using optical fluctuation analysis. Nature 408:589-593.

Sanders DB (2003) Lambert-eaton myasthenic syndrome: diagnosis and treatment. Ann N Y Acad Sci 998:500-508.

Sanders DB, Massey JM, Sanders LL, Edwards LJ (2000) A randomized trial of 3,4-diaminopyridine in Lambert-Eaton myasthenic syndrome. Neurology 54:603-607.

Santafe MM, Lanuza MA, Garcia N, Tomas J (2006) Muscarinic autoreceptors modulate transmitter release through protein kinase C and protein kinase A in the rat motor nerve terminal. Eur J Neurosci 23:2048-2056.

Santafe MM, Salon I, Garcia N, Lanuza MA, Uchitel OD, Tomas J (2003) Modulation of ACh release by presynaptic muscarinic autoreceptors in the neuromuscular junction of the newborn and adult rat. Eur J Neurosci 17:119-127.

Satzler K, Sohl LF, Bollmann JH, Borst JG, Frotscher M, Sakmann B, Lubke JH (2002) Three-dimensional reconstruction of a calyx of Held and its postsynaptic principal neuron in the medial nucleus of the trapezoid body. J Neurosci 22:10567-10579.

Schara U, Della Marina A, Abicht A (2012) Congenital myasthenic syndromes: current diagnostic and therapeutic approaches. Neuropediatrics 43:184-193.

Schinder AF, Gage FH (2004) A hypothesis about the role of adult neurogenesis in hippocampal function. Physiology (Bethesda) 19:253-261.

Schneggenburger R, Neher E (2000) Intracellular calcium dependence of transmitter release rates at a fast central synapse. Nature 406:889-893.

Scimemi A, Diamond JS (2012) The number and organization of $Ca^{2+}$ channels in the active zone shapes neurotransmitter release from Schaffer collateral synapses. J Neurosci 32:18157-18176.

Seagar M, Leveque C, Charvin N, Marqueze B, Martin-Moutot N, Boudier JA, Boudier JL, Shoji-Kasai Y, Sato K, Takahashi M (1999) Interactions between proteins implicated in exocytosis and voltage-gated calcium channels. Philos Trans R Soc Lond B Biol Sci 354:289-297.

Sedehizadeh S, Keogh M, Maddison P (2012) The use of aminopyridines in neurological disorders. Clinical neuropharmacology 35:191-200.

Shahidullah M, Le Marchand SJ, Fei H, Zhang J, Pandey UB, Dalva MB, Pasinelli P, Levitan IB (2013) Defects in synapse structure and function precede motor neuron degeneration in Drosophila models of FUS-related ALS. J Neurosci 33:19590-19598.

Shahrezaei V, Cao A, Delaney KR (2006) $Ca^{2+}$ from one or two channels controls fusion of a single vesicle at the frog neuromuscular junction. J Neurosci 26:13240-13249.

Sheng J, He L, Zheng H, Xue L, Luo F, Shin W, Sun T, Kuner T, Yue DT, Wu LG (2012) Calcium-channel number critically influences synaptic strength and plasticity at the active zone. Nat Neurosci 15:998-1006.

Sheng ZH, Westenbroek RE, Catterall WA (1998) Physical link and functional coupling of presynaptic calcium channels and the synaptic vesicle docking/fusion machinery. J Bioenerg Biomembr 30:335-345.

Simon SM, Llinas RR (1985) Compartmentalization of the submembrane calcium activity during calcium influx and its significance in transmitter release. Biophys J 48:485-498.

Smith DO, Conklin MW, Jensen PJ, Atchison WD (1995) Decreased calcium currents in motor nerve terminals of mice with Lambert-Eaton myasthenic syndrome. J Physiol 487 ( Pt 1):115-123.

Sorra KE, Mishra A, Kirov SA, Harris KM (2006) Dense core vesicles resemble active-zone transport vesicles and are diminished following synaptogenesis in mature hippocampal slices. Neuroscience 141:2097-2106.

Stanley EF (1993) Single calcium channels and acetylcholine release at a presynaptic nerve terminal. Neuron 11:1007-1011.

Stock L, Souza C, Treptow W (2013) Structural basis for activation of voltage-gated cation channels. Biochemistry 52:1501-1513.

Sudhof TC (2012) The presynaptic active zone. Neuron 75:11-25.

Südhof TC (2013) Neurotransmitter Release: The Last Millisecond in the Life of a Synaptic Vesicle. Neuron 80:675-690.

Tabares L, Ruiz R, Linares-Clemente P, Gaffield MA, Alvarez de Toledo G, Fernandez-Chacon R, Betz WJ (2007) Monitoring synaptic function at the neuromuscular junction of a mouse expressing synaptopHluorin. J Neurosci 27:5422-5430.

Takahashi M, Seagar MJ, Jones JF, Reber BF, Catterall WA (1987) Subunit structure of dihydropyridine-sensitive calcium channels from skeletal muscle. Proc Natl Acad Sci U S A 84:5478-5482.

Takamori M (2008) Lambert–Eaton myasthenic syndrome: Search for alternative autoimmune targets and possible compensatory mechanisms based on presynaptic calcium homeostasis. J Neuroimmunol 201–202:145-152.

Takamori S, Holt M, Stenius K, Lemke EA, Gronborg M, Riedel D, Urlaub H, Schenck S, Brugger B, Ringler P, Muller SA, Rammner B, Grater F, Hub JS, De Groot BL, Mieskes G, Moriyama Y, Klingauf J, Grubmuller H, Heuser J, Wieland F, Jahn R (2006) Molecular anatomy of a trafficking organelle. Cell 127:831-846.

Takano H, Tanaka M, Koike R, Nagai H, Arakawa M, Tsuji S (1994) Effect of intravenous immunoglobulin in Lambert-Eaton myasthenic syndrome with small-cell lung cancer:

correlation with the titer of anti-voltage-gated calcium channel antibody. Muscle Nerve 17:1073-1075.

Tanabe T, Takeshima H, Mikami A, Flockerzi V, Takahashi H, Kangawa K, Kojima M, Matsuo H, Hirose T, Numa S (1987) Primary structure of the receptor for calcium channel blockers from skeletal muscle. Nature 328:313-318.

Tarr TB, Dittrich M, Meriney SD (2013a) Are unreliable release mechanisms conserved from NMJ to CNS? Trends Neurosci 36:14-22.

Tarr TB, Lacomis D, Reddel SW, Liang M, Valdomir G, Frasso M, Wipf P, Meriney SD (2014) Complete reversal of Lambert-Eaton myasthenic syndrome synaptic impairment by the combined use of a K+ channel blocker and a $Ca^{2+}$ channel agonist. J Physiol 592:3687-3696.

Tarr TB, Malick W, Liang M, Valdomir G, Frasso M, Lacomis D, Reddel SW, Garcia-Ocano A, Wipf P, Meriney SD (2013b) Evaluation of a novel calcium channel agonist for therapeutic potential in Lambert-Eaton myasthenic syndrome. J Neurosci 33:10559-10567.

Tarr TB, Wipf P, Meriney SD (2015) Synaptic Pathophysiology and Treatment of Lambert-Eaton Myasthenic Syndrome. Mol Neurobiol 52:456-463.

Taschenberger H, Leao RM, Rowland KC, Spirou GA, von Gersdorff H (2002) Optimizing synaptic architecture and efficiency for high-frequency transmission. Neuron 36:1127-1143.

Taschenberger H, von Gersdorff H (2000) Fine-tuning an auditory synapse for speed and fidelity: developmental changes in presynaptic waveform, EPSC kinetics, and synaptic plasticity. J Neurosci 20:9162-9173.

Tavalin SJ, Shepherd D, Cloues RK, Bowden SE, Marrion NV (2004) Modulation of single channels underlying hippocampal L-type current enhancement by agonists depends on the permeant ion. J Neurophysiol 92:824-837.

Thevenaz P, Ruttimann UE, Unser M (1998) A pyramid approach to subpixel registration based on intensity. IEEE Trans Image Process 7:27-41.

Thompson EE, Kornev AP, Kannan N, Kim C, Ten Eyck LF, Taylor SS (2009) Comparative surface geometry of the protein kinase family. Protein Sci 18:2016-2026.

Thomsen RH, Wilson DF (1983) Effects of 4-aminopyridine and 3,4-diaminopyridine on transmitter release at the neuromuscular junction. The Journal of pharmacology and experimental therapeutics 227:260-265.

Tim RW, Massey JM, Sanders DB (1998) Lambert-Eaton myasthenic syndrome (LEMS). Clinical and electrodiagnostic features and response to therapy in 59 patients. Ann N Y Acad Sci 841:823-826.

Tim RW, Massey JM, Sanders DB (2000) Lambert-Eaton myasthenic syndrome: electrodiagnostic findings and response to treatment. Neurology 54:2176-2178.

Titulaer MJ, Lang B, Verschuuren JJ (2011a) Lambert-Eaton myasthenic syndrome: from clinical characteristics to therapeutic strategies. Lancet Neurol 10:1098-1107.

Titulaer MJ, Maddison P, Sont JK, Wirtz PW, Hilton-Jones D, Klooster R, Willcox N, Potman M, Sillevis Smitt PA, Kuks JB, Roep BO, Vincent A, van der Maarel SM, van Dijk JG, Lang B, Verschuuren JJ (2011b) Clinical Dutch-English Lambert-Eaton Myasthenic syndrome (LEMS) tumor association prediction score accurately predicts small-cell lung cancer in the LEMS. J Clin Oncol 29:902-908.

Titulaer MJ, Wirtz PW, Kuks JB, Schelhaas HJ, van der Kooi AJ, Faber CG, van der Pol WL, de Visser M, Sillevis Smitt PA, Verschuuren JJ (2008) The Lambert-Eaton myasthenic syndrome 1988-2008: a clinical picture in 97 patients. J Neuroimmunol 201-202:153-158.

tom Dieck S, Specht D, Strenzke N, Hida Y, Krishnamoorthy V, Schmidt KF, Inoue E, Ishizaki H, Tanaka-Okamoto M, Miyoshi J, Hagiwara A, Brandstatter JH, Lowel S, Gollisch T, Ohtsuka T, Moser T (2012) Deletion of the presynaptic scaffold CAST reduces active zone size in rod photoreceptors and impairs visual processing. J Neurosci 32:12192-12203.

Tsien RW (1983) Calcium channels in excitable cell membranes. Annu Rev Physiol 45:341-358.

Upreti C, Otero R, Partida C, Skinner F, Thakker R, Pacheco LF, Zhou ZY, Maglakelidze G, Veliskova J, Velisek L, Romanovicz D, Jones T, Stanton PK, Garrido-Sanabria ER (2012) Altered neurotransmitter release, vesicle recycling and presynaptic structure in the pilocarpine model of temporal lobe epilepsy. Brain 135:869-885.

Urbano FJ, Pagani MR, Uchitel OD (2008) Calcium channels, neuromuscular synaptic transmission and neurological diseases. J Neuroimmunol 201-202:136-144.

Urbano FJ, Piedras-Renteria ES, Jun K, Shin HS, Uchitel OD, Tsien RW (2003) Altered properties of quantal neurotransmitter release at endplates of mice lacking P/Q-type $Ca^{2+}$ channels. Proc Natl Acad Sci U S A 100:3491-3496.

van Sonderen A, Wirtz PW, Verschuuren JJ, Titulaer MJ (2013) Paraneoplastic syndromes of the neuromuscular junction: therapeutic options in myasthenia gravis, lambert-eaton myasthenic syndrome, and neuromyotonia. Current treatment options in neurology 15:224-239.

Verschuuren JJ, Wirtz PW, Titulaer MJ, Willems LN, van Gerven J (2006) Available treatment options for the management of Lambert-Eaton myasthenic syndrome. Expert Opin Pharmacother 7:1323-1336.

Vesely J, Havlicek L, Strnad M, Blow JJ, Donella-Deana A, Pinna L, Letham DS, Kato J, Detivaud L, Leclerc S, et al. (1994) Inhibition of cyclin-dependent kinases by purine analogues. Eur J Biochem 224:771-786.

Vincent A, Lang B, Newsom-Davis J (1989) Autoimmunity to the voltage-gated calcium channel underlies the Lambert-Eaton myasthenic syndrome, a paraneoplastic disorder. Trends Neurosci 12:496-502.

von Bohlen Und Halbach O (2007) Immunohistological markers for staging neurogenesis in adult hippocampus. Cell Tissue Res 329:409-420.

von Bohlen und Halbach O (2011) Immunohistological markers for proliferative events, gliogenesis, and neurogenesis within the adult hippocampus. Cell Tissue Res 345:1-19.

Wachman ES, Poage RE, Stiles JR, Farkas DL, Meriney SD (2004) Spatial Distribution of Calcium Entry Evoked by Single Action Potentials within the Presynaptic Active Zone. J Neurosci 24:2877-2885.

Wang LY, Fedchyshyn MJ, Yang YM (2009) Action potential evoked transmitter release in central synapses: insights from the developing calyx of Held. Mol Brain 2:36.

Wang S, Bruzzi J, Rodriguez-Garza VP, Komaki RR (2006) Lambert-eaton myasthenic syndrome in a patient with small-cell lung cancer. Clinical lung cancer 7:282-284.

Wang X, Pinter MJ, Rich MM (2010) $Ca^{2+}$ dependence of the binomial parameters p and n at the mouse neuromuscular junction. J Neurophysiol 103:659-666.

Waterman SA, Lang B, Newsom-Davis J (1997) Effect of Lambert-Eaton myasthenic syndrome antibodies on autonomic neurons in the mouse. Ann Neurol 42:147-156.

White MG, Crumling MA, Meriney SD (1997) Developmental changes in calcium current pharmacology and somatostatin inhibition in chick parasympathetic neurons. J Neurosci 17:6302-6313.

Wipf P, George KM (2010) Regioselective Palladium-Catalyzed Cross-Coupling Reactions of 2,4,7-Trichloroquinazoline. Synlett 2010:644-648.

Wirtz PW, Nijnuis MG, Sotodeh M, Willems LN, Brahim JJ, Putter H, Wintzen AR, Verschuuren JJ, Dutch Myasthenia Study G (2003) The epidemiology of myasthenia gravis, Lambert-Eaton myasthenic syndrome and their associated tumours in the northern part of the province of South Holland. Journal of neurology 250:698-701.

Wirtz PW, Verschuuren JJ, van Dijk JG, de Kam ML, Schoemaker RC, van Hasselt JG, Titulaer MJ, Tjaden UR, den Hartigh J, van Gerven JM (2009) Efficacy of 3,4-diaminopyridine and pyridostigmine in the treatment of Lambert-Eaton myasthenic syndrome: a randomized, double-blind, placebo-controlled, crossover study. Clin Pharmacol Ther 86:44-48.

Wiser O, Trus M, Hernandez A, Renstrom E, Barg S, Rorsman P, Atlas D (1999) The voltage sensitive Lc-type $Ca^{2+}$ channel is functionally coupled to the exocytotic machinery. Proc Natl Acad Sci U S A 96:248-253.

Wondolowski J, Dickman D (2013) Emerging links between homeostatic synaptic plasticity and neurological disease. Front Cell Neurosci 7:223.

Wood SJ, Slater CR (2001) Safety factor at the neuromuscular junction. Prog Neurobiol 64:393-429.

Wyatt RM, Balice-Gordon RJ (2008) Heterogeneity in synaptic vesicle release at neuromuscular synapses of mice expressing synaptopHluorin. J Neurosci 28:325-335.

Xu YF, Hewett SJ, Atchison WD (1998) Passive transfer of Lambert-Eaton myasthenic syndrome induces dihydropyridine sensitivity of ICa in mouse motor nerve terminals. J Neurophysiol 80:1056-1069.

Yan Z, Chi P, Bibb JA, Ryan TA, Greengard P (2002) Roscovitine: a novel regulator of P/Q-type calcium channels and transmitter release in central neurons. J Physiol 540:761-770.

Yang YM, Fedchyshyn MJ, Grande G, Aitoubah J, Tsang CW, Xie H, Ackerley CA, Trimble WS, Wang LY (2010) Septins regulate developmental switching from microdomain to nanodomain coupling of Ca(2+) influx to neurotransmitter release at a central synapse. Neuron 67:100-115.

Yang YM, Wang LY (2006) Amplitude and kinetics of action potential-evoked $Ca^{2+}$ current and its efficacy in triggering transmitter release at the developing calyx of held synapse. J Neurosci 26:5698-5708.

Yazejian B, DiGregorio DA, Vergara JL, Poage RE, Meriney SD, Grinnell AD (1997) Direct measurements of presynaptic calcium and calcium-activated potassium currents regulating neurotransmitter release at cultured Xenopus nerve-muscle synapses. J Neurosci 17:2990-3001.

Yazejian B, Sun XP, Grinnell AD (2000) Tracking presynaptic $Ca^{2+}$ dynamics during neurotransmitter release with $Ca^{2+}$-activated K+ channels. Nat Neurosci 3:566-571.

Yokoyama CT, Myers SJ, Fu J, Mockus SM, Scheuer T, Catterall WA (2005) Mechanism of SNARE protein binding and regulation of Cav2 channels by phosphorylation of the synaptic protein interaction site. Mol Cell Neurosci 28:1-17.

Yoshikami D, Bagabaldo Z, Olivera BM (1989) The inhibitory effects of omega-conotoxins on Ca channels and synapses. Ann N Y Acad Sci 560:230-248.

Zador A (1998) Impact of synaptic unreliability on the information transmitted by spiking neurons. J Neurophysiol 79:1219-1229.

Zefirov A, Benish T, Fatkullin N, Cheranov S, Khazipov R (1995) Localization of active zones. Nature 376:393-394.

Zhai RG, Bellen HJ (2004) The architecture of the active zone in the presynaptic nerve terminal. Physiology (Bethesda) 19:262-270.

Zhai RG, Vardinon-Friedman H, Cases-Langhoff C, Becker B, Gundelfinger ED, Ziv NE, Garner CC (2001) Assembling the presynaptic active zone: a characterization of an active one precursor vesicle. Neuron 29:131-143.

Zheng W, Rampe D, Triggle DJ (1991) Pharmacological, radioligand binding, and electrophysiological characteristics of FPL 64176, a novel nondihydropyridine $Ca^{2+}$ channel activator, in cardiac and vascular preparations. Mol Pharmacol 40:734-741.

Zhu Y, Xu J, Heinemann SF (2009) Two pathways of synaptic vesicle retrieval revealed by single-vesicle imaging. Neuron 61:397-411.

Zucker RS, Regehr WG (2002) Short-term synaptic plasticity. Annu Rev Physiol 64:355-405.